MXenes for Rechargeable Batteries Beyond the Lithium-Ion

ADVANCED MATERIALS
www.advmat.de

MXenes for Rechargeable Batteries Beyond the Lithium-Ion

Fangwang Ming, Hanfeng Liang, Gang Huang, Zahra Bayhan, and Husam N. Alshareef*

Research on next-generation battery technologies (beyond Li-ion batteries, or LIBs) has been accelerating over the past few years. A key challenge for these emerging batteries has been the lack of suitable electrode materials, which severely limits their further developments. MXenes, a new class of 2D transition metal carbides, carbonitrides, and nitrides, are proposed as electrode materials for these emerging batteries due to several desirable attributes. These attributes include large and tunable interlayer spaces, excellent hydrophilicity, extraordinary conductivity, compositional diversity, and abundant surface chemistries, making MXenes promising not only as electrode materials but also as other components in the cells of emerging batteries. Herein, an overview and assessment of the utilization of MXenes in rechargeable batteries beyond LIBs, including alkali-ion (e.g., Na^+, K^+) storage, multivalent-ion (e.g., Mg^{2+}, Zn^{2+}, and Al^{3+}) storage, and metal batteries are presented. In particular, the synthetic strategies and properties of MXenes that enable MXenes to play various roles as electrodes, metal anode protective layers, sulfur hosts, separator modification layers, and conductive additives in these emerging batteries are discussed. Moreover, a perspective on promising future research directions on MXenes and MXene-based materials, ranging from material design and processing, fundamental understanding of the reaction mechanisms, to device performance optimization strategies is provided.

1. Introduction

Environmentally friendly renewable energy sources such as wind, solar, and tide are becoming increasingly important for global sustainable development. However, these renewable energy sources are naturally intermittent, which makes the energy storage devices indispensable. Owing to the high energy conversion efficiency, relatively long lifespan, a wide range of energy and power densities, and low maintenance cost, electrochemical energy storage (EES) technologies have been playing vital roles in meeting the rapidly increasing demands of portable devices, electric vehicles, grid storage, and stationary markets.[1] Since the successful commercialization by SONY in 1991, lithium-ion batteries (LIBs) have been dominating the market of energy storage systems over the past few decades.[2] In spite of the great success of the LIBs in consumer electronics and electric vehicles, their grid-scale implementation is hindered by the limited lithium resources (only 20 ppm in the earth's crust) as well as the safety concerns.[3] In this regard, many other EES systems based on more abundant and less active elements, such as sodium (2.3%), potassium (2.1%), magnesium (2.3%), aluminum (8.2%), and zinc (75 ppm), have been developed and have already achieved significant progress.[1d,4]

Historically, 2D layered materials have been employed as electrodes for batteries (e.g., graphite,[5] $LiCoO_2$,[6] and TiS_2[7]). Since the discovery of monolayer graphene in 2004,[8] more and more emerging 2D materials have quickly become popular electrode materials for various EES devices. This is not surprising given the unique structure and property of 2D materials. Their relatively large interlayer space allows fast ion (de)intercalation, whereas the highly anisotropic 2D structure enables fast charge transfer. Recently, a new class of 2D transition metal carbides, nitrides, and carbonitrides, known as MXenes,[9] was discovered and has attracted increasing research interest. Up to date, more than 30 MXenes have been successfully synthesized.[10] Similar to other 2D layered materials, MXenes also possess large/tunable interlayer spaces and high aspect ratios. In addition, MXenes show excellent hydrophilicity (contact angle is ≈21.5°–35°)[11] and extraordinary conductivity (e.g., ≈9880 S cm^{-1} for $Ti_3C_2T_x$, 3250 ± 100 S cm^{-1} for V_2CT_x).[12] Further, MXenes are coupled with various terminations (e.g., −OH, −O, and −F), which endow rich surface chemistries. These unique properties make them appealing in various applications, especially for energy storage devices such as batteries and supercapacitors.[1d,4i,13]

We noted that there have already been several excellent reviews on the application of MXenes for energy storage and conversion, which cover a wide range of topics including for LIBs, supercapacitors, electrocatalysis, photocatalysis, electromagnetic interference, and so on.[10a,14] However, a more specific summary focuses on the rechargeable batteries is required and beneficial for the researchers working on next-generation batteries. Moreover, the study and investigation on MXenes for other EES systems beyond LIB are rapidly developing and have achieved great progress very recently. For example, great research efforts have been invested in exploring the application of MXenes in Li–sulfur batteries

F. Ming, Dr. H. Liang, Dr. G. Huang, Z. Bayhan, Prof. H. N. Alshareef
Materials Science and Engineering
Physical Science and Engineering Division
King Abdullah University of Science Technology (KAUST)
Thuwal 23955, Saudi Arabia
E-mail: husam.alshareef@kaust.edu.sa
The ORCID identification number(s) for the author(s) of this article can be found under https://doi.org/10.1002/adma.202004039.

DOI: 10.1002/adma.202004039

(Li-SBs), sodium-ion batteries (SIBs), potassium-ion batteries (PIBs), and multivalent-ion (i.e., Mg^{2+}, Zn^{2+}, Al^{3+}). Besides being directly used as electrodes, MXenes are also employed as protective layers for metal anodes to prevent the growth of dendrites. Thus, a timely and comprehensive review of the latest progress of MXenes in emerging EES applications is needed. However, the use of MXenes for LIBs, supercapacitors, and energy conversion will not be covered in this review. Readers who are interested in these topics can refer to the information provided elsewhere[14c–e,15]. In the present review, we will start with a brief introduction to MXenes, followed by an overview of the preparation strategies and the properties of MXenes. Next, we will highlight the recent advances in using MXenes for rechargeable batteries beyond LIBs, including Li-SBs, SIBs, PIBs, multivalent-ion (i.e., Mg, Al, Zn) batteries as well as the utilization of MXenes for metal anode protection. Finally, we will present our perspective on the current challenges and problems, and promising future research directions.

2. MXene in Brief

MXenes are a new class of 2D transition metal carbides, carbonitrides, and nitrides that are generally produced by selectively removing the A" layer from their parent MAX phases. The term "MXene" was coined aiming at emphasizing the removal of "A" layer from the MAX phase as well as its 2D nature that is analogous to "graphene."[9,10b] The general formula of their parental MAX phases can be expressed as $M_{n+1}AX_n$ (n = 1, 2, 3 or 4), where "M" represents the early transition metal (e.g., Ti, V, Nb, Mo), "A" is an A-group (mostly groups 13 and 14, i.e., groups IIIA and IVA) element (e.g., Al, Si, Ga), and "X" is carbon and/or nitrogen (**Figure 1**a). All known MAX phases are layered structures with P63/mmc symmetry, where the XM_6 octahedra "$M_{n+1}X_n$" layers are separated by the atomic "A" layers. In other words, the structure of MAX phase can be viewed as the alternative stacking of "$M_{n+1}X_n$" layers and "A" layers along with the c direction (Figure 1b). In addition to the ordered transition metal structural crystals, MAX phases can also be solid

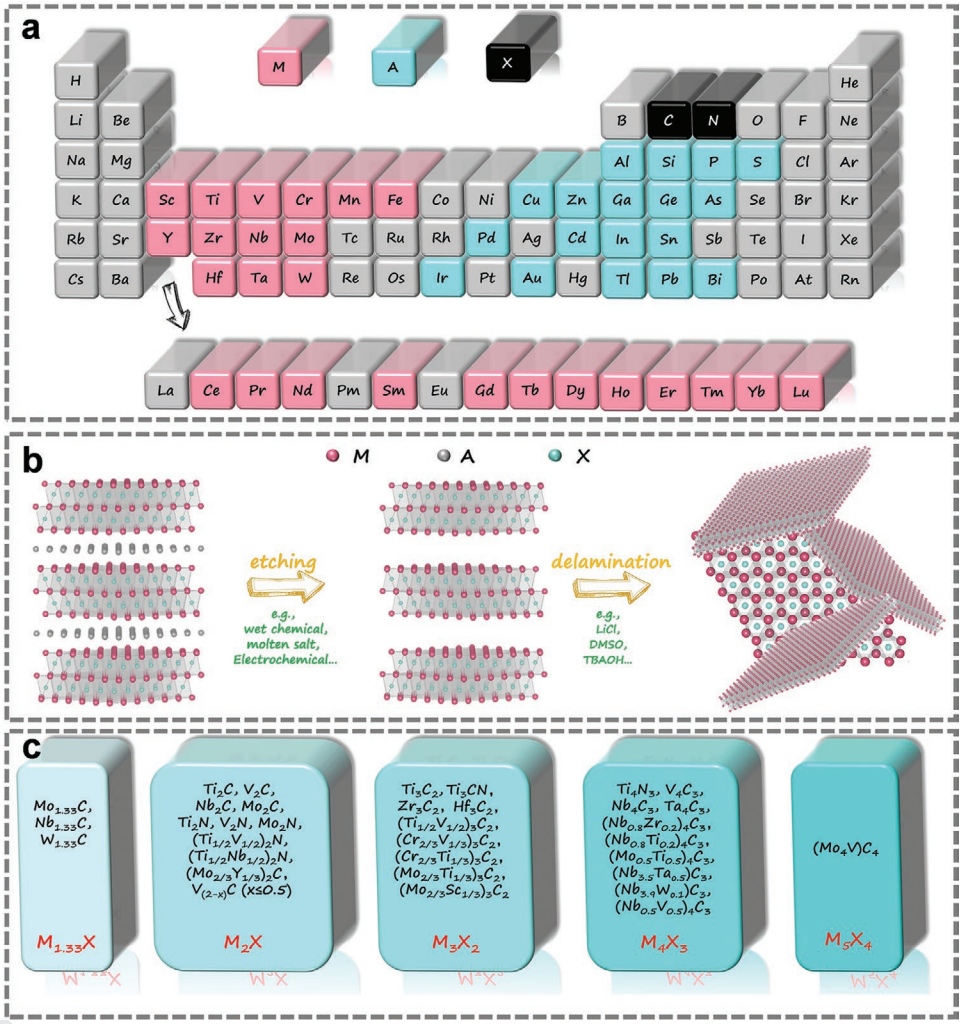

Figure 1. a) Fragment of periodic table showing the "M," "A," and "X" elements of the known MAX phases. b) The typical preparation process of M_3X_2 MXene from the corresponding M_3AX_2 phase. c) Reported MXenes up to date. Three $M_{1.33}X$,[16] 11 M_2X,[13e,17] 9 M_3X_2,[9,17a,18] 10 M_4X_3,[17a,18d,19] and 1 M_5X_4[20] MXenes. Note that the terminal functional groups (T_x) are omitted here.

solutions of "M," "A," and "X," as seen in $(Nb_{0.8},Ti_{0.2})_4AlC_3$,[19i] $(Nb_{0.8},Zr_{0.2})_4AlC_3$,[19i] $Ti_2Al_{(1-x)}Sn_xC$,[21] $Ti_3Al(C_{0.5},N_{0.5})_2$,[22] and $Ti_2Al(C_{0.5},N_{0.5})$.[22] This enables the possibility of preparing MXenes with diverse compositions,[18d,19i,23] leading to different chemical/physical properties that could be used in specific scenarios as needed. Up to now, more than 150 kinds of MAX phases and over 30 kinds of MXenes (Figure 1c) have been experimentally prepared, and the list is still rapidly expanding. It should be mentioned that, during the etching process, the "A" layers are often replaced by some functional groups, which appear as the surface terminations on the MXenes. Therefore, the general formula of MXene is denoted as $M_{n+1}X_nT_x$, where T_x represents the functional groups such as −OH, −O, −F, and −Cl.

As mentioned above, most of the MXenes are made from MAX phases, however, there are some exceptions. For example, Mo_2CT_x is the first MXene that has been derived from Mo_2Ga_2C,[17d,e] which is a non-MAX phase, regardless of its similar crystal structure to MAX phase. Two layers of Ga need to be selectively etched off, which makes it more challenging to obtain the Mo_2CT_x MXene. Later, other MXenes, such as $Zr_3C_2T_x$ and $Hf_3C_2T_x$ were also successfully synthesized from the non-MAX phases, i.e., $Zr_3Al_3C_5$ and $Hf_3[Al(Si)_4]C_6$, respectively.[18b,c] In most MXenes, the n is an integer between 1 and 3, such as in $Ti_3C_2T_x$, V_2CT_x, $Mo_2TiC_2T_x$, and $Nb_4C_3T_x$. However, very recently, Yury's group synthesized a $Mo_4VC_4T_x$ MXene from the Mo_4VAlC_4 MAX phase (i.e., a "514" phase), which means the n has now been extended to 4.[20] In addition, a series of new MXene phases with a general formula of $M_{1.33}CT_x$ (M = transition metal, e.g., Mo, Nb, W) was discovered by Rosen's group.[16,24] These MXenes were synthesized from quaternary $(M^1_{2/3}M^2_{1/3})_2AX$, wherein the M^1 and M^2 are ordered in-plane (*i*-MAX,[16a,f,25] distinguished from those out-of-plane MAX phases, i.e., *o*-MAX). Up to date, more than 10 different *i*-MAX phases were reported.[16a,c,25,26] Different from other MXenes that only selectively remove the "A" layer, the $M_{1.33}CT_x$ MXenes are prepared by selectively etching both "M^2" and "A" layers, which consequently leads to the formation of ordered divacancies in MXenes. For instance, $Mo_{1.33}CT_x$ MXene was obtained by simultaneously removing Sc and Al in $(Mo_{2/3}Sc_{1/3})_2AlC$ using hydrofluoric acid (HF).[16a] Similarly, $V_{2-x}C$ MXene was also prepared from a solid solution of $(V_{2-x}Sc_x)_2AlC$ ($x \leq 0.05$) MAX phase.[17j] The discovery of $M_{1.33}CT_x$ and $V_{2-x}C$ MXenes greatly increases the ability and possibility to regulate and control the physical/chemical properties of the MXene family. The presence of vacancies also makes this kind of material more appealing for energy-related and catalysis applications.

3. Synthesis Strategies

Graphene and some other 2D materials (e.g., black phosphorus) have their corresponding natural 3D bulk precursors. Generally, the weak van der Waal force between adjacent layers makes it possible to directly exfoliate/delaminate the 3D precursors into the ultrathin single/few-layer 2D flakes by simple physical or chemical exfoliation strategies.[8,27] In contrast, MXenes do not have the straightforward precursors in nature, and instead are generally derived from the corresponding MAX phases, where the M−X and M−A bonds possess much stronger interaction force compared to the van der Waals force. Fortunately, thanks to the difference in the formation energy of the M−X (covalent and ionic bonds) and M−A bonds (metallic bonds), the selective removal of "A" layers from the MAX phases is possible.[10] In this way, 3D multilayer MXenes can be synthesized from their parent MAX phases. Through further delamination/exfoliation (will be discussed later), 2D single/few-layer MXene sheets could be readily obtained. A typical etching and delamination process from M_3AX_2 phase to M_3X_2 MXene is schematically displayed in Figure 1b.

3.1. Etching (Removal of "A" Layers)

Since the first discovery of $Ti_3C_2T_x$ MXene in 2011, which was obtained by selectively etching off Al layers from the Ti_3AlC_2 MAX using HF,[9] increasing efforts have been devoting to developing various etching approaches. Among them, the wet chemical etching is the most prevalent and mature method, which can generally be divided into HF-containing (direct use of HF or in situ formed HF) and HF-free routes. The HF-containing routes are dominant and proven to be the most efficient ways, though HF is extremely harmful and requires extra caution during the operation. The HF-free strategies are much safer and thus are highly desired yet quite challenging. In addition, new etching methods such as molten salt and electrochemical routes have also been explored for the preparation of MXenes.

3.1.1. Wet Chemical Routes

Although the M-A bonds are intrinsically weaker than the M−X bonds in MAX phases, they are still much stronger than the van der Waals force between the adjacent layers in the typical bulk 2D materials (e.g., graphite). Prior to the use of HF for etching, researches also tried other methods but did not succeed. For instance, Barsoum et al. heated the MAX phases at high temperature under various ambiances, including in molten salts (cryolite,[28] LiF[124]), molten metals (e.g., molten Al with Ti_3SiC_2),[29] and vacuum[30] to selectively remove the "A" elements. However, detwinning of the "MX" layers occurs at elevated temperatures, which consequently leads to 3D "MX" rock salt structures rather than 2D MXenes. Thereafter, chemical etching has become the dominant route for producing MXenes. It should be noted that weak etchants cannot completely remove the "A" layers, whereas strong etchants (e.g., Cl_2 gas[31]) could possibly destroy the "MX" 2D structure, resulting in the formation of carbons. Besides the chemical activity of etchants, the reaction temperature should also be carefully investigated. For example, the reaction of Ti_2AlC and HF at 55°C would result in Ti_2AlF_9 but not Ti_2AlC MXene.[32] In this regard, a thorough understanding of the etching reactions is required to optimize the etching process and thus to produce high-quality MXenes. Using Ti_3AlC_2 MAX as an example, the etching reactions in HF at room temperature can be reasonably described as follows[9] Q5

$$Ti_3AlC_2 + 3HF \rightarrow AlF_3 + 3/2H_2 + Ti_3C_2 \quad (1)$$

$$Ti_3C_2 + 2H_2O \rightarrow Ti_3C_2(OH)_2 + H_2 \quad (2)$$

$$Ti_3C_2 + 2HF \rightarrow Ti_3C_2F_2 + H_2 \quad (3)$$

Reaction (1) is essential to produce MXenes from MAX phases. Upon etching, the "A" layers are replaced by −OH, −F surface terminations. Reactions (2) and (3) are simplified based on the assumption that the terminations are −OH, or −F. The HF is proven to be an effective MAX etchant and has been used to prepare many MXenes, including V_2CT_x, Ti_2CT_x, Nb_2CT_x, Mo_2CT_x, Ti_2NT_x, $(Ti_{0.5},Nb_{0.5})_2CT_x$, $Mo_{1.33}CT_x$, $Nb_{1.33}CT_x$, $W_{1.33}CT_x$, $V_{(2-x)}CT_x$, $(V_{0.5}Cr_{0.5})_3C_2T_x$, Ti_3CNT_x, $Mo_2TiC_2T_x$, $Mo_2Ti_2C_3T_x$, $Ta_4C_3T_x$, $V_4C_3T_x$, $Nb_4C_3T_x$, $Zr_3C_2T_x$, $Hf_3C_2T_x$, etc.[13e,16a,c,e,f,17a,c–f,j,18b–d,19b–g,23c,33] The concentration, temperature, and reaction time vary from case to case, mainly depending on the particle size of MAXs and the strength of the M−A bonds. Consequently, appropriate etching conditions are essential and critical for obtaining well-defined, high quality, as well as high yield MXenes.

Although HF can effectively etch MAX phases while preserving their 2D nature, it is highly hazardous and toxic. Other approaches have therefore been explored to either reduce or even avoid the use of HF. A straightforward route would be using mixtures of a small amount of HF and other acids. For example, Dirscoll et al. successfully etched Ti_3AlC_2 MAX powder by a mixture of HCl, deionized water, and HF with a volumetric ratio of 6:3:1.[34] This method greatly reduces the amount of HF by 90% compared to the method that use HF solely. In addition, MXene nanosheets with large lateral size and fewer defects can be obtained with high throughput at room temperature (25 °C). In 2014, a milder synthesis route was developed by Ghidiu et al., in where the HF acid was in situ formed by the reaction of LiF and HCl (the molar ratio of Ti_3AlC_2:LiF:HCl is 1:0.5:11.7).[11a] This method not only avoids the direct use of HF, but also results in nanosheets with larger lateral sizes and fewer defects compared to HF-etched MXenes.[35] Later, the LiF/HCl route was optimized by increasing the amount of LiF salt and HCl acid.[36] The optimal method is referred to as Minimally Intensive Layer Delamination (MILD) method. It is worth mentioning that the MILD method doesn't require sonication but instead only manual handshaking, which can produce even larger MXene flakes with fewer defects compared to the original HF/HCl process.[36b] A comparison of the LiF/HCl route followed by sonication and the MILD route is shown in **Figure 2** and **Table 1**. Similarly, $NaBF_4$/HCl was also shown to be able to etch Ti_3AlC_2 MAX in hydrothermal conditions at

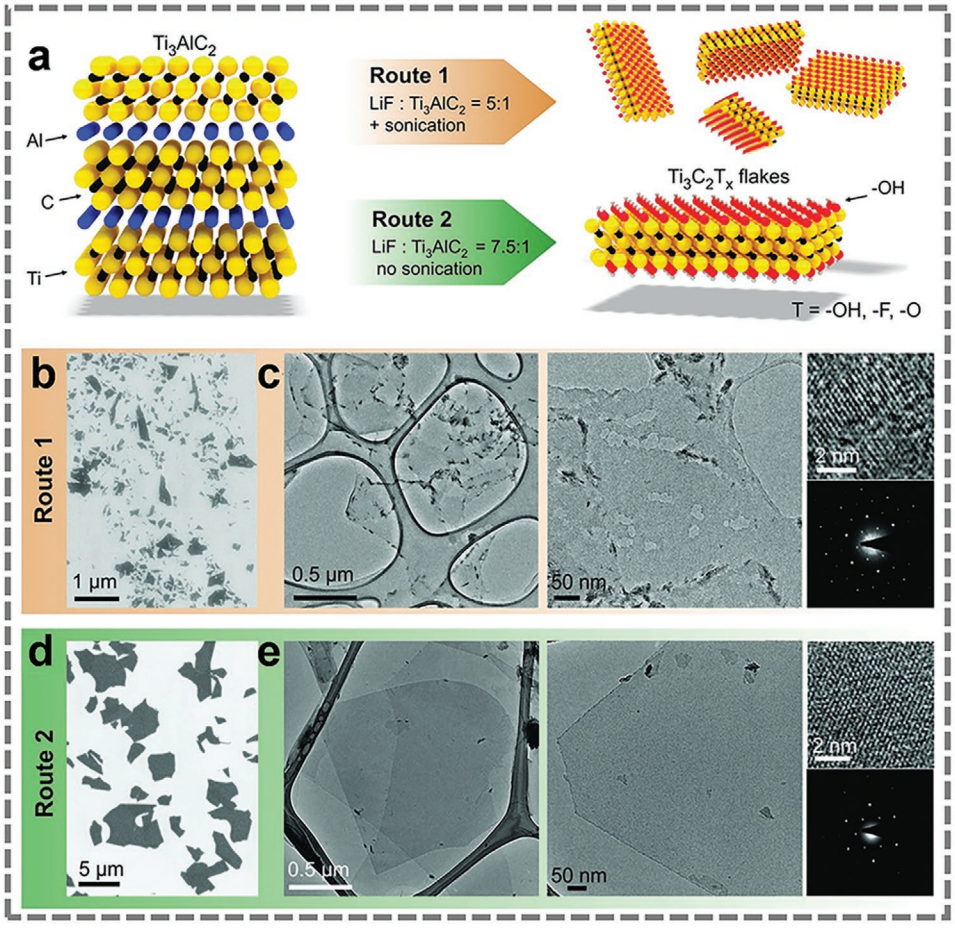

Figure 2. a) Schematic summary of Routes 1 (HF + HCl etching followed by sonication) and 2 (MILD method). b,c) Scanning electron microscope (SEM) and transmission electron microscopy (TEM) characterizations of $Ti_3C_2T_x$ flakes produced through Route 1. d,e) SEM and TEM characterizations of $Ti_3C_2T_x$ flakes synthesized through Route 2. Reproduced with permission.[36b] Copyright 2016, Wiley.

Table 1. Summary of the experimental parameters for Route 1 and Route 2. Reproduced with permission.[36b] Copyright 2016, Wiley.

Method	Mass (Ti_3AlC_2) [g]	Mass (LiF) [g]	Volume (6 M HCl) [mL]	Molar ratio Ti_3AlC_2:LiF:HCl	Etching time [h]	Centrifugation speed/time	Sonication
LiF/HCl (route 1)	1	0.67	10	1.0: 5.0: 11.7	24	3500 rpm/1 h	Yes, 1 h
MILD (route 2)	1	1	20	1.0: 7.5: 23.4	24	3500 rpm/1 h	No

180°C without the use of HF.[37] Importantly, such a fluoride salt (e.g., LiF, NaF, KF, NH_4F, CsF, CaF_2, and tetrabutylammonium fluoride) and acid (e.g., HCl and H_2SO_4) combination protocol can be extended to synthesize other MXenes (e.g., V_2CT_x, Nb_2CT_x, Mo_2CT_x, Ti_2CT_x, Ti_3CNT_x, $Cr_2TiC_2T_x$, $W_{1.33}CT_x$).[17e,37,38] Generally, the kind of fluoride salts does not have a significant impact on the resulting products.[38c] Interestingly, it was found that only the NaF/HCl combination could efficiently etch the V_2AlC MAX while LiF/HCl and KF/HCl could not.[38a,b] Though the reason is unclear, it might be associated with the hydrated cation radius and the solubility of the fluoride salts.[38b]

Apart from the fluoride salt/acid combinations, NH_4HF_2, an environmentally friendly weak acid, was also able to etch Ti_3AlC_2 MAX, though a much longer time was needed compared to HF.[39] The resulting $Ti_3C_2T_x$ MXene exhibits a larger interlayer spacing (the *c* lattice parameter is 24.7 Å) than the HF etched one (19.8 Å). This strongly indicates that the intercalation of the cations (NH^{4+}) and/or NH_3 takes place during the etching process, as confirmed by X-ray photoelectron spectroscopy (XPS) and TEM analysis. Besides, NH_4F was also introduced solely as an etchant to synthesize $Ti_3C_2T_x$ MXene using a hydrothermal method at 150 °C for 24 h.[40] Furthermore, it is noteworthy that inspired by the Bayer process, Li et al. demonstrated that the multilayer $Ti_3C_2T_x$ powder with a high purity of ≈92 wt% could be obtained via an alkali treatment (27.5 M NaOH) at 270 °C.[41] Additionally, very recently, Mei et al. successfully synthesized the fluorine-free mesoporous Mo_2C MXene using a UV light-induced method in the phosphoric acid etching solution.[42] These new HF-free approaches are of great importance and interest as they are much safer and endow the possibility to obtain MXenes with surface terminations other than F, which could have significant impacts on the properties and thus the electrochemical performance of the MXenes.

In order to obtain high quality MXenes, the etching process and condition should be carefully manipulated. Usually, longer etching time and/or higher reaction temperatures are expected for weak etchants (e.g., LiF/HCl, NH_4HF_2, NH_4F). When using the same etchant for etching different MAX phases, the reaction conditions should also be regulated accordingly. Generally, the reaction time, reaction temperature, and the fluorine ion concentration need to be adjusted according to the following parameters: the atomic number of M and the number of *n*. In most cases, the energy of the M—A bonds increases with the increase of the atomic number of M, thus longer time and/or higher temperatures are needed. A larger *n* value also requires a higher fluorine ion concentration and longer reaction time.[18h]

3.1.2. Molten Salt Method

The molten salt method was also applied to etch MAX phases. Urbankowski et al. used the molten salt as the etchant to synthesize $Ti_4N_3T_x$ MXene, which is the first nitride compound of MXene family (**Figure 3**a).[19a] Besides, Huang's group recently reported an element replacement approach to the synthesis of novel Zn-MAX phases, such as Ti_3ZnC_2, Ti_2ZnC, Ti_2ZnN, and V_2ZnC, and further the preparation of Cl-terminated MXenes (such as $Ti_3C_2Cl_2$ and Ti_2CCl_2).[43] As schematically shown in Figure 3b, the strong Lewis acidity of molten $ZnCl_2$ enables the Zn atoms to occupy the A sites in the MAX (i.e., Al in Ti_3AlC_2). When excessive $ZnCl_2$ salt was used, the Zn atoms could be removed, and thus the Cl-terminated MXenes were obtained. More importantly, they extended this strategy to a wide range of A-site elements not only Zn, but also Al, Si, and Ga from various MAX precursors (e.g., Ti_2AlC, Ti_3AlCN).[44] This is achieved by selectively etching A elements through a redox substitution reaction between the Lewis acid molten salts and the A elements. Such an approach further expands the MAX family and is able to synthesize MXenes without —F terminations. Very recently, Talapin et al. developed a general strategy to install and remove surface functional groups by using the molten salts method.[45] Specifically, MXenes with —O, —NH, —S, —Cl, —Se, —Br, and —Te terminations, as well as bare MXenes without any surface groups were successfully synthesized (Figure 3c). These MXenes exhibit distinctive properties. Notably, it was found that Nb_2C MXenes display surface group dependent superconductivity. This work suggests that the surface terminations are controllable and the bare MXenes are achievable via post treatments. More importantly, it also enables more potential applications of MXenes.

3.1.3. Electrochemical Method

Electrochemical etching was also proven to be an efficient way to obtain MXenes without the involvement of fluorine. Specifically, Ti_2CT_x and $Ti_3C_2T_x$ MXenes can be synthesized by electrochemically etching off Al from Ti_2AlC and Ti_3AlC_2 MAX in the electrolyte of 2 M HCl, and 1 M NH_4Cl + 0.2 M tetramethylammonium hydroxide (TMAOH), respectively.[46] Moreover, in the latter case, the resulting $Ti_3C_2T_x$ possesses an average lateral size of 2.4 µm (ranging from 1 to 5 µm with some flakes up to 18.6 µm in diameter), which is comparable to that prepared by MILD method.[46b] It should be noted that the excessive etching would convert the MAX phase to carbon due to the simultaneous dissolution of "A" and "M" elements.[46a]

3.1.4. Other Methods

Bottom-up approaches such as chemical vapor deposition are possible for MXene synthesis. For instance, 2D ultrathin Mo_2C crystals were produced by chemical vapor deposition (CVD).[47] The MXenes obtained from this method possess a large lateral

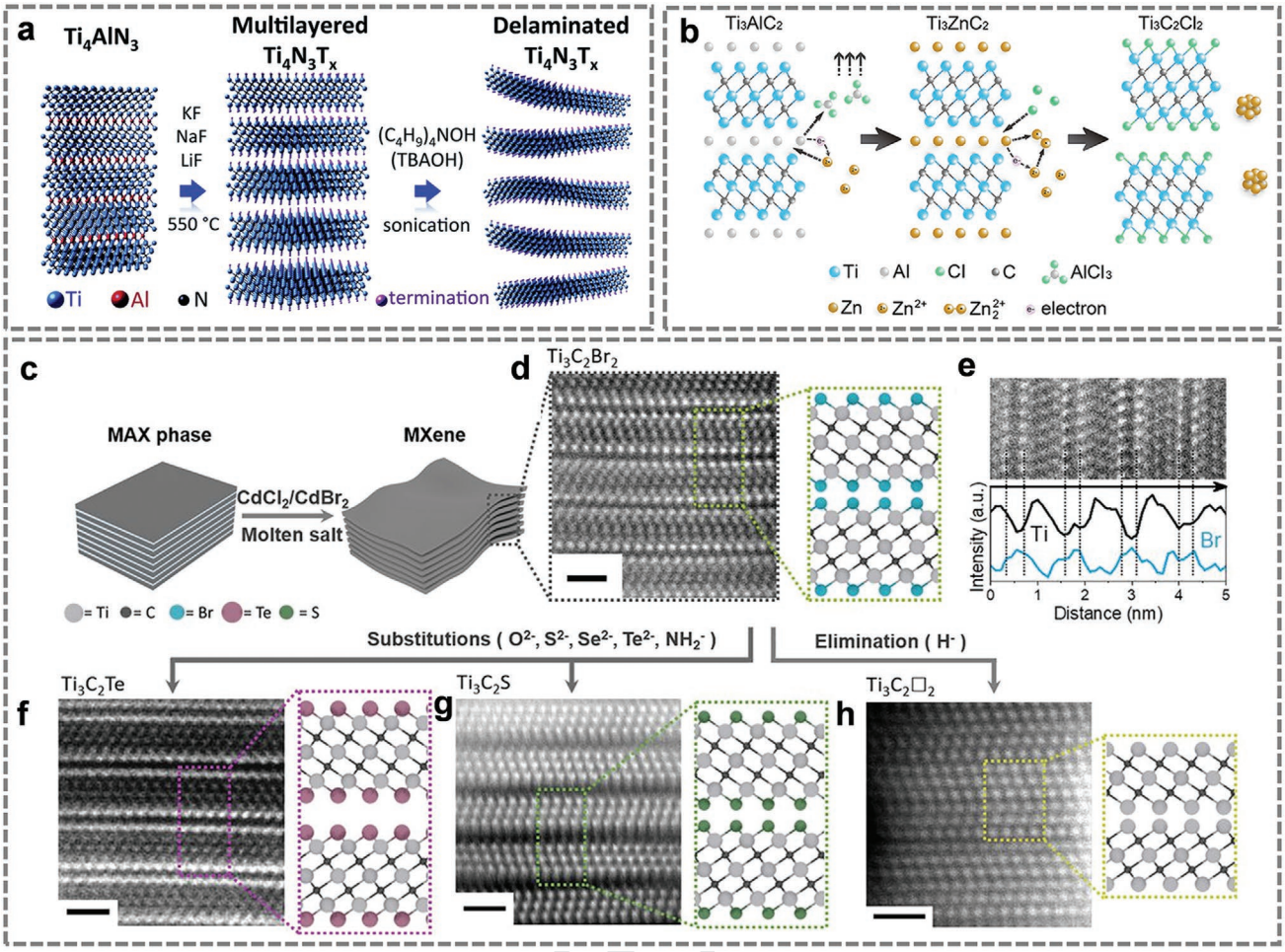

Figure 3. Schematic illustration of the synthesis of a) $Ti_4N_3T_x$ MXene using molten fluoride salts. Reproduced with permission.[19a] Copyright 2016, Royal Society of Chemistry, and b) Schematic illustration of the synthesis of $Ti_2C_2Cl_2$ using molten $ZnCl_2$. Reproduced with permission.[43] Copyright 2019, American Chemical Society. c) Schematics for etching of MAX phases in Lewis acidic molten salts. d–h) Atomic resolution TEM images of MXenes terminated with various surface groups obtained via direct molten salt etching, substitution, and elimination, respectively. Reproduced with permission.[45] Copyright 2020, American Association for the Advancement of Science.

size and few defects, which are beneficial for investigating their intrinsic properties. Besides, a two-step approach that involves the deposition of MAX thin films and the subsequent etching process was also demonstrated to synthesis MXene thin films. For example, magnetron sputtering was used to deposit Ti_3AlC_2 MAX thin films on the surface of TiC. Then, the $Ti_3C_2T_x$ MXene was synthesized by a subsequent HF or NH_4HF_2 etching.[39] Mo_2CT_x MXene thin films were also synthesized by a similar strategy except using the Mo_2Ga_2C MAX as the precursor.[17d]

Table 2 summarizes the different etching approaches to the preparation of MXenes reported in the literature. Overall, the most efficient and prevalent methods are the HF-containing ones, whereas other methods, especially those HF-free protocols are still challenging but under rapid development. Since the surface terminations of MXenes are largely determined by the etchants, different etching methods therefore not only affect the etching result but could also tune the properties of MXenes. HF-free methods provide the possibility to synthesize F terminations-free MXenes, thus new fundamental properties of MXenes with various terminations can be further investigated. It is worth mentioning that, currently, the HF-free methods are mainly applied to synthesize Ti-based MXenes (i.e., Ti_2CT_x and $Ti_3C_2T_x$), their versatility in preparing many other MXenes remains to be explored.

3.2. Delamination

After the etching process, the "A" layers are selectively removed and replaced by various functional groups. The resulting MXene layers are held together by the weak van der Waals and/or hydrogen bonds. This allows the formation of single/few-layer MXene flakes by further delamination/exfoliation treatment. Typically, the delamination process involves the intercalation of inorganic cations, organic or ionic molecules, and the subsequent handshaking and/or ultrasonication. Thanks to their negatively charged surfaces, the as-obtained flakes can be well suspended in water or organic solvents without the need of surfactants. Many cations (e.g., Na^+, K^+, NH^{4+}, Mg^{2+}, Al^{3+}) have been used for the chemical/electrochemical intercalation

Table 2. A summary of different etching approaches used to prepare MXenes.

Type of etching methods		Etchant	Type of MXenes	References
Wet chemical etching	HF containing	HF, HF + HCl	$Ti_3C_2T_x$, V_2CT_x, Ti_2CT_x, Nb_2CT_x, Mo_2CT_x, Ti_2NT_x, $(Ti_{0.5},Nb_{0.5})_2CT_x$, $Mo_{1.33}CT_x$, $Nb_{1.33}CT_x$, $W_{1.33}CT_x$, $V_{(2-x)}CT_x$, $(V_{0.5}Cr_{0.5})_3C_2T_x$, Ti_3CNT_x, $Mo_2TiC_2T_x$, $Mo_2Ti_2C_3T_x$, $Ta_4C_3T_x$, $V_4C_3T_x$, $Nb_4C_3T_x$, $Zr_3C_2T_x$, etc.	[9,13e,16a,c,e,f,17a,c–f,j, 18b–d,19b–g,23c,33,34]
	Fluoride salt/acid	Salt: LiF, NaF, KF, NH_4F, CsF, CaF_2, etc. Acid: HCl, H_2SO_4	$Ti_3C_2T_x$, V_2CT_x, Nb_2CT_x, Mo_2CT_x, Ti_2CT_x, Ti_3CNT_x, $Cr_2TiC_2T_x$, $W_{1.33}CT_x$, etc.	[11a,17e,36–38]
	Fluoride salt	NH_4HF_2, NH_4F	$Ti_3C_2T_x$	[39,40]
	Alkali treatment	NaOH	$Ti_3C_2T_x$	[41]
	UV-induced	UV light + H_3PO_4	Mo_2CT_x	[42]
Molten salt etching	Fluoride salt	KF + LiF + NaF	$Ti_4N_3T_x$	[19a]
	Lewis acid salt	$ZnCl_2$, $CuCl_2$, $NiCl_2$, $FeCl_2$, AgCl, $CoCl_2$, $CdCl_2$, $CdCl_2$, $CdBr_2$, etc.	$Ti_3C_2T_x$, Ti_3CNT_x, Nb_2CT_x, Ta_2CT_x, Ti_2CT_x, etc.	[43–45]
Electrochemical etching		HCl, NH_4Cl + TMAOH	Ti_2CT_x, $Ti_3C_2T_x$	[46]

of MXene hosts.[50] It is worth mentioning that in the case of MILD method, the Li^+ ions simultaneously intercalate into the MXene layers during the etching of Ti_3AlC_2 MAX, which weakens the interactions of layers thus allows the delamination by simple handshaking.[36] However, it turns out that some intercalants such as Li^+ ions and dimethyl sulfoxide (DMSO) are not effective in delaminating other MXenes. In light of this, organic isopropylamine has been chosen as the intercalant of Nb_2CT_x MXene for the following reasons: a) it can form positively charged R-NH^{3+} (ammonium cation) in aqueous solution, which would then intercalate into the Nb_2CT_x layers because of the electrostatic attractions; b) the three-carbon-atom alkyl tail of isopropylamine molecule is small enough to overcome the steric hindrance upon intercalation, on the other hand, is large enough to push the MXene layers apart.[48] The delaminated single/few-layer Nb_2CT_x sheets can be obtained by subsequent sonication (**Figure 4**a). Naguib et al. also found that several organic bases (e.g., tetrabutylammonium hydroxide (TBAOH), choline hydroxide, *n*-butylamine) could be used as intercalants (Figure 4b).[49] This method can be extended to delaminate various MXenes, including $Ti_3C_2T_x$, V_2CT_x, Ti_3CN, Mo_2C, $Mo_{1.33}CT_x$, $Mo_2TiC_2T_x$, and $Mo_2Ti_2C_3T_x$, etc.[12c,16a,17e,23c,49] Among those organic intercalants investigated, compounds with long chains (e.g., TBAOH) are generally more difficult to intercalate into the layers than those with short molecular chains (e.g., TMAOH) because of the steric hindrance, thus are often less efficient in delaminating MXenes.[51]

4. Properties of MXenes

4.1. Structural Properties

As mentioned earlier, the "MX" and "A" layers are alternatively stacked in the MAX phases. The arrangement of the "M" and "X" atoms in MXenes is almost the same as that in their parent MAX phases, where X atoms occupy the center of "XM_6" octahedrons (Figure 1b). Owing to the unique synthetic routes of MXenes, the exposed metal elements of MXenes are always terminated with surface functional groups (e.g., −O, −OH, and −F), which could significantly affect their properties. For example, it is predicted that the −O terminated MXenes exhibit the highest theoretical metal ion (e.g., Li^+, Na^+, K^+, Mg^{2+}, Ca^{2+} Al^{3+}) storage capacity.[52] The S-functionalized Ti_3C_2 MXene not only shows high capacity for sodium-ion storage, but also exhibits excellent affinity to polysulfide species that could be potentially used as the host for Li-SBs.[53] The −OH terminations are vulnerable and can be replaced by metals (Li, Na, K, Mg, Ca, Pb).[52a,b,54] Further, the −OH groups can also be converted into −O by high-temperature annealing, similar to the hydroxide/oxide conversion. Obviously, the terminations play a pivotal role in determining the surface chemistry of MXenes. Tuning the type of terminations, therefore, could serve as a powerful approach to improve the electrochemical performance of MXenes, which fortunately can be achieved

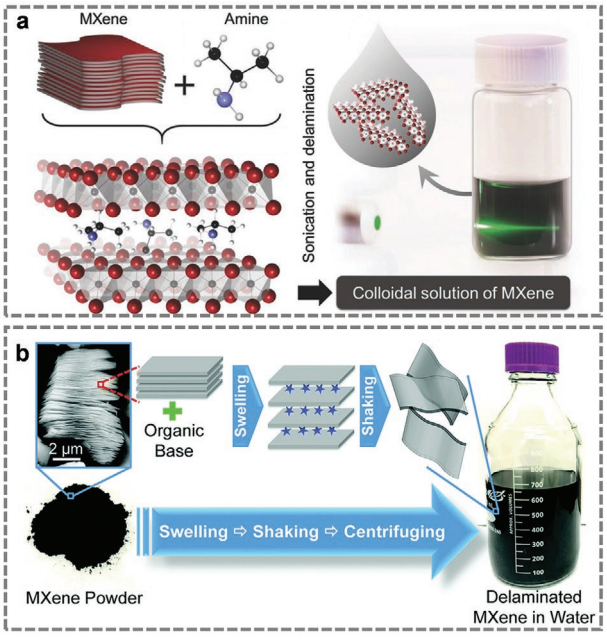

Figure 4. Schematic of a) Nb_2CT_x MXene delamination process. Reproduced with permission.[48] Copyright 2015, Wiley. b) MXene delamination process by reacting MXenes with an organic base. Reproduced with permission.[49] Copyright 2015, Royal Society of Chemistry.

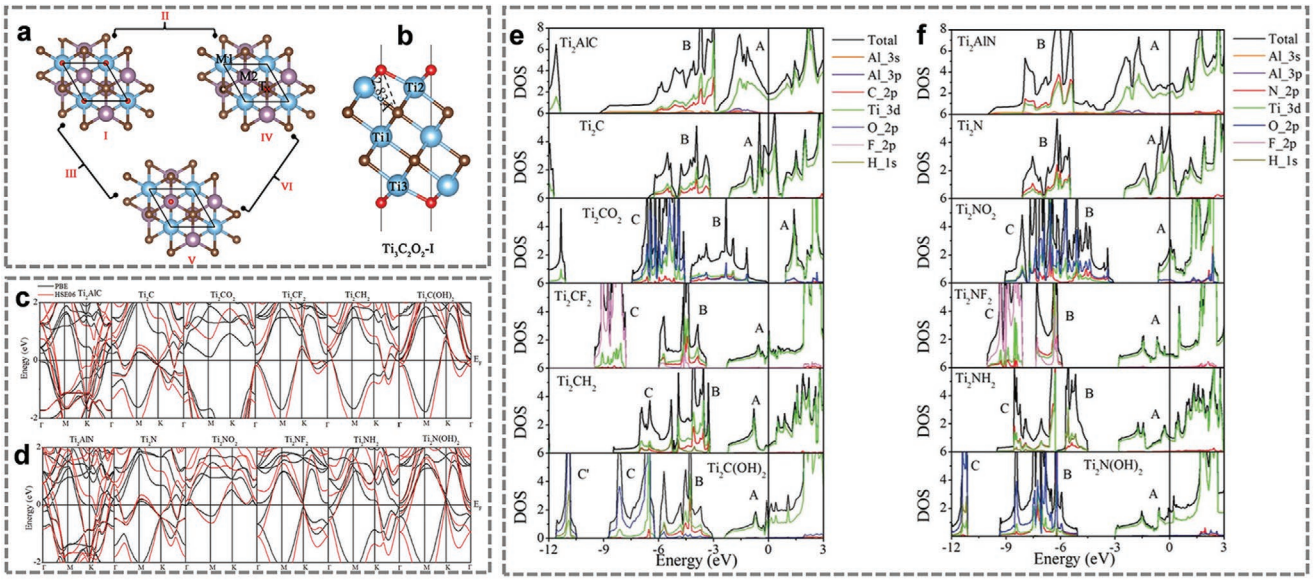

Figure 5. Structural configurations of functionalized MXenes with different arrangements of the surface atoms T_x. a) Top views of configurations I, IV, and V. The mixture configurations II, III, and VI are not shown. Light turquoise (M1): Ti; light purple (M2): Ti; red (T_x): O/OH/F; and brown: carbon. b) Side views of the most energy favorable structure of $Ti_3C_2O_2$. Reproduced with permission.[56] Copyright 2016, Elsevier. Band structures of c) Ti_2CT_2 and d)Ti_2NT_2. PDOS of e) Ti_2CT_2 and f) Ti_2NT_2, and related MXenes and MAX phases. Reproduced with permission.[57a] Copyright 2013, American Physical Society.

by using different etchants. For instance, etching MAX by HF-containing aqueous solutions could result in MXenes with −O, −OH, and −F terminations,[55] while the use of Lewis acid salts ($ZnCl_2$, $CuCl_2$, etc.) etchants leads to the formation of MXenes with −Cl termination.[43,44] In addition, the relative content of the terminations can be regulated by adjusting the concentration of etchants. For example, the HF etching results in more −F terminations in $Ti_3C_2T_x$ than the MILD method, in which a much smaller amount of HF is used.[55b]

Multiple terminations might lead to enhanced performance but also bring about complexity. Understanding their configurations can be helpful for the design and synthesis of MXenes with specific terminations. Li investigated the stability of $Ti_3C_2T_x$ with various terminations (e.g., −O, −OH, and −F) using the density functional theory (DFT) calculations.[56] As shown in **Figure 5**a,b, six possible configurations are taken into consideration: I) the T_x groups are on the hollow site of the M2 (topmost three Ti atoms) and point to the M1 (Ti atom in the second layer) on both sides of $Ti_3C_2T_x$; IV) both two T_x groups are above the hollow site of the M2 and point to the C atom in the first layer; V) T_x groups are located on the M2 on both sides; II) a combination of types I and IV; III) a combination of I and V; VI) a combination of IV and V. The result suggests that configuration I is the most energy favorable structure with lowest total energy regardless of the type of terminations.[56] This is mainly because in type I, the terminations are close to carbon atoms, which can provide electrons.[57] It should be noted that there are also studies that predicted type IV is the most stable geometry.[58] Therefore, further studies, especially through experimental characterizations, are required. Fortunately, the surface chemistry of MXenes can now be investigated at the atomic level using advanced techniques such as nuclear magnetic resonance (NMR) and aberration-corrected STEM-electron energy loss spectroscopy (EELS).[9,50b,55a,59] For example, it has been experimentally demonstrated that the surface of $Ti_3C_2T_x$ MXene is covered by both the functional groups and TiO_x adatom complexes. The O-based surface groups are found to draw valence charge from the MXene. It is also observed that the atoms and terminations at the surfaces are mobile, leading to the migration and ripening of the TiO_x adatom complexes and terminations.[59b]

In addition to the surface functional group, the interlayer spacing of MXenes is also tunable, depending on the composition of MXenes and the size of intercalants. A comparison of the *c*-lattice parameter for various MXenes is shown in **Table 3**. Generally, the *c*-lattice parameter increases with increasing *n* value ($M_{n+1}X_nT_x$). For example, $Ti_3C_2T_x$ (20.51 Å) and $Nb_4C_3T_x$ (30.47 Å) exhibit larger *c*-lattice parameters than that of Ti_2CT_x (15.04 Å) and Nb_2CT_x (22.34 Å). The particle size of the parent MAXs also plays an important role in determining the *c* value of MXenes. For example, V_2CT_x MXene with a *c*-lattice parameter of 23.96 Å can be obtained by using the attrition milled V_2AlC MAX, while this value is only 19.73 Å using the unmilled one. The interlayer spacing can also be adjusted by using different intercalant species. Mashtalir et al. demonstrated that the intercalation of hydrazine and further its cointercalation with *N*,*N*-dimethylformamide increased the *c*-lattice parameter of $Ti_3C_2T_x$ from 19.5 to 25.48 and further to 26.8 Å.[50b] It was also reported the cation (e.g., Li^+, Na^+, K^+, Rb^+, Mg^{2+}, Ca^{2+})-intercalated $Ti_3C_2T_x$ MXenes showed reversible humidity-dependent expansion and the interlayer spacing varied from 12.5 to 15.5 Å.[61] Luo et al. systematically investigated the influence of cationic surfactants with various lengths of hydrophobic alkyl chains on the interlayer spacing of $Ti_3C_2T_x$ MXene. Remarkably, the cetyltrimethylammonium bromide (CTAB)-intercalated $Ti_3C_2T_x$ MXene with pillared structure exhibits an expanded interlayer

Table 3. A comparison of *c*-lattice parameter for MAX phases and corresponding MXenes. Reproduced with permission.[10b] Copyright 2014, Wiley.

MAX structure	MAX	MXene	RT etching conditions		*c* lattice parameter [Å]		Ref.
			HF conc. [%]	Time [h]	MAX	MXene	
211	Ti_2AlC	Ti_2CT_x	10	10	13.6	15.04	[17a]
	V_2AlC	V_2CT_x	50	8	13.13	23.96	[17c]
				90		19.73	
	Nb_2AlC	Nb_2CT_x	50	90	13.88	22.34	[17c]
	$(Ti_{0.5},Nb_{0.5})_2AlC$	$(Ti_{0.5},Nb_{0.5})_2CT_x$	50	28	13.79	14.88	[17a]
312	Ti_3AlC_2	$Ti_3C_2T_x$	50	2	18.42	20.51	[9,17a]
			40	20	18.62	20.89	[60]
	$(V_{0.5},Cr_{0.5})_3AlC_2$	$(V_{0.5},Cr_{0.5})_3C_2T_x$	50	69	17.73	24.26	[17a]
	Ti_3AlCN	Ti_3CNT_x	30	18	18.41	22.28	[17a]
413	Ta_4AlC_3	$Ta_4C_3T_x$	50	72	24.08	30.34	[17a]
	Nb_4AlC_3	$Nb_4C_3T_x$	50	90	24.19	30.47	[17c]

spacing of 2.708 nm, which is 177% larger than that of the pristine MXene (0.977 nm).[62] Besides, TBA^+, TMA^+, and a series of alkylammonium cations have also been intercalated into the MXenes.[17e,23c,63] The easily tunable interlayer spacing of MXenes makes them promising candidates for energy storage applications, especially as intercalation-type electrodes.

4.2. Electronic Properties

Electronic properties have a critical impact on the electrochemical performance of MXene electrodes for energy-related applications. Both theoretical studies and experimental characterizations have been employed to study the electronic properties of MXenes.[57a,64] The band structure and density of states (DOS) of MXenes have been investigated by DFT calculation (Figure 5c–f). The Fermi energy of the bare MXene shifts down compared to the MAX precursor, and further shifts down after adding the surface terminations. The DOS at Fermi level ($N(E_f)$) is dominated by Ti 3d orbitals of the MAX phases. The valence states below the Fermi level can be divided into two sub-bands, i.e., band A (formed by hybridized Ti 3d–C 2p and Ti 3d–Al 3s orbitals) and band B (Ti 3d–Al 3p orbitals). After the removal of Al atoms, both bands A and B are narrowed. The $N(E_f)$ increases from 1.88 to 3.15 eV and from 2.77 to 4.84 eV for the conversions of Ti_2AlC to Ti_2C and Ti_2AlN to Ti_2N, respectively, because of the breaking of Ti–Al bonds. With the addition of functional groups, the Fermi level shifts down to lower energy and the $N(E_f)$ decreases due to the interactions between Ti and terminations.[57a] Shein et al. reported that the $N(E_f)$ of the $Ti_{n+1}C_n$ and $Ti_{n+1}N_n$ MXenes is 2.5–4.5 times higher than that of the corresponding MAX precursors.[65] Though most bare MXenes are predicted to be metallic,[57c,66] in reality, the electronic properties are greatly influenced by the surface terminations and the M elements. For instance, the small bandgaps of 0.05 and 0.1 eV were revealed for $Ti_3C_2(OH)_2$ and $Ti_3C_2F_2$, respectively.[9] In fact, because of the hybridization of p orbitals in F and O, and d orbitals in M, the metallic M_2C and M_2N MXenes could become semiconductors after surface functionalization. $Sc_2C(OH)_2$ exhibits a direct semiconducting characteristic, while Sc_2CF_2 has an indirect bandgap of 1.03 eV.[57c] It was also found that not only the type but also the arrangement/orientation of terminations could alter the electronic properties of MXenes.[58,67] Additionally, transition metal M also plays a vital role in regulating the electronic properties. Anasori et al.[68] demonstrated the transition from metallic to semiconducting behavior by replacing Ti with Mo atoms in the outer layers of Ti_3C_2 and Ti_4C_3 MXenes. Moreover, Zr_2CO_2 has been predicted to have a bandgap of 0.88 eV while the bandgap for Hf_2CO_2 is 1 eV.[57c] Interestingly, the oxygen functionalized M_2C (M = W, Mo, and Cr) MXenes and some ordered double transition metals MXenes, $M'_2M''C_2$ (M′ = Mo, W; M″ = Ti, Zr, Hf) are predicted to be topological insulators.[57b,69]

Besides the simulations, efforts have also been devoted to directly measure the conductivity of MXenes. Hu et al. demonstrated the anisotropic electronic conduction of individual $Ti_3C_2T_x$ particulates using *I–V* measurement.[70] Lipatov et al. reported that individual $Ti_3C_2T_x$ flakes exhibit a high conductivity of 4600 ± 1100 S cm^{-1}, and a field-effect electron mobility of 2.6 ± 0.7 cm^2 V^{-1} s^{-1}.[36b] Zhang et al. demonstrated that $Ti_3C_2T_x$ MXene films (≈88 nm) have a DC conductivity of ≈9880 S cm^{-1}.[12b] It was also reported that $Ti_3C_2T_x$ films exhibit metallic characteristic down to 100 K and below.[39] Interestingly, the conductivity of $Ti_3C_2T_x$ transparent thin films obtained by spin coating was measured to be as high as 6500 S cm^{-1}, superior to other solution-processed 2D materials. The high conductivity can be ascribed to the metal-like free-electron density and the high degree of coplanar alignment of individual MXene flakes.[71] Apart from $Ti_3C_2T_x$,[72] the electronic properties of many other MXenes, including V_2CT_x,[12c] $Mo_{1.33}CT_x$,[16a] Mo_2CT_x,[17e] and Ti_2CT_x,[73] were also experimentally investigated. In summary, both the computational and experimental studies imply that most of the MXenes have outstanding electronic conductivities that are favorable for fast electron transport and charge transfer for electrochemical applications.

5. Applications in Electrochemical Energy Storage

Since the discovery of $Ti_3C_2T_x$, research on MXene electrodes for emerging EES systems (batteries and supercapacitors) has flourished. Most studies focus on $Ti_3C_2T_x$ MXene for LIBs,

despite the big family of MXenes and various EES systems. Nevertheless, the investigations on MXenes for other EES technologies beyond LIBs are rapidly developing and great progress has been achieved very recently. In the following sections, we will summarize the recent developments of MXene-based materials for EES beyond LIBs, including Li-SBs, SIBs, PIBs, and multivalent ion (e.g., Mg^{2+}, Zn^{2+}, Al^{3+}) batteries.

5.1. Lithium–Sulfur Batteries

In recent years, Li-SBs have attracted intensive attention by virtue of their very high capacity/energy density and low cost, yet still face significant obstacles, including the lithium polysulfide (LiPS) shuttle effect, the intrinsic insulating characteristic of sulfur and the growth of Li dendrites.[74] MXene materials with high electronic conductivity, large surface area, and rich and tunable functional groups hold promising potentials for Li-SBs, where MXenes can be used for the sulfur host, separator modification/interlayer, and anode protection. The following section discusses the recent progress in theoretical computations, experimental findings and reaction mechanisms in Li-SBs.[74d,75]

5.1.1. Theoretical Investigations

The pioneering work of Ti_2CT_x MXene materials for Li-SBs was conducted by Nazar's group in 2015.[76] Later in 2017, a more comprehensive study on Ti-based MXenes (Ti_2C, Ti_3C_2, and Ti_3CN) for Li-SBs was carried out with the support of theoretical calculations.[77] Based on the XPS and DFT results, a unique double mechanism of entrapping polysulfides was proposed. It has been demonstrated that the −OH terminations on the surface of Ti-based MXenes would gradually react with the polysulfides upon the formation of thiosulfate intermediates, followed by the Ti−S bond formation through a Lewis acid-base interaction.[76,77] Rao et al. explored the behaviors of LiPSs on bare Ti-based MXenes (Ti_nX_{n-1}, where X = C, N; n = 2, 3, 4) and terminated Ti_2C.[78] They found that both the long-chain and short-chain sulfides can be entrapped by bare MXenes. However, selectivity can be achieved by modifying the surface group of MXenes. The −OH terminations are effective in entrapping long-chain sulfides such as Li_2S_4, Li_2S_6, and Li_2S_8, while the short-chain sulfides can be entrapped by the −O terminations. The Coulombic interactions between LiPSs and bare MXene or MXene terminations result in the formation of Ti−S, H−S, and Li−O bonds, contributing to the binding between them.[78]

The anchoring effects of various MXenes functionalized by different terminal groups has also been intensively investigated. Zhao et al. demonstrated that Ti_2CF_2 and $Ti_3C_2F_2$ MXenes have low binding energies with LiPSs, resulting in their inability to suppress the shuttle effect, while $Ti_2C(OH)_2$ and $Ti_3C_2(OH)_2$ MXenes show poor stability toward Li-SBs. In contrast, Ti_2CO_2 and $Ti_3C_2O_2$ MXenes could effectively immobilize the soluble LiPS species and maintain the LiPSs intact thanks to the moderate attractions between the O groups in MXene (Ti_2CO_2 or $Ti_3C_2O_2$) monolayers and the Li ions in LiPS species. Interestingly, Chung's group reported that both Ti_2CF_2 and Ti_2CO_2 can suppress the shuttle effect, however, through different mechanisms.[79] The former is owing to the fact that the binding energies of LiPS intermediates with the MXene are always larger than those with electrolytes. Whereas the latter is due to the conversion of soluble long-chain LiPSs to insoluble elemental sulfur on the Ti_2CO_2 MXene surfaces.[79] Despite some discrepancies in these theoretical simulations, both studies clearly indicate that the oxygen functionalized Ti-based MXenes exhibit good anchoring effect toward LiPSs.

To better simulate the actual situation, Chung's group further studied the anchoring behavior of both F- and O-terminated Ti_2C MXene in a nonuniform surface form.[80] Specifically, the models with the vacancy, substitutional and S-trapped sites of F- and O-terminated Ti_2C MXenes were designed. In addition, the adsorption energy of LiPS, the reactivity of the matrix with Li atoms, and the reduction states of S atoms were taken into consideration (**Figure 6**a–f). The result implies that on the F-substituted sites of the O-functionalized surface, the suppression mechanism changes from neutralization of the S atoms to anchoring of the LiPSs. On the other hand, at the vacancy sites, the strong interaction between the exposed Ti atoms and the S atoms in LiPSs leads to the trapping of the S atoms. As a result, the amount of active materials decreases (Figure 6g). It is therefore important to minimize the formation of vacancies in Ti_2C MXene in order to achieve the optimal anchoring effect.[80] Liu et al. also investigated the anchoring effect of S-terminated Ti_2C MXene for Li-SBs. They found that compared to Ti_2CO_2 and Ti_2CF_2 MXenes, Ti_2CS_2 has the highest binding energy with LiPSs, thus the best performance in suppressing the shuttling effect.[53a] Moreover, the electrocatalytic mechanism of the $Ti_3C_2T_2$ MXenes was proposed by Wang et al.[81] It was found that the energy barrier of Li_2S decomposition can be significantly reduced from 3.390 to 0.4 eV when $Ti_3C_2S_2$ or $Ti_3C_2O_2$ was used as the host material, resulting in a fast Li^+ diffusion.

Apart from Ti-based carbide MXenes, research on other MXenes was also carried out.[85,86] For instance, Li et al. thoroughly studied the interactions between LiPSs and Ti_2CO_2 as well as six other MXenes ($M_3C_2O_2$, where M = Cr, V, Ti, Nb, Hf, and Zr) host materials using DFT computations.[85] Benefiting from the strong Li−O interactions between the −O termination on MXene surface and the Li in LiPSs, all MXenes exhibit anchoring ability toward LiPSs. Among them, the $Cr_3C_2O_2$ shows the largest binding energy toward both the Li_2S_8 and Li_2S_4 (Figure 6h), which is possibly associated with its small lattice constant. As shown in Figure 6i, the binding energy decreases with the increasing lattice constant of the $M_3C_2O_2$ MXene. It is noted that the metallic character of all six $M_3C_2O_2$ MXenes is well preserved during the whole adsorption process as verified by the DOS computations.[85] Additionally, sulfur-terminated vanadium carbide (V_2CS_2) MXene and $Li_2S@V_2CT_x$ hybrid composite were also predicted to be promising anchoring materials for Li-SBs via the first-principles calculations.[87]

As discussed above, the theoretical predictions strongly indicate that various MXenes exhibit excellent anchoring effects to immobilize the LiPSs. It should be noted that these simulations are mostly based on ideal models, whereas in reality, the situation is much more complicated. Nonetheless, these investigations shed light on the modeling of MXenes and provide guidance for the design of MXene matrixes for high-performance Li-SBs.

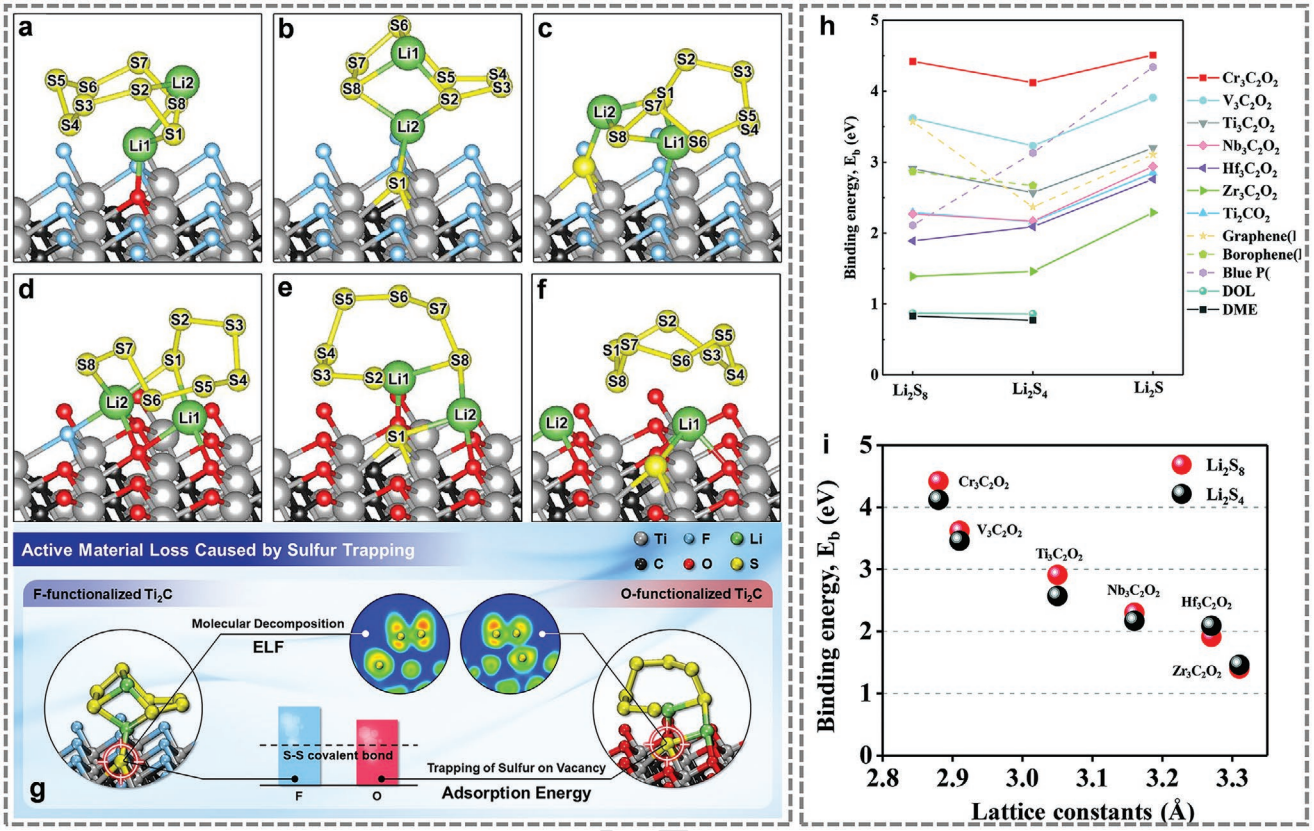

Figure 6. Optimized configurations of Li_2S_8 anchored on the a) substitutional, b) vacancy, and c) S-trapped sites of F-functionalized Ti_2C, and on the d) substitutional, e) vacancy, and f) S-trapped sites of O-functionalized Ti_2C. g) Schematic illustration of the anchoring behavior of both F- and O-terminated Ti_2C MXene in a nonuniform surface form. Reproduced with permission.[80] Copyright 2017, Elsevier. h) Plots of the calculated binding energies between LiPSs and various MXenes, graphene,[82] borophene,[83] blue P,[84] and 1,3-dioxolane (DOL), 1,2-dimethoxyethane (DME) electrolytes. i) The binding energies between the MXenes and Li_2S_8 and Li_2S_4 species, as a function of the lattice constants of MXenes. Reproduced with permission.[85] Copyright 2019, Royal Society of Chemistry.

Please replace Figure 6 with uploaded one

5.1.2. MXene Sulfur Host

Since the pioneering work by Nazar's group, the use of MXenes for Li-SBs has quickly attracted intensive attention. Zhao et al. first reported the use of accordion-like structural $Ti_3C_2T_x$ MXene as a matrix to host sulfur. The resulting cathode with 57.6 wt% sulfur loading displayed a high initial discharge capacity of 1291 mAh g^{-1}, while 970 mAh g^{-1} could be maintained after 100 cycles at a current density of 200 mA g^{-1}.[88] Note that this performance was achieved on multilayer MXenes that with limited surface area, mechanical flexibility, and utilization of Lewis acidic properties. The performance is expected to be enhanced by further delamination of MXenes, while the restacking of thin MXene flakes would become an issue. In this regard, fabricating porous 3D architectures is one of the most effective solutions. For example, Wang's group rationally synthesized a crumpled N-doped $Ti_3C_2T_x$ (N-$Ti_3C_2T_x$) by annealing the mixture of negatively charged $Ti_3C_2T_x$ and positively charged melamine (**Figure 7**a–e).[89] Benefiting from the high surface area, porous structure, remarkable physical confinement effect and chemisorption property, the as-designed N-$Ti_3C_2T_x$/S electrodes showed a reversible capacity of 1144 mAh g^{-1} at 0.2 C rate (1 C rate = 1673 mA g^{-1}) and good cycling stability.[89] Very recently, Song et al. prepared porous N-doped MXene (P-NTC) via a similar protocol for Li-SBs (Figure 7f).[90] As illustrated in Figure 7g, the porous structure of the P-NTC can provide rich active sites for the adsorption and conversion of LiPS species. The nitrogen doping not only enhances the interfacial interaction between the P-NTC and Li atoms and Li_2S cluster, thus facilitating the Li_2S nucleation kinetics, but also decreases the dissociation barrier of Li_2S on P-NTC, resulting in accelerated Li_2S decomposition. Moreover, the low diffusion barrier of Li atoms on the surface of P-NTC promotes the sulfur redox kinetics. Based on these findings, a multifunctional electrocatalytic mechanism was proposed instead of conventional chemical adsorption behavior. The as-fabricated P-NTC not only immobilizes the LiPSs, but also acts as a multifunctional catalyst to enhance both the decomposition and precipitation of Li_2S.[90] In addition, Zhang et al. developed robust, flexible, highly conductive free-standing S@$Ti_3C_2T_x$ ink and $Ti_3C_2T_x$/S paper as sulfur hosts by two different strategies.[91] Remarkably, the $Ti_3C_2T_x$/S electrode exhibited outstanding stability with a low capacity decay rate of 0.014% per cycle for 1500 cycles, which is due to the conversion of initially formed thiosulfate species to sulfates during cycling.[91b] Wang's group presented a $Ti_3C_2T_x$ nanodots-interspersed $Ti_3C_2T_x$ nanosheets structure that could significantly reduce the interfacial resistance and accelerate the redox kinetics of the reactions for Li-SBs.[92]

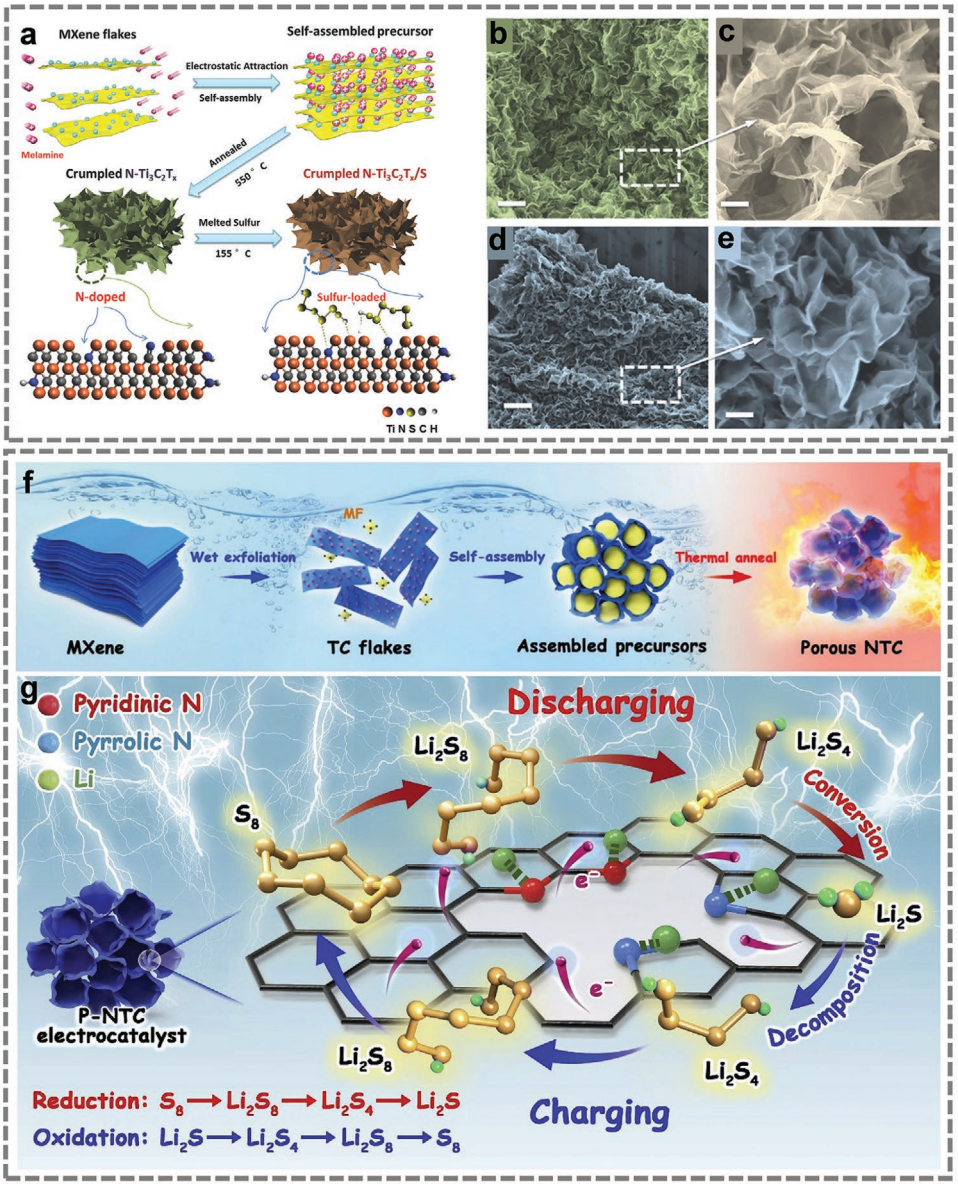

Figure 7. a) Schematic of the synthesis of N-$Ti_3C_2T_x$/S electrode. SEM images of the b,c) N-$Ti_3C_2T_x$ and d,e) N-$Ti_3C_2T_x$/S samples, respectively. Reproduced with permission.[89] Copyright 2018, Wiley. f) Schematic illustration of the synthesis of P-NTC. g) Schematic illustration of the mechanism of the P-NTC electrocatalyst in Li-SBs. Reproduced with permission. Copyright 2020,[90] Elsevier.

Meanwhile, they also synthesized a 3D flower-like porous $Ti_3C_2T_x$ to accommodate sulfur. The electrode exhibited a high areal capacity of 10.04 mAh cm^{-2} and ultrahigh volumetric capacity of 2009 mAh cm^{-3}.[93]

5.1.3. MXene Composite-Based Sulfur Hosts

MXene–Carbon Composites: Besides building up 3D MXene structures, combining MXene with other materials is also an effective strategy to improve the overall performance toward Li-SBs. Among various materials, carbons (graphene, carbon nanotube (CNT), porous carbon, etc.) with high conductivity and strong mechanical strength are popular candidates.[94] Their merits of lightweight, high surface area and large pore volume could adequately accommodate solid charge/discharge products of S/Li_2S, and inhibit the restacking of MXene flakes simultaneously. On the other hand, the weak adsorption and conversion abilities of carbons toward LiPS species can be compensated by MXenes. For example, CNTs have been widely used for Li-SBs, however, they suffer from weak interactions with sulfur species.[95] Therefore, MXenes with polar property and rich surface functional groups are ideal candidates to hybridize with CNTs to tackle this issue. In return, the introduction of CNTs can enlarge the specific surface area, buffer the volumetric variation and maintain the structural integrity of the composites.[94e,f] For instance, the Mo_2C-CNT/S cathodes deliver a high reversible capacity of 1235 mAh g^{-1}, with 925 mAh g^{-1} maintained

after 250 cycles. In contrast, the capacity falls from 1034 to 639 mAh g^{-1} after 250 cycles for the Mo_2C/S cathodes. Incorporating MXene into reduced graphene oxide (rGO) aerogels is also an efficient way (note that the preparation of MXene aerogels without additives is challenging). Wang et al. fabricated free-standing 3D porous $Ti_3C_2T_x$ MXene/rGO hybrid aerogels to accommodate the liquid Li_2S_6 electrolyte.[94b] The MXene can provide rich functional groups to anchor the LiPSs, while the rGO aerogels can inhibit the restacking of MXene. Consequently, the optimized composite electrode (30 wt% MXene) can deliver a high reversible capacity of 1270 mAh g^{-1} at 0.1 C, compared to only 753 mAh g^{-1} of bare rGO. Metal–organic framework (MOF) derived mesoporous carbon has also been used as a space vector to prevent the restacking of MXene nanosheets (**Figure 8**a–e).[94c] Thanks to the MOF-derived carbon, the 2D MXene nanosheets can be homogeneously distributed without aggregation. The as-prepared $Ti_3C_2T_x$@Meso-C host material can achieve a significantly improved cycling performance with a capacity of 704.6 mAh g^{-1} retained after 300 cycles at 0.5 C (against 470.2 mAh g^{-1} for the Meso-C/S cathode).[94c]

MXene–Metal Oxides Composites: Metal oxides were among the first investigated anchoring materials for stabilizing soluble LiPSs. They can efficiently inhibit the leakage of active materials into the electrolytes, thus preventing the commonly observed fast irreversible capacity fading and ultimately battery failure in Li-SBs.[97] The high surface polarity in metal oxides induced by the difference in electronegativity between oxygen and transition metal atoms endows them strong interactions with polar LiPSs.[96] However, most metal oxides are semiconductors with low electronic conductivity. Hybridizing metal oxides with highly conductive MXenes is therefore a reasonable approach to enhance the conductivity and thus the overall performance.[96,98] On the other hand, the metal oxides can improve surface adsorption ability of MXenes toward LiPSs. For instance, TiO_2 is a polar metal oxide with strong polysulfide adsorption ability, but suffers from low electronic conductivity (10^{-12} to 10^{-7} S cm^{-1}) and poor Li^+ ion diffusion coefficient (10^{-12} to 10^{-9} cm^2 s^{-1}). To solve this issue, Gao et al. developed a simple CTAB-assisted approach for the growth of TiO_2 quantum dots (QDs) on the highly conductive $Ti_3C_2T_x$ MXene flakes (Figure 8f).[96] The DFT simulation (Figure 8g–j) suggests weak chemical interactions of −2.62 and −0.29 eV between Li_2S_4 and the $Ti_3C_2(OH)_x$ and $Ti_3C_2F_x$, respectively. However, the introduction of TiO_2 QDs on MXene surface

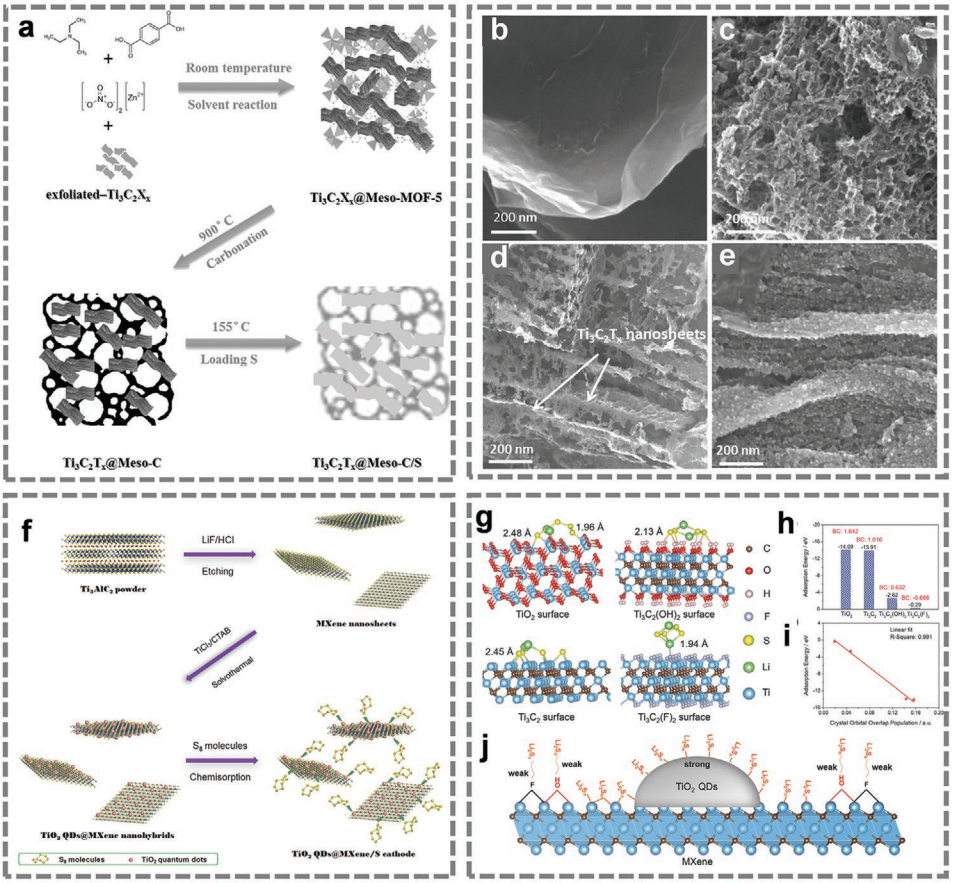

Figure 8. a) Synthesis strategy of the $Ti_3C_2T_x$@Meso-C/S electrode. SEM images of b) delaminated $Ti_3C_2T_x$, c) Meso-C, d) $Ti_3C_2T_x$@Meso-C, and e) $Ti_3C_2T_x$@Meso-C/S composites. Reproduced with permission.[94c] Copyright 2016, Wiley. f) Synthesis route of the TiO_2 QDs@MXene/S cathode. g) Optimized structures of Li_2S_4 adsorbed on TiO_2, Ti_3C_2, $Ti_3C_2(OH)_2$, and $Ti_3C_2(F)_2$ surfaces. h) Adsorption energies of Li_2S_4 on different surfaces. i) Linear fit between adsorption energy and the crystal orbital overlap populations. j) Proposed strategy for suppressing the shuttling effect of LiPSs by the growth of TiO_2 QDs on MXene nanosheets. Reproduced with permission.[96] Copyright 2018, Wiley.

Please replace Figure 8 with uploaded one

could significantly enhance the polysulfides fixation ability of MXene with an adsorption energy of –14.09 eV. As a result, the TiO_2 QDs@MXene/S cathode shows superior performance to that of MXene/S cathode in terms of long-term stability and rate performance.[96] What's more, by taking advantage of Ti-based MXene (e.g., $Ti_3C_2T_x$) and their intrinsic susceptibility to oxidation, TiO_2/MXene composites can be easily achieved by in-situ partial oxidation of the MXene precursors and further serve as sulfur host.[98a,c]

MXene–Polymer Composites: Although 2D materials exhibit many advantages as sulfur hosts, a serious drawback is that the openly accessible structure could eventually lead to the leakage of the active materials into the electrolytes. Although the dissolution of LiPS species can be mitigated by the strong chemisorption of MXenes to some degree, the leakage of active materials is inevitable when the interaction between the host and outermost LiPS is insufficiently strong. In fact, the LiPS dissolution into the electrolytes is intensified with their accumulation on the outer surface. To solve this problem, organic polydopamine (PDA) has been proposed as an overcoat of MXene/S composites.[99] The PDA coating layer could trap sulfur species in the MXene nanosheets physically and chemically. In the meantime, it can protect sulfur from direct contact with the liquid electrolyte. The shuttle effect of LiPSs can be mitigated by the strong Ti—S bonds originating from the Lewis acid-base mechanism of MXene and the polar-polar interaction/chemical adsorption between the PDA and LiPSs.[99] It is worth mentioning that the PDA coating process in aqueous solution requires violent stirring overnight, which may cause active sulfur loss and therefore it is hard to precisely control the sulfur loading. Yu et al. developed a similar PDA coating process that shortened the reaction time to 6 h, which effectively improves the performance.[100] Furthermore, a self-assembly strategy was developed to fabricate $Ti_3C_2T_x$ MXene/polyethyleneimine functionalized CNT (T@CP) composite for both sulfur host and antifouling separator. The as-prepared T@CP product exhibits superb mechanical strength, high conductivity, dual polarity and well-organized porosity, which enable excellent electrochemical performance toward the Li-SBs.[101]

5.1.4. MXenes for Separator Modification and Lithium Anode Protection

As summarized above, structural and compositional engineering of the sulfur host can effectively mitigate the shuttle effect of LiPS species. Apart from that, the modification of other components of Li-SBs allows further improvement of the electrochemical performance and operational lifespan. For example, coating separator with a polymer or carbon layer, or adding an interlayer between the cathode and separator, can provide a protective barrier to hinder the shuttling of LiPSs.[102] Besides, the formation of lithium dendrites and the pulverization of the lithium metal anode cause serious safety issues. Fortunately, it has been demonstrated that the rational modification of metal anodes can greatly relieve such situations.[103] In this section, the use of MXene-based materials for the modification of the separator and lithium anode is summarized.

The first MXene-functionalized separator for Li-SBs was reported by Lin et al.[104] In the case of the Ti_3C_2 MXene modified glass fiber separator, the batteries can deliver an initial capacity of 1462 mAh g^{-1}, which is 395 mAh g^{-1} higher than the pure glass fiber separator. Moreover, after 100 cycles, 820 mAh g^{-1} of capacity can be retained compared to ≈ 320 mAh g^{-1} using the commercial separator. Ti_3C_2 modified polypropylene separator was also developed for Li-SBs.[105] The uniform surface MXene coating can be considered as a second current collector that decreases the internal resistance of the battery and thus facilitates the redox kinetics. Besides, the ultrathin (mass loading: 0.1 mg cm^{-2}, thickness: 522 nm) but dense MXene coating can inhibit the shutting effect of LiPSs by its polar surface and Lewis acid-base mechanism, confining the polysulfides in the cathode region (**Figure 9**a).[105] Later, Yin et al. developed a functional separator by coating $Ti_3C_2T_x$ MXene debris on the eggshell membrane (MXene/ESM) (Figure 9b).[106] The as-obtained MXene/ESM separator showed a porous structure, good conductivity, excellent mechanical strength, and high thermal stability. By using MXene/ESM separator, the cycling performance was greatly enhanced with 74% capacity retention after 250 cycles at 0.5 C, in sharp contrast to only 11% for

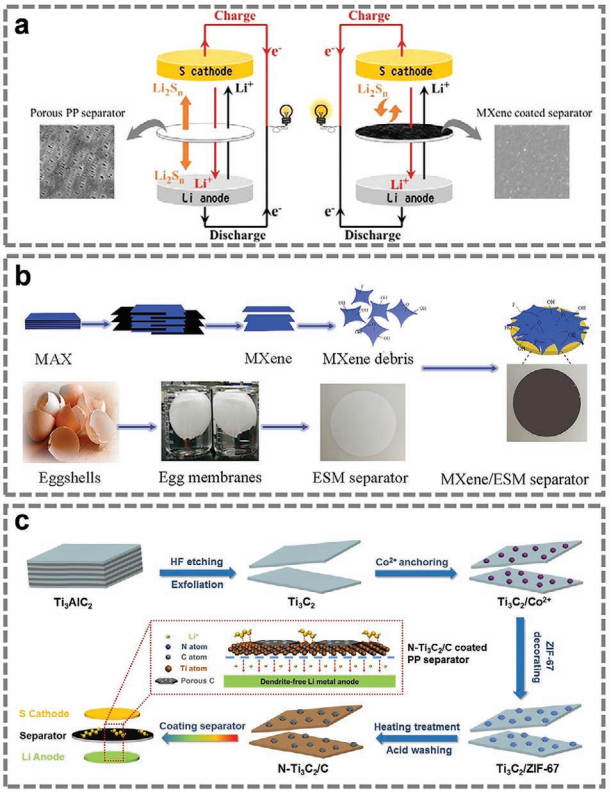

Figure 9. a) Schematic configurations of Li-SBs using commercial polypropylene (PP) membrane and MXene-modified polypropylene (MPP) separator, respectively. Reproduced with permission.[105] Copyright 2016, American Chemical Society. b) Scheme of synthesis route of the MXene/ESM. Reproduced with permission.[106] Copyright 2018, Elsevier. c) Schematic illustration of the preparation process of N-Ti_3C_2/C nanosheets and the modified PP separator. Reproduced with permission.[108] Copyright 2019, Elsevier.

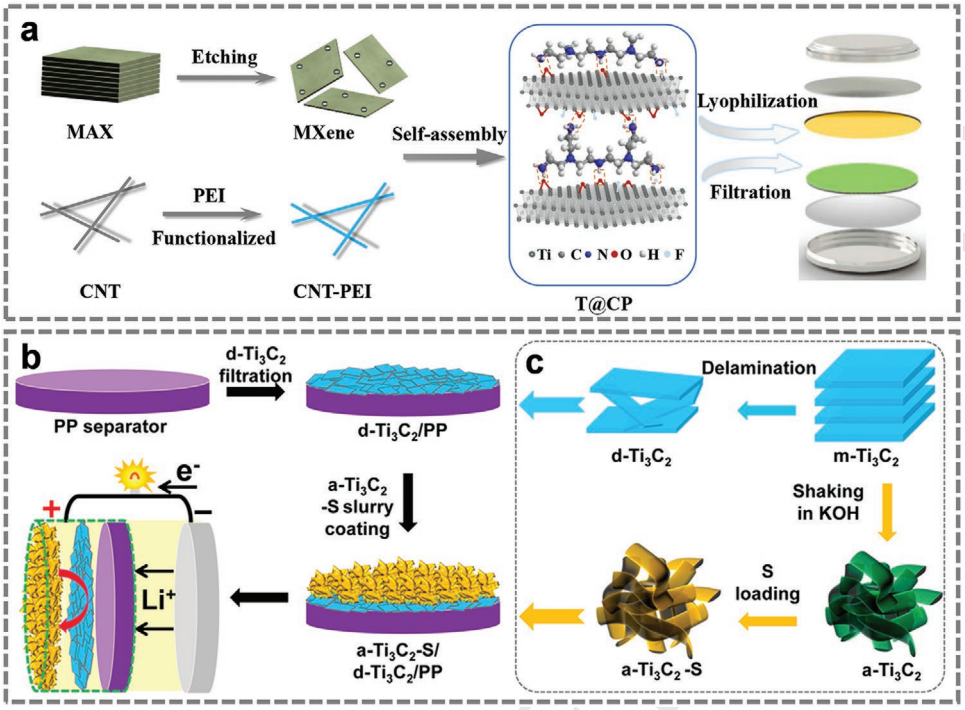

Figure 10. a) Schematic of the fabrication of T@CP nanohybrids for sulfur cathode and modified separator. Reproduced with permission.[101] Copyright 2019, Elsevier. b) Schematic of the fabrication of the dual-functional a-Ti_3C_2–S/d-Ti_3C_2/PP electrode for Li–S batteries. c) Schematic of the synthesis of $Ti_3C_2T_x$ nanosheets and a-Ti_3C_2–S hybrid. Reproduced with permission.[109] Copyright 2018, American Chemical of Society.

the commercial separator.[106] Han et al. further studied the thickness-dependent electrochemical performance of MXene modified separator for Li-SBs.[107] They found that the lithium ion diffusion coefficient increases with the decrease of thickness of MXene layers on the separator. The shuttling of LiPS species was efficiently inhibited even at the lowest MXene mass loading of 0.016 mg cm^{-2}, corresponding to a thickness of 100 nm.[107] Though ultrathin MXenes show excellent performance, they suffer from serious restacking. To solve this problem, a MXene/MOF derivative 2D hybrid (N-Ti_3C_2/C) was synthesized by in situ growth of zeolitic imidazolate framework (ZIF-67) particles on delaminated MXene nanosheets, followed by vacuum annealing (Figure 9c).[108] The resulting N-Ti_3C_2/C can prevent MXene flakes from restacking and preserve their 2D nature. In this way, the N-Ti_3C_2/C ensures the exposure of active Lewis acidic surface that has a strong interaction with the LiPSs. The theoretical calculation showed that N-doped MXene has higher adsorption energy than pristine MXene. The as-fabricated N-Ti_3C_2/C@PP separator not only enabled the good ability to prevent the LiPSs migration, but also suppressed the dendrite growth of lithium anode.[108] Other MXene-based composites including 3D CNTs/MXene[94f] and TiO_2/MXene[98c] have also been used as the separator coating or interlayer between separator and cathode and achieved improved electrochemical performance.

In some cases, MXenes and their composites can be employed as dual-functional materials. For instance, Guo et al. fabricated a 3D MXene/polyethyleneimine (PEI) grafted CNTs composite and used it as both the sulfur host and interlayer for Li-SBs. The integrated design could simultaneously suppress the LiPSs shuttling and the growth of lithium dendrite (**Figure 10**a). Consequently, a high reversible capacity of 980 mAh^{-1} cm^{-2} at 5 mA cm^{-2} for 500 cycles was achieved.[101] Wu et al. used alkali treated Ti_3C_2 MXene nanoribbons as S/polysulfides host and 2D exfoliated Ti_3C_2 MXene nanosheets as interlayer and achieved a high reversible capacity of 1062 mAh g^{-1} at 0.2 C (Figure 10b,c).[109] It should be mentioned that Yang et al. pointed out that the alkali treatment of Ti_3C_2 MXene would lead to the formation of amorphous titanium oxides.[110]

Metal lithium has been regarded as an optimal anode material owing to its high theoretical capacity (3680 mAh g^{-1}) and low redox potential (−3.04 V vs standard hydrogen electrode). Nevertheless, the flammable characteristic and the formation of dendrite during the repeated charge/discharge cycles pose a safety hazard. Moreover, these issues are even severer in Li-SBs because LiPS species also involve in the formation of solid electrolyte interphase (SEI) layers. Recently, MXene has been successfully used to protect the lithium anode in Li-SB system.[111] We will systematically discuss this topic later in Section 5.4.

In this section, we have summarized both the theoretical and experimental progress of MXene-based materials for Li-SBs. A summary of the electrochemical performance of MXene-based materials for Li-SBs is shown in **Table 4**. The use of versatile MXene-based composites for the sulfur host, separator modification, and anode protection is proven to be able to effectively suppress the shuttling effects of LiPS species, as well as the lithium dendrite formation, therefore resulting in high reversible capacity, enhanced rate capability, and better cycling stability.

Table 4. Summary of the electrochemical performance of MXene-based materials for Li-SBs (1 C rate = 1675 mA g^{-1}).

Material		Sulfur loading [mg cm^{-2}]	Cycling performance				Rate performance Capacity at current density [mAh g^{-1} @ C rate]	Ref.
			Current density [C]	Initial Capacity [mAh g^{-1}]	Cycle number	Capacity retention		
Sulfur host	Ti_2C	1	0.5 C	1090	650	723	660 @ 4C	[76]
	Ti_3C_2	/	200 mA g^{-1}	1291	100	970	520 @ 3.2 A g^{-1}	[88]
	$Ti_3C_2T_x$ @Meso-C	2	0.5 C	1225.8	300	704.6	544.3 @ 4C	[94c]
	$Ti_3C_2T_x$/rGO	1.5	0.2 C	1190	100	984.6	923 @ 2C	[94a]
			0.5 C	1144.2	300	878.4	750 @ 5C	
	CNT- $Ti_3C_2T_x$	1.5	0.5 C	1216	1200	450	1216 @ 0.5 C	[77]
		5.5	0.2 C	910	300	≈450		
	N-$Ti_3C_2T_x$	1.5	0.2 C	1144	200	950	947 @ 0.5 C	[89]
		5.1	2 C	825	1000	610	835 @ 1 C	
			0.2 C	765	500	588		
	$Ti_3C_2T_x$/1T-2H MoS_2-C	1	0.5 C	1014.1	300	799.3	905.1 @ 1 C	[98d]
							677.2 @ 2 C	
	TiO_2 QDs@ $Ti_3C_2T_x$	1.5	2 C	812	500	680	1037 @ 0.5 C	[96]
		5.5	0.2 C	≈ 900	100	533	663 @ 5 C	
	$Ti_3C_2T_x$ ink	≈2.5	0.2 C	1184	800	724	1244 @ 0.1 C	[91a]
							1004 @ 2 C	
	$Ti_3C_2T_x$ nanodot/xnanosheet	1.8	2 C	1058	400	815	882 @ 3 C	[92]
		9.2	0.05 C	9.5 mAh cm^{-2}	100	7.6 mAh cm^{-2}		
	$Ti_3C_2T_x$/Ultramicroporous carbon	1	0.1 C	1029	200	946.7	502.3 @ 2 C	[94d]
	S@TiO_2/Ti_2CT_x	1.8-2.0	2 C	782.9	200	464.0	879.2 @ 0.2 C	[98b]
	$Ti_3C_2T_x$/rGO	1.57	1 C	946	500	596	1270 @ 0.1 C	[94b]
							977 @ 1 C	
	Mo_2C-CNTs	1.5	0.1 C	1235	250	925	≈832 @ 2 C	[94e]
							≈673 @ 5 C	
	$Ti_3C_2T_x$ flower	4.2	1/30 C	1178	75	855	/	[93]
		6.8	1/30 C	1120	75	805		
		10.5	1/30 C	957	75	746		
	TiO_2–Ti_3C_2	/	1C	1417	1000	662	969 @ 5 C	[98a]
	$Ti_3C_2T_x$ paper	1	1 C	1169	1500	970	1075 @ 2 C	[91b]
	S@Ti_3C_2@PDA	1	0.2 C	1439	150	1044	624 @ 6 C	[100]
		4.4	0.5 C	798	330	556	735 @ 1 C	
	Ti_3C_2/S@PDA	1.5	0.5 C	1197	200	1096	442 @ 4 C	[99]
		5	0.2 C	1001	1000	651		
	Ti_3C_2/C	1.0	0.5 C	1180	200	790	1669 @ 0.1 C	[94h]
			1 C	≈707	500	530	520 @ 5 C	
	MnO_2@Ti_3C_2	1.2	1 C	≈716	500	501	615 @ 2 C	[98e]
	Ti_3C_2@carbon fiber	4	1 C	1058.4	1000	626	1508.1 @ 0.1 C	[94g]
							795.5 @ 2 C	
	N–Ti_3C_2	1.4–1.6	2 C	820	1200	≈495	1082 @ 0.5 C	[90]
							792 @ 3 C	
Separator	Ti_3C_2/glass fiber	1.9	500 mA g^{-1}	820	100	721	476 @ 2 A g^{-1}	[104]
	$Ti_3C_2T_x$/ Eggshell membrane	2.07	0.5 C	1185	250	862	948 @ 1 C	[106]
			1 C	948	150	672		
	CNT/$Ti_3C_2T_x$	0.8	0.1 C	1415	100	992	728 @ 2 C	[94f]
		2.5	1 C	987	600	614		
			1C	≈570	600	400		
	$Ti_3C_2T_x$	1.2	0.5 C	848.7	500	550	743.7 @ 1 C	[105]
			1 C	743.7	500	495		
	TiO_2–$Ti_3C_2T_x$/graphene	1.2	2 C	≈800	1000	≈576	800 @ 2 C	[98c]
	N–Ti_3C_2/C	3.4	0.5 C	945	500	716	675 @ 2 C	[108]

Table 4. Continued.

Material		Sulfur loading [mg cm^{-2}]	Cycling performance				Rate performance Capacity at current density [mAh g^{-1} @ C rate]	Ref.
			Current density [C]	Initial Capacity [mAh g^{-1}]	Cycle number	Capacity retention		
Separator/ sulfur host	a-$Ti_3C_2T_x$ nanoribbon/nanosheet	0.7–1	0.5 C	≈900	200	≈400	691 @ 1 C	[109]
			2 C	≈800	200	≈350	403 @ 4 C	
							288 @ 10 C	
	$Ti_3C_2T_x$/CNTs/PEI	2.6	0.25 C	1227	200	1100	950 @ 2.5 C	[101]
			1 C	1035	500	980		
Anode	Ti_3C_2/lithium film	/	/	/	/	/	/	[111]

5.2. Sodium- and Potassium-Ion Storage

SIBs and PIBs based on earth-abundant elemental Na and K have been gaining increasing interest in the battery research community. However, the large ionic radii of Na^+ and K^+ make them much more challenging to intercalate into many well-established LIB anode materials. In this regard, MXenes with tunable interlayer spacing, high electronic conductivity, and rich surface chemistry are predicted to be promising anodes for both the SIBs and PIBs.[52b,c,112] Particularly, Xie et al. revealed both theoretically and experimentally that Na^+ and K^+ could be intercalated into functionalized MXene electrodes.[52b] They found that the surface functional groups and transition metal species have a significant impact on the capacity and voltage of MXenes. The M_2C MXenes (M = Sc, V, Ti, V, etc.) with oxygen termination or without any functional groups, are demonstrated to be the most promising for metal ion storage.[52c] In addition, a large number of experimental studies have confirmed the feasibility of MXenes for sodium/potassium-ion storage. In this section, we divide the MXene-based materials into three categories (MXenes, MXene-based hybrid materials, and MXene-derived materials) and discuss their utilization for sodium/potassium-ion storage.

5.2.1. MXene Electrodes

Up to date, various MXenes have been studied for SIBs and PIBs.[13f,113] With the accelerating development of MXene battery research, it is particularly important to investigate the charge storage mechanism in MXenes. It was found that the MXene electrode in nonaqueous Na^+ electrolyte behaves differently from that in aqueous Na^+ electrolyte or in nonaqueous Li^+ electrolyte. For instance, the Na^+ ions can spontaneously intercalate into the MXene interlayer spaces by simple immersion, while such a phenomenon cannot be observed in a nonaqueous electrolyte (i.e., $NaPF_6$/ethylene carbonate/diethyl carbonate mixture)[114] Interestingly, Yamada et al. demonstrated that the pillared Ti_2CT_x structure was formed during the first cycle because of the "activation" process.[113d] The activated electrode allowed both reversible Na^+ interaction/deintercalation into the layers and Na^+ adsorption/desorption on the surfaces. Later, a similar storage behavior was observed in $Ti_3C_2T_x$ by the same group.[115] As schematically shown in **Figure 11**a, during the activation process, residual Na^+ along with the penetrated solvent molecules are trapped in between the MXene layers. Such a Na^+-pillared structure can stabilize the electrode by minimizing

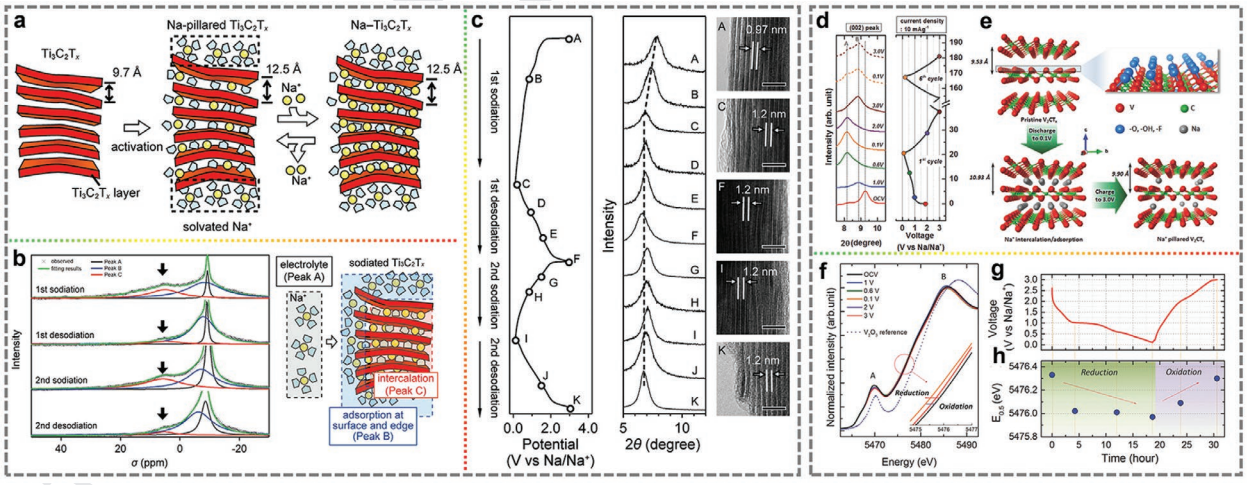

Figure 11. a) Schematic illustration for the proposed mechanism of reversible Na^+ insertion/desertion into $Ti_3C_2T_x$. b) ^{23}Na NMR spectra during the initial two cycles. c) Ex situ XRD patterns and TEM images for $Ti_3C_2T_x$ upon sodium intercalation and deintercalation. Scale bar: 5 nm. Reproduced with permission.[115] Copyright 2016, American Chemical of Society. d) Ex situ XRD patterns of V_2CT_x during Na^+ insertion/desertion at the 1st and 6th cycles. e) Schematic illustration of the expansion/contraction behavior of V_2CT_x during Na^+ intercalation/deintercalation. f) Ex situ V K-edge hard X-ray absorption near edge spectroscopy results of V_2CT_x at selected cell voltages during the first cycle (from open circuit voltage to fully discharged status and then recharged to 3 V). g) Corresponding voltage profile, and c) variation of V edge energy at selected cell voltages. Reproduced with permission.[116] Copyright 2017, Wiley.

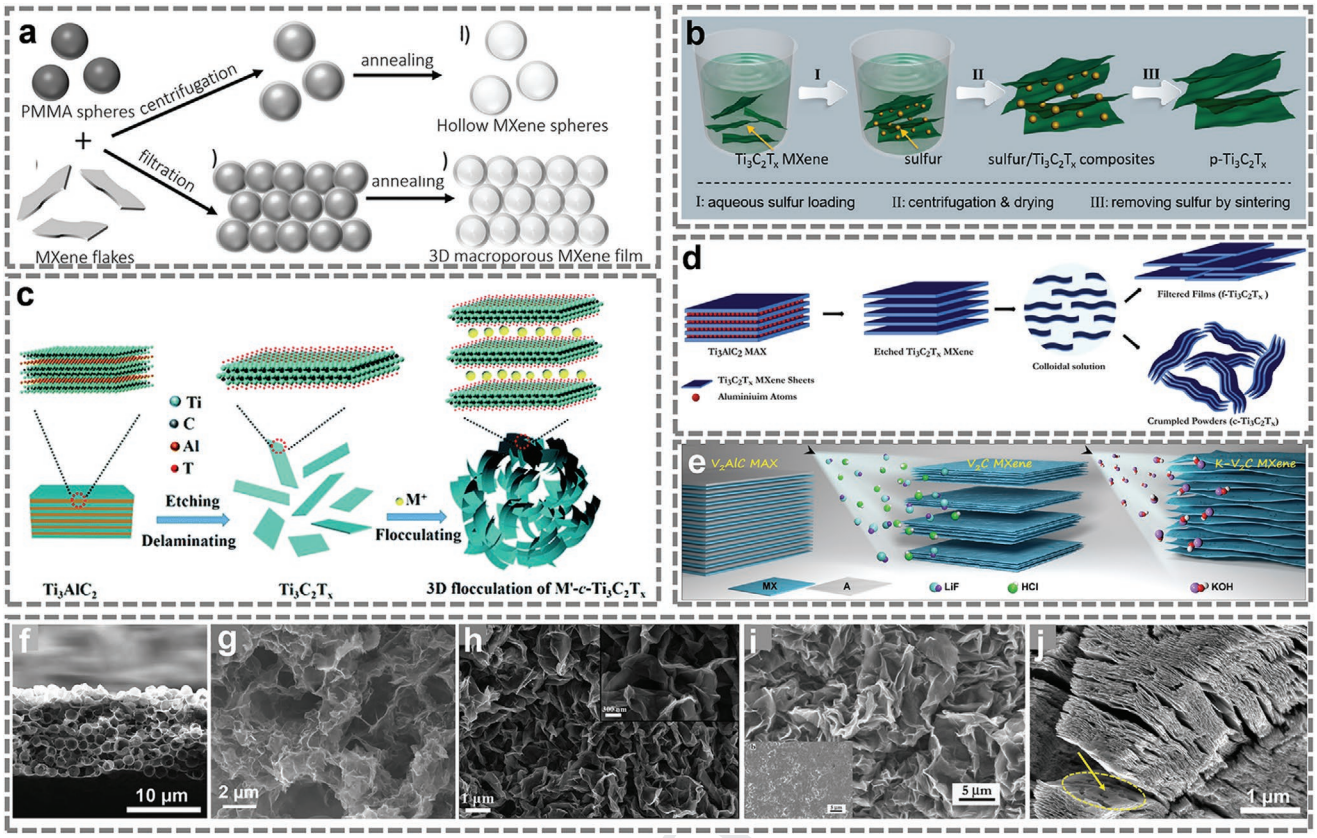

Figure 12. Synthesis strategies and corresponding SEM images of a,f) 3D hollow MXene spheres, b,g) porous $Ti_3C_2T_x$ (p- $Ti_3C_2T_x$), c,h) alkali-induced crumpled $Ti_3C_2T_x$, d,i) acid-induced crumpled $Ti_3C_2T_x$, and e,j) porous K-V_2C MXene, respectively. a,f) Reproduced with permission.[11b] Copyright 2017, Wiley. b,g) Reproduced with permission.[124] Copyright 2018, American Chemical of Society. c,h) Reproduced with permission.[117a] Copyright 2018, Royal Society of Chemistry. d,i) Reproduced with permission.[117b] Copyright 2018, Taylor & Francis. e,j) Reproduced with permission.[4i] Copyright 2019, Elsevier.

the structural expansion/shrinkage during the subsequent cycles, as confirmed by a wide spectrum of characterizations (Figure 11b,c) as well as DFT calculations. Meanwhile, the Na^+ ion interaction and charge storage mechanism in V_2CT_x MXene were studied by Yang et al.[116] Except for the similar structural evolution as in the cases of Ti_2CT_x and $Ti_3C_2T_x$, the reduction and oxidation of the vanadium element during the Na^+ intercalation/deintercalation was confirmed (Figure 11d–h), implying that the redox reaction of the transition metals contributes to the charge storage.[116]

Although MXenes have shown promising performance toward alkali ion storage, there are still some challenges that need to be addressed. For example, the etched MXene with a multilayer accordion-like structure could lead to low material utilization and poor flexibility. Whereas the restacking of exfoliated MXene nanosheets originating from van der Waals force and/or hydrogen bonds would severely hinder the electrolyte diffusion and permeation. Both of these effects could result in inferior electrochemical performance. In order to effectively address these issues, efforts have been devoted to fabricating various 3D architectures, such as porous MXenes, crumpled MXenes, and MXene hollow spheres, via different strategies. Zhao et al. synthesized the 3D microporous MXene films using spherical polymethylmethacrylate (PMMA) as the template.[11b] As depicted in **Figure 12**a, upon mixing the MXene nanosheets with PMMA spheres suspension, MXene nanosheets would spontaneously warp the surface of PMMA driven by the electrostatic force. The MXene hollow spheres and the 3D free-standing films can be readily obtained by facile centrifugation or vacuum filtration with the subsequent annealing process. More importantly, the size of the spheres is tunable, and this method can be extended to prepare other MXene compositions, such as V_2CT_x and Mo_2CT_x. The as-prepared 3D Mo_2CT_x film electrode can achieve a high reversible capacity of 370 mAh g^{-1} at 0.25 C (1 C = 200 mA g^{-1}), along with excellent rate capability and long-term stability for SIBs. After 1000 cycles, a reversible capacity of 290 mAh g^{-1} at 2.5 C can be maintained.[11b] Later, Xie et al. reported the synthesis of a porous and anisotropic structure by a sulfur loading-removal strategy (Figure 12b).[117] Because of the metallic conductivity, low charge diffusion barrier and efficient electrolyte contact, the 3D porous $Ti_3C_2T_x$ (p-$Ti_3C_2T_x$) exhibited outstanding rate performance. Furthermore, similar crumpled MXene structures can also be achieved by simple acid or alkali treatment (Figure 12c,d). The resultant products showed much superior performance compared to pristine MXenes. Additionally, Ming et al. presented a simple method involving dual acid/alkali treatment to prepared 3D porous

accordion-like K-V_2C MXene (Figure 12e), which shows greatly enhanced performance for K^+ storage with a high capacity of 152 mAh g^{-1} at 100 mA g^{-1}.[4i] Bao et al. also presented the preparation of Ti_3C_2 MXene nanoribbons by alkalized treatment.[118] Benefiting from the expanded interlayer distance and the 3D interconnected porous frameworks, the resulting MXene nanoribbons showed excellent sodium/potassium storage performance in terms of high capacity and stability compared to the pristine MXene. Apart from being used as anode electrodes, Simon et al. demonstrated the possibility of using V_2C MXene as a cathode electrode for sodium-ion capacitors, which expands the potential applications of the MXene family.[119]

It is also demonstrated that elemental doping or incorporation can effectively modify the properties of MXenes, leading to enhanced electrochemical performance toward alkali ion storage. Particularly, Luo et al. synthesized the S atom intercalated Ti_3C_2 MXene (CT-S@Ti_3C_2) by multiple steps, i.e., CTAB preintercalation, thermal diffusion with sulfur, and vacuum annealing process (**Figure 13**a).[120] The interlayer distance of the pristine MXene expands from 0.98 to 1.37 nm upon S intercalation (Figure 13b–g). The as-obtained CT-S@Ti_3C_2-450 sample exhibited a high reversible sodium-ion storage capacity of 492 mAh g^{-1} after 100 cycles. According to the DFT computations (Figure 13h–i), both the first and second adsorption layers of $Ti_3C_2S_2$ have lower

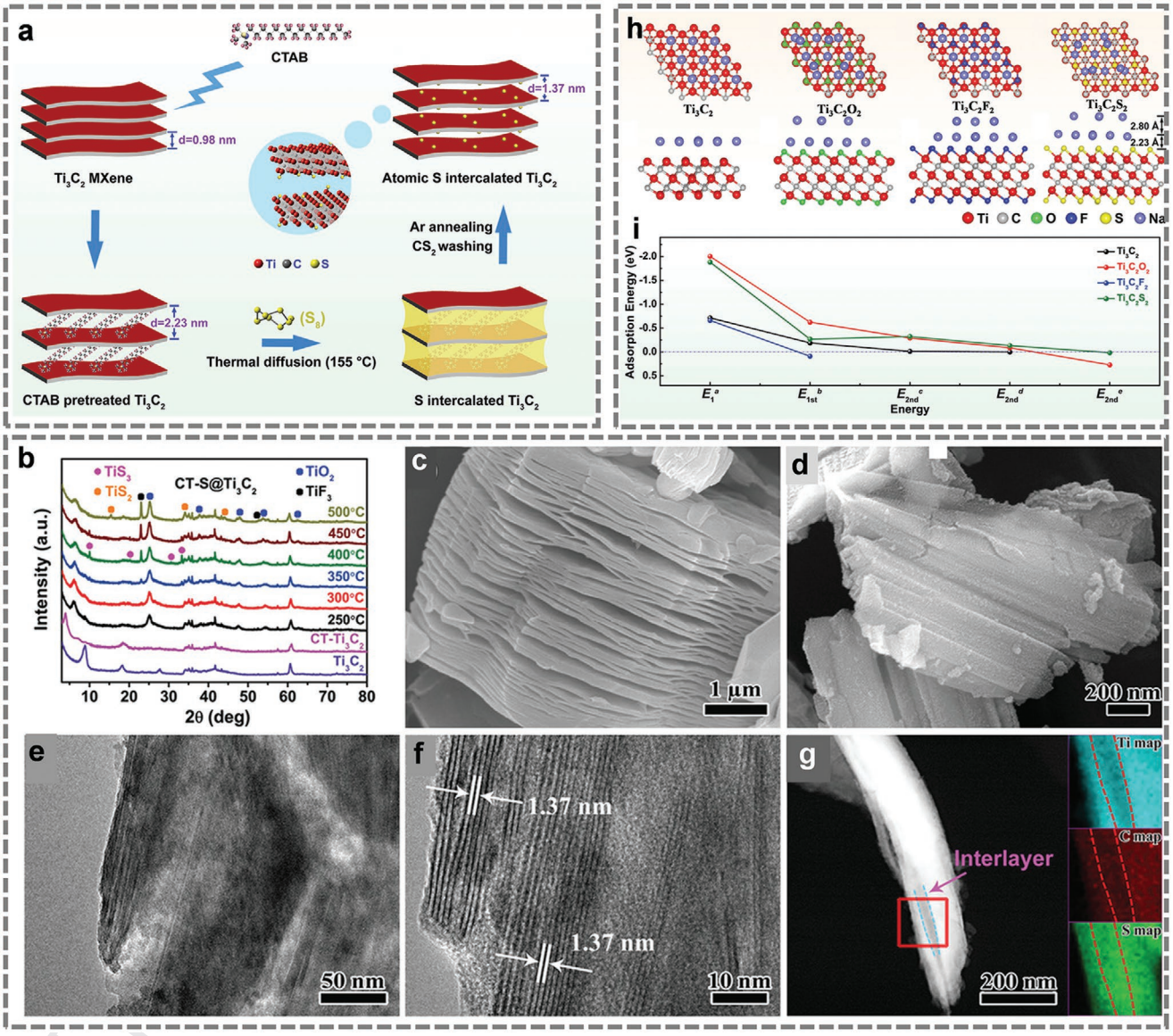

Figure 13. a) Schematic illustration of the preparation of S atoms intercalated Ti_3C_2. b) XRD patterns of Ti_3C_2, CTAB-pretreated Ti_3C_2 (CT-Ti_3C_2), and S atoms intercalated Ti_3C_2 MXenes (CT-S@Ti_3C_2) obtained at different annealing temperatures. SEM images of c) Ti_3C_2 and d) CT-S@Ti_3C_2-450. e,f) TEM images of CT-S@Ti_3C_2-450. g) STEM images of CT-S@Ti_3C_2-450 and the corresponding elemental maps. h) DFT calculations and geometric structures for Na adsorption on the Ti_3C_2, $Ti_3C_2O_2$, $Ti_3C_2F_2$, and $Ti_3C_2S_2$ monolayer of top and side views. i) The calculated Na adsorption energies on the Ti_3C_2, $Ti_3C_2O_2$, $Ti_3C_2F_2$, and $Ti_3C_2S_2$ monolayer. Reproduced with permission.[120] Copyright 2019, Wiley.

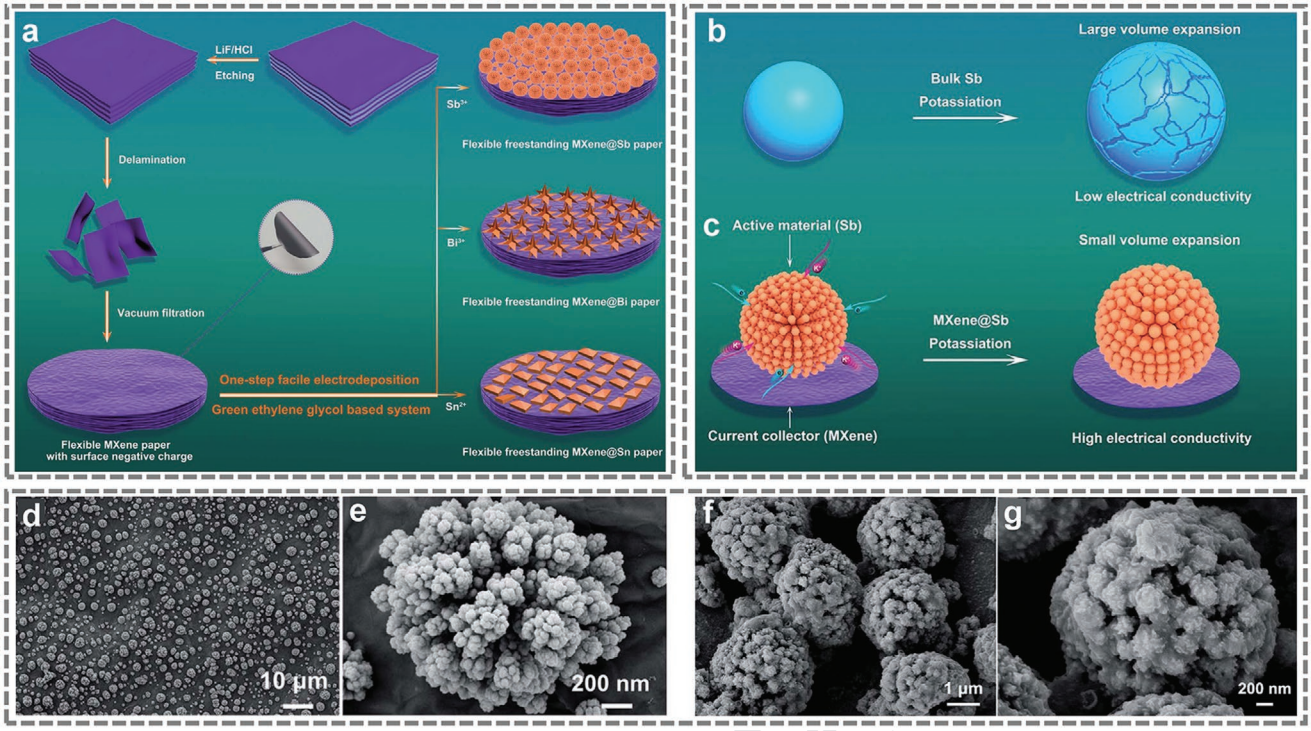

Figure 14. a) Schematic illustration of the synthesis process of flexible free-standing MXene@M paper (M = Sb, Bi, or Sn). SEM images of MXene@Sb electrode b,c) before electrochemical test, and d,e) after 100 cycles at 50 mA g^{-1}. f,g) Potassiation schematics for bulk Sb and MXene@Sb electrodes for KIBs. Reproduced with permission.[129] Copyright 2019, Royal Society of Chemistry.

adsorption energies to sodium ions, indicating the more energetically stable configurations of $Ti_3C_2S_2$. Besides, it was also found that the distance between the second layer and the host $Ti_3C_2S_2$ (0.5 nm) is smaller than the increment of interlayer distance (0.81 nm) of CT-S@Ti_3C_2-450, revealing the stable structure and the feasibility of "pillar effect" of the as-prepared electrode. Finally, sodium-ion capacitors were fabricated by coupling with activated carbon cathode, showing both good rate performance and stability.[120] Additionally, other approaches including sulfur decoration,[121] sulfur doping,[122] and cation pillaring[123] are also proven to be efficient for enabling high-performance sodium-ion storage.

5.2.2. MXene-Based Hybrid Electrodes

Though MXenes possess high conductivity and thus high rate capability, they generally suffer from low capacity and therefore low energy density. In this regard, hybridizing MXenes with other materials (e.g., Sn, Bi, Sb, P, and their compounds) with high capacity would further boost the performance in terms of both the energy and power densities. On the one hand, such compositions can prevent MXene from restacking to some degree, thus are beneficial for the ion/electrolyte diffusion and material utilization.[125] On the other hand, MXene could serve as a buffer layer to relieve the dramatic volumetric change of the electrode. In light of these facts, many MXene-based hybrid systems such as $Sb_2O_3/Ti_3C_2T_x$,[126] $Ti_3C_2T_x/SnS_2$,[127] and $SnS/Ti_3C_2T_x$[128] have been developed as anodes of SIBs and they generally exhibit good structural stability and superior electrochemical performance. Notably, Qian et al. developed a general electrodeposition strategy to fabricate robust, flexible and free-standing MXene@M (M = Sb, Sn, and Bi) anodes for PIBs (**Figure 14**a).[129] Thanks to the MXene buffer layer, these hybrids exhibited outstanding structural stability compared to the bulk metal anodes without the use of MXene (Figure 14b–g). For example, the MXene@Sb anode can stably deliver a high reversible capacity of 516.8 mAh g^{-1} for over 500 cycles.[129] Apart from alloy-based metals and their compounds, phosphorus (e.g., red phosphorus, black phosphorus), and phosphides have also been hybridized with MXenes for high-performance SIBs.[130] For example, Yang et al. demonstrated the black phosphorus quantum dot/Ti_3C_2 MXene nanosheets (BPQD/TNS) for both the LIBs and SIBs.[130b] The composite was synthesized by an interfacial assembly strategy, which resulted in well-dispersed BPQDs anchored on the surface of MXenes. Specifically, the BPQDs with improved conductivity and relieved stress endowed a high capacity and stable cycling performance. In the meantime, the pseudocapacitive MXene provides a fast charge transfer, thus high rate performance. Wang et al. fabricated a phosphorene/MXene hybrid material with in situ formed fluorinated interphase as anode for SIBs.[130d] The as-prepared anode not only promotes the transport of electrons and sodium ions, but also mitigates the volumetric expansion, leading to both the improved cycling stability and rate capability of the anode. Yin et al. coupled NiCoP bimetallic phosphide nanoparticles with crumpled porous Ti_3C_2 MXene as an anode for SIBs.[130a]

The interconnected 3D Ti_3C_2 crumpled architectures provide a conductive framework, rich open pores and large surface area, leading to a rapid charge transfer and electrolyte diffusion. Meanwhile, the NiCoP owns abundant redox reaction sites. The synergistic effect of these two components leads to an outstanding electrochemical performance. Remarkably, a capacity of 261.7 mAh g^{-1} can be maintained after 2000 cycles at a current density of 1 A g^{-1}.

Additionally, conversion-type electrodes such as transition metal sulfides, selenides, and oxides have also attracted considerable attention for SIBs and PIBs. However, they suffer from poor conductivity and dramatic volumetric expansion caused by the phase change during discharge and charge, therefore inferior long-term stability and unsatisfied rate performance. Hybridizing these materials with MXenes can improve the conductivity and stability. Such a concept has been proven to be effective as confirmed in many MXene-based hybrid systems such as $MoS_2/Ti_3C_2T_x$,[131] $MoSe_2/Ti_3C_2T_x$,[132] $FeS_2/Ti_3C_2T_x$,[133] $CoS/Ti_3C_2T_x$,[134] $CoNiO_2/Ti_3C_2T_x$,[135] $VO_2/Ti_3C_2T_x$,[136] $TiO_2@Ti_3C_2T_x$,[137] and so on. Particularly, Zhang et al. rationally designed a hierarchical carbon-coated $MoSe_2/Ti_3C_2$ MXene hybrid material as a superior anode for PIBs.[132] The 3D porous network of $MoSe_2$ and Ti_3C_2 can prevent the restacking or aggregation of each other, while the MXene significantly boosts the electronic conductivity. Furthermore, the carbon layer serves as a protective layer that can reinforce the stability and conductivity of the hybrid materials. Notably, the strong interactions at the interfaces of the $MoSe_2$ and MXene flakes promote the charge transfer and improve the stability. Consequently, the resulting $MoSe_2$/MXene@C composites exhibited unprecedented rate performance for PIBs, with capacities of 355 and 183 mAh g^{-1} at current densities of 200 mA g^{-1} and 10 A g^{-1}, respectively.[132]

5.2.3. MXene-Derived Materials

In addition to being directly used as electrodes or conductive media, MXenes are also used as the precursor/template to prepare various materials, including oxides, nitrides, sulfide, MOF, etc.[51d,110,138] This is particularly attractive for synthesizing materials with 1D or 2D morphologies that otherwise are more challenging to synthesize by common methods. For instance, Dong et al. synthesized sodium titanate (M-NTO) and potassium titanate (M-KTO) nanoribbons by simultaneous oxidation and alkalization of $Ti_3C_2T_x$ MXene in NaOH or KOH solution, respectively (**Figure 15**a–g).[138d] These highly anisotropic M-NTO and M-KTO nanoribbons with marcoporous 3D framework delivered high reversible capacities of 191 mAh g^{-1} for SIBs (at 200 mA g^{-1}) and 151 mAh g^{-1} for PIBs (at 50 mA g^{-1}), respectively. Similarly, sandwich-like $Na_{0.23}TiO_2$ nanobelt/Ti_3C_2 composites were prepared by Yang et al. through a partial oxidation process of Ti_3C_2.[110] The as-prepared product showed superior high rate capability and long cycling stability with negligible capacity fading over 4000 cycles for SIBs. In addition, a confined transformation of assembled 2D MXene ($Ti_3C_2T_x$) and rGO nanosheets was used to prepare composite with ultrathin sodium titanate (NTO)/potassium titanate (KTO) sandwiched between graphene layers (Figure 15h).[138i] The excellent flexibility of the sandwiched structure was confirmed by physical characterizations (Figure 15i–n). Both the NTO/KTO and rGO layers showed a small thickness of 5–10 nm and were stacked alternatively. The incorporation of highly conductive graphene into the binder-free films can efficiently reduce the diffusion barriers. Consequently, the NTO/rGO electrodes retained 72 mAh g^{-1} at 5 A g^{-1} even after 10 000 cycles for SIBs, whereas the KTO/rGO electrodes exhibited 75 mAh g^{-1} at 2 A g^{-1} after 700 cycles for PIBs. Zhang's group and Cao's group also demonstrated the feasibility of MXene-derived TiO_2/rGO for alkali ion storage.[138e,f] Apart from oxides, MXene-derived TiS_2 nanosheets were successfully prepared by the in-situ conversion of polyvinylpyrrolidone modified $Ti_3C_2T_x$ MXene under H_2S gas flow. The as-obtained carbon-coated TiS_2 nanosheets exhibited both extraordinary rate performance and excellent stability.[138c]

Given the high conductivity, fast charge transfer, low diffusion barrier, tunable interlayer distance, and rich surface chemistry, MXene-based electrodes and conductive matrixes/additives have already shown great potential for SIBs and PIBs, while delicate nanostructuring such as assembling 2D MXene nanosheets into 3D hierarchical networks can further boost the electrochemical performance. A brief summary of MXene-based materials in the applications of SIBs and PIBs is shown in **Table 5**.

5.3. Multivalent Ion Storage (Mg, Al, Zn)

5.3.1. Magnesium-Ion Storage

Owing to the high abundance (23 300 vs 20 ppm of lithium), high theoretical capacity, and dendrite free features of Mg anode, magnesium-ion batteries (MIBs) have drawn much attention since the pioneering work conducted by Aurbach et al. in 2000.[140] However, the divalent charge of Mg^{2+} ions results in strong ion-electrode bonds and sluggish ion diffusion kinetics. Currently, MIBs still suffer from the lack of suitable cathodes that allow fast diffusion/intercalation of Mg^{2+} ions as well as stable electrolytes.[141] Previous simulations imply that the Mg^{2+} ions are able to form bilayers and trilayers on MXene surface, leading to a theoretical capacity as high as 1050 mAh g^{-1}.[52b,c] Several attempts have therefore been made to use MXene-based materials for MIBs. For example, Xu et al. demonstrated the capability of CTAB intercalated $Ti_3C_2T_x$ MXene for Mg-ion storage, while the pristine $Ti_3C_2T_x$ exhibited poor performance (**Figure 16**a,b).[142] The as-prepared $Ti_3C_2T_x$/CTAB electrode achieved a high capacity of 300 mAh cm^{-3} at 50 mA g^{-1} and excellent rate capability. The DFT results indicated that the significantly improved performance could be ascribed to the reduced diffusion barrier (about 0.19 eV) of Mg^{2+} ions on the MXene surface (Figure 16c–h). The same group also synthesized $Ti_3C_2T_x$ MXene supported MoS_2 composite for MIBs.[143] Gao et al. found that the preintercalation of K^+ into $Ti_3C_2T_x$ MXene leads to improved Mg-ion storage in 1 M $MgSO_4$ electrolyte.[144] Gogotsi et al. also showed that the Mg^{2+} preintercalated $Ti_3C_2T_x$ ($Mg_{0.21}Ti_3C_2T_x$) microporous films could be used as the cathode for MIBs, though the rate performance and stability need to be further optimized.[145] Besides, Fan et al. fabricated

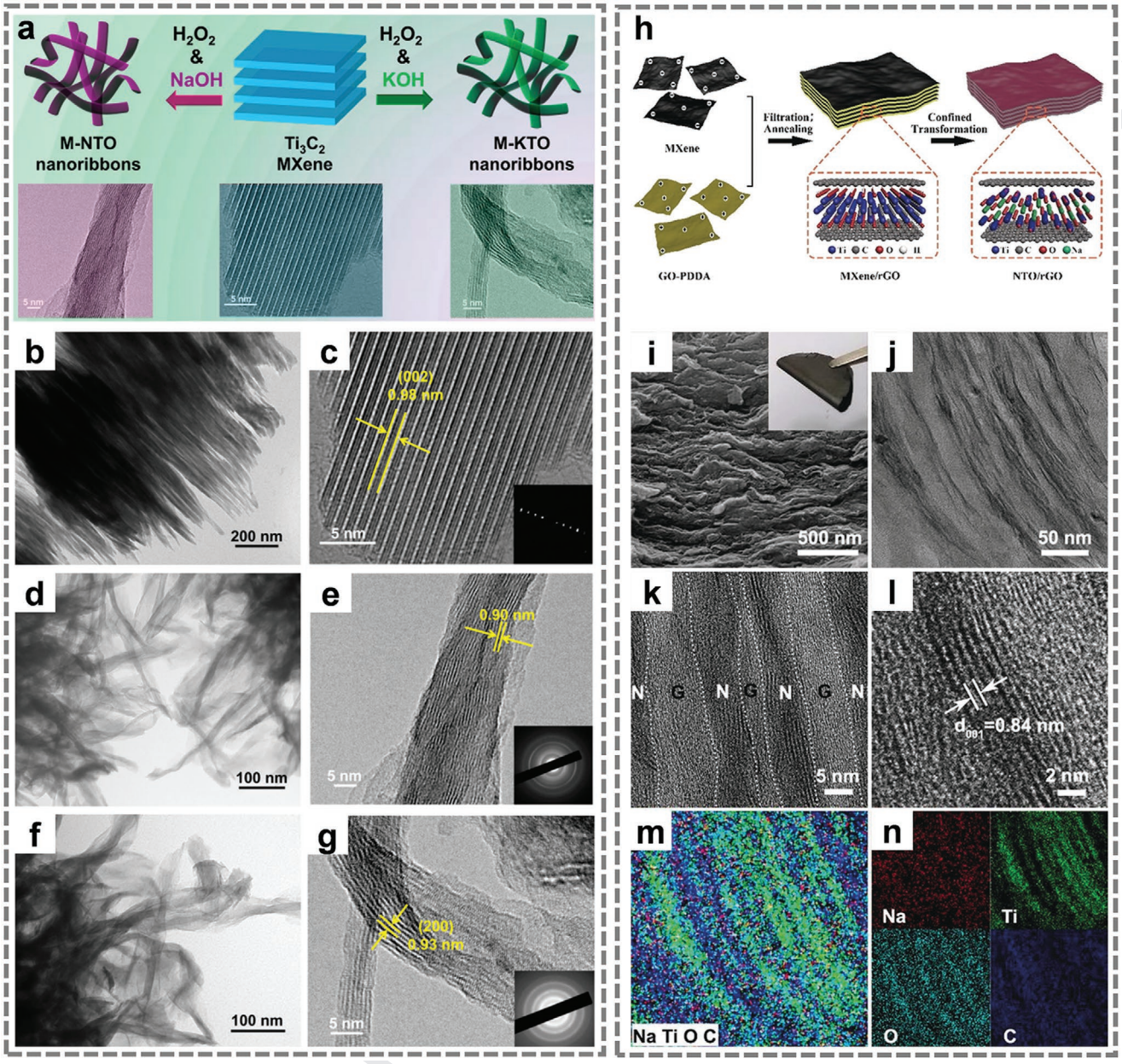

Figure 15. a) Schematic of the synthesis process of MXene derived M-NTO and M-KTO nanoribbons. TEM images of b,c) pristine $Ti_3C_2T_x$ MXene, d,e) M-NTO nanoribbons, and f,g) M-KTO nanoribbons. Reproduced with permission.[138d] Copyright 2017, American Chemistry of Society. h) Schematic of the preparation of flexible NTO/rGO films. SEM and TEM characterizations of NTO/rGO-10% hybrid film. i) SEM, j) TEM, and k,-l) HRTEM images ("N" refers to NTO, and "G" refers to rGO). e,f) TEM elemental maps of Na, Ti, O, and C elements. Reproduced with permission.[138i] Copyright 2018, American Chemistry of Society.

a sandwich-like $Ti_3C_2T_x$@C spheres structure as a cathode for MIBs.[146] The theoretical calculations revealed that the Mg ions are not affected by the steric hindrance caused by the incorporation of the carbon spheres. On the contrary, the expanded interlayer distance enabled by the C intercalation provides additional diffusion channels. Moreover, such a strategy can be extended to other MXenes, such as V_2CT_x.

Since MXene-based cathodes deliver a relatively high reversible capacity (≈100–200 mAh g^{-1}) for MIBs, it is therefore of great interest to investigate the charge storage mechanism. Very recently, Schnell et al. studied the Mg-ion storage performance of multilayer MXene particles (i.e., $Ti_3C_2T_x$ and V_2CT_x) in various electrolytes at room and elevated temperatures.[147] The results demonstrated that almost no Mg-ion intercalation takes place at both room temperature and 60 °C (the capacity is less than 5 mAh g^{-1}). Furthermore, DFT computations revealed that the average voltage of F- and OH-terminated $Ti_3C_2T_2$ MXene falls in the negative region, while the O-terminated $Ti_3C_2T_2$ MXene shows high migration barriers. What's more, it was found that upon discharge of multilayer F- and OH-terminated

Table 5. Summary of the electrochemical performance of MXene-based materials for sodium/potassium ion storage.

Material		Cycling performance				Rate performance Capacity [mAh g^{-1}]	Ref.
		Ion storage system	Current density [mA g^{-1}]	Cycle number	Capacity retention		
MXene	Ti_2CT_x	Na^+	20	100	138	113 @ 1 A g^{-1} 63 @ 5 A g^{-1}	[113d]
	a-$Ti_3C_2T_x$	Na^+	200	500	53	85 @ 0.3 A g^{-1}	[118]
	a-$Ti_3C_2T_x$	K^+	200	500	42	60 @ 0.3 A g^{-1}	[118]
	f-$Ti_3C_2T_x$–DMSO	Na^+	1000	1500	76	110 @ 2 A g^{-1}	[113a]
	Ti_3CNT_z	K^+	20	100	75	32 @ 0.5 A g^{-1}	[113e]
	Hollow $Ti_3C_2T_x$ MXene spheres	Na^+	500	1000	210	120 @ 5 A g^{-1}	[11b]
	d-D-$Ti_3C_2T_x$	Na^+	100	500	103	85 @ 0.5 A g^{-1}	[113c]
	p-$Ti_3C_2T_x$	Na^+	1000	1000	189	124 @ 10 A g^{-1} 24 @ 100 A g^{-1}	[124]
	Ti_3CN	Na^+	100	500	85.6	157.3 @ 0.5 A g^{-1}	[113b]
			500	500	60		
	S-doped $Ti_3C_2T_x$	Na^+	500	2000	138.2	165.8 @ 1 A g^{-1} 113.9 @ 4 A g^{-1}	[122]
	Na-*c*-$Ti_3C_2T_x$	Na^+	100	300	130	61 @ 1 A g^{-1}	[117a]
	Na-Ti_3C_2	Na^+	2000	2000	85	≈110 @ 3 A g^{-1}	[123]
	c-$Ti_3C_2T_x$	Na^+	20	50	246	120 @ 0.5 A g^{-1}	[117b]
	Bistacked $Ti_3C_2T_x$	Na^+	25	70	≈113	58 @ 0.5 A g^{-1}	[13f]
	Sulfur-decorated Ti_3C_2 MXenes	Na^+	2000	1000	135	185.6 @ 2 A g^{-1} 136.6 @ 5 A g^{-1}	[121]
	CT-S@Ti_3C_2	Na^+	10 000	5000	≈75	358 @ 1 A g^{-1} 223 @ 5 A g^{-1} 120 @ 15 A g^{-1}	[120]
	Porous K-V_2C	K^+	500	400	87	97 @ 1 A g^{-1} 70 @ 3 A g^{-1}	[4i]
MXene-based composites	Ti_3C_2 MXene/CNT	Na^+	100	500	345 mAh cm^{-3}	421 @ 0.02 A g^{-1} 89 @ 5 A g^{-1}	[125]
	$MoS_2/Ti_3C_2T_x$	Na^+	100	100	250.9	162.7 @ 1 A g^{-1}	[131a]
	$Sb_2O_3/Ti_3C_2T_x$	Na^+	500	100	≈400	295 @ 2 A g^{-1}	[126]
	$CoNiO_2/Ti_3C_2T_x$	Na^+	100	140	223	188 @ 0.3 A g^{-1}	[135]
	$Ti_3C_2T_x/SnS_2$	Na^+	100	200	322	134 @ 1 A g^{-1} 78 @ 2 A g^{-1}	[127]
	$SnS/Ti_3C_2T_x$	Na^+	500	50	320	255.9 @ 1 A g^{-1}	[128]
	BPQDs/$Ti_3C_2T_x$	Na^+	1000	2400	520	280 @ 1 A g^{-1} 167 @ 2 A g^{-1}	[130b]
	Phosphorene/$Ti_3C_2T_x$	Na^+	1000	1000	343	343 @ 1 A g^{-1} 193 @ 5 A g^{-1}	[130d]
	$TiO_2@Ti_3C_2T_x$	Na^+	960	5000	116	93 @ 1.92 A g^{-1} 68 @ 3.84 A g^{-1}	[137]
	PDDA-BP/Ti_3C_2	Na^+	1000	2000	658	461 @ 2 A g^{-1}	[130c]
	$MoSe_2/Ti_3C_2$@C	K^+	1000	300	317	212 @ 5 A g^{-1}	[132]
			5000	300	207	183 @ 10 A g^{-1}	
	VO_2/Ti_3C_2	Na^+	5000	200	98.5	206 @ 1.6 A g^{-1}	[136]
	CoS/Ti_3C_2	Na^+	2000	1700	267	272 @ 5 A g^{-1}	[134]
	Ti_3C_2@Sb	K^+	500	500	≈214	270.81 @ 0.5 A g^{-1}	[129]
	Ti_3C_2/NiCoP	Na^+	1000	2000	261.7	240.1 @ 2 A g^{-1}	[130a]
	MoS_2/Ti_3C_2	K^+	200	50	145.5	168.2 @ 0.5 A g^{-1}	[131b]

Table 5. Continued.

Material		Cycling performance				Rate performance Capacity [mAh g^{-1}]	Ref.
		Ion storage system	Current density [mA g^{-1}]	Cycle number	Capacity retention		
MXene-derived materials	$NaTi_{1.5}O_{8.3}$	Na^+	200	150	≈135	101 @ 2 A g^{-1}	[138d]
	$K_2Ti_4O_9$	K^+	200	900	≈45	81 @ 0.3 A g^{-1}	[138d]
	M-TiO_2–rGO	Na^+	1000	8000	≈87	79 @ 2 A g^{-1}	[138e]
	$Na_{0.23}TiO_2/Ti_3C_2$	Na^+	2000	4000	56	47 @ 3 A g^{-1}	[110]
	NTO/rGO	Na^+	5000	10 000	72	97 @ 5 A g^{-1}	[138i]
	KTO/rGO	K^+	2000	700	75	84 @ 1 A g^{-1}	[138i]
	TiO_2/rGO	K^+	1000	1000	≈85	107.1 @ 1 A g^{-1}	[138f]
	TiO_xN_y/C	K^+	200	1200	150	72 @ 1.6 A g^{-1}	[138h]
	$Na_2Ti_3O_7$@C	Na^+	2000	200	119	115 @ 2 A g^{-1}	[138g]
	TiS_2@C	Na^+	10 000	5000	321.4	387 @ 10 A g^{-1}	[138c]
	CoS_2/CNTs/TiO_xN_y	Na^+	1000	100	72	166 @ 2 A g^{-1}	[139]

V_2CT_2 MXene, MgF_2 or MgH_2 is formed instead of Mg-ion intercalation. Nevertheless, multilayer V_2CO_2 MXene displayed a relatively high average voltage of about 1.5 V with a low migration barrier of 480 meV, suggesting the potential for MIB anodes.[147] The findings here also reveal the importance of regulating the surface chemistry of MXenes in enhancing their electrochemical performance as MIB electrodes.

Because of the huge challenges facing the development of suitable cathode materials for MIBs, the concept of hybrid Mg^{2+}/Li^+ battery has been proposed. Such a hybrid system

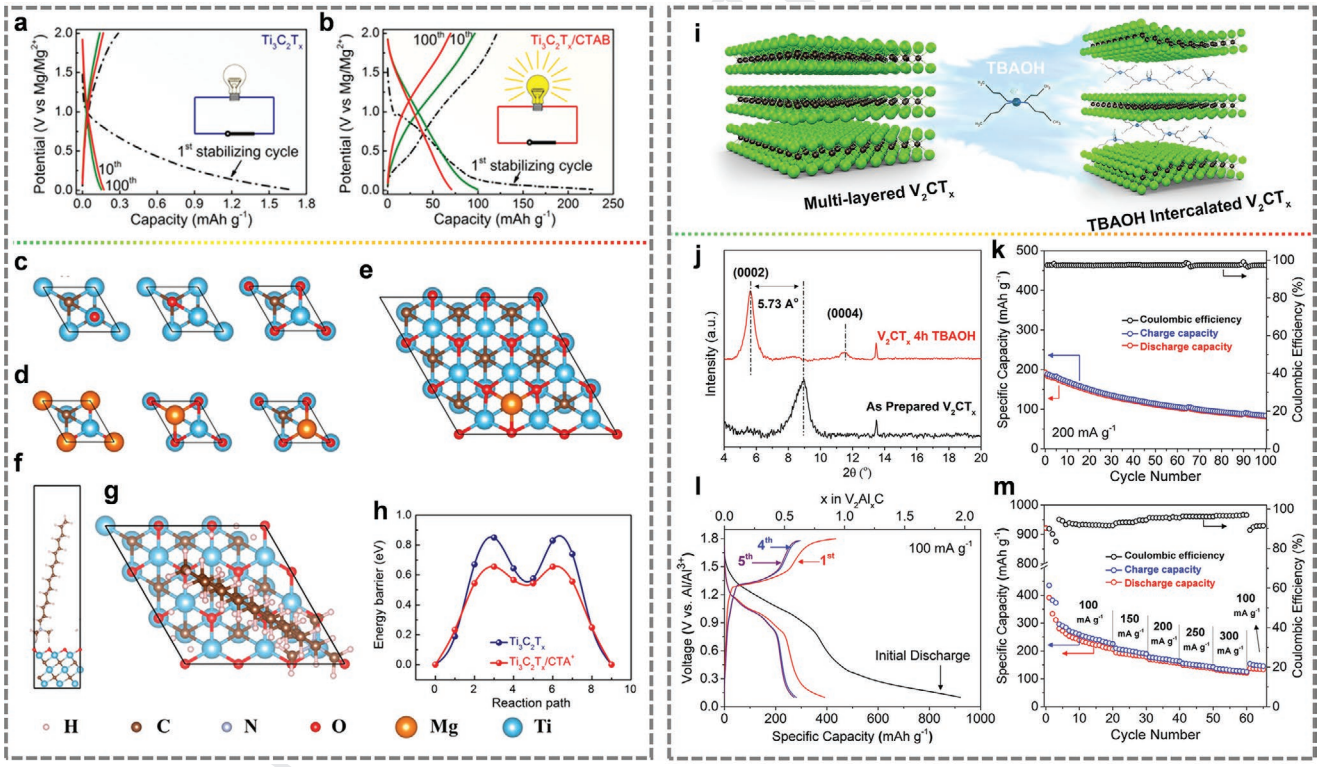

Figure 16. Charge/discharge profiles of a) $Ti_3C_2T_x$ electrode, and b) $Ti_3C_2T_x$/CTAB electrode at the 10th (green lines) and the 100th (red lines) cycles at 50 mA g^{-1}. Top view of the structures of c) an O atom and d) a Mg atom adsorbed on the 1×1 Ti_3C_2 surface at the top site, body-centered cubic (bcc) site, and face-centered cubic (fcc) site, respectively. Top view of e) Mg^{2+} and g) CTA^+ as well as f) side view of CTA^+ adsorbed on the 3×3 Ti_3C_2O surface. h) Diffusion profile of Mg^{2+} on Ti_3C_2O and CTA^+/Ti_3C_2O surface in nudged elastic band calculations. Reproduced with permission.[142] Copyright 2018, American Chemistry of Society. i) Schematic illustration of interlayer expansion of multilayer V_2CT_x MXene through TBAOH intercalation. j) XRD patterns of V_2CT_x and TBAOH intercalated V_2CT_x. k) Cyclic performance, l) charge–discharge curves of the first five cycles, and m) rate performance of TBAOH intercalated few-layer V_2CT_x. Reproduced with permission.[33a] Copyright 2017, American Chemistry of Society.

consists of an Mg anode, a lithium-ion intercalation cathode, and a Mg^{2+}/Li^+ dual-salt electrolyte. The hybrid Mg^{2+}/Li^+ battery could potentially inherit the advantages of fast Li^+ intercalation kinetics, high voltage and high capacity of LIB cathodes, as well as the low cost, dendrite-free features of Mg anodes.[148] Mo_2CT_x, $Ti_3C_2T_x$, and prelithiated V_2CT_x MXenes have shown promising applications for hybrid Mg^{2+}/Li^+ batteries.[149] Notably, the prelithiated V_2CT_x electrode exhibits a reversible capacity of up to 230.3 mAh g^{-1} at 20 mA g^{-1} with 82% capacity retention after 480 cycles.[149b]

5.3.2. Zinc-Ion Storage

Zinc-based batteries are technologies that have been around for centuries. Since the first utilization of zinc anode in 1799,[150] it has been regarded as an ideal negative electrode because of its high theoretical capacity (820 mAh g^{-1} or 5855 mAh cm^{-3}), low cost, low redox potential (–0.76 V vs standard hydrogen electrode) and high safety. Unlike the rechargeable alkaline Zn–MnO_2 batteries, whose cycle life is severely hampered by the formation of zinc dendrite and irreversible ZnO and $Zn(OH)_2$ formation, the rechargeable aqueous ZIBs that use neutral or slightly acidic electrolytes (e.g., $ZnSO_4$) pioneered by Yamamoto et al. in 1986 virtually eliminate the dendritic zinc deposition.[151] Recently, aqueous rechargeable zinc-ion storage has regained significant attention. Previous studies have shown that MXenes are capable of storing zinc ions and can be used for zinc-ion capacitors.[152] For example, a degradable Zn-MXene capacitor was fabricated by Zhi et al.[152b] The capacitor can maintain 82.5% of the capacitance after 1000 cycles, along with a very low self-discharge rate of 6.3 mV h^{-1}. More importantly, the whole capacitor can be totally degraded within 7.25 days. The performance and degradation rate surpass many reported supercapacitor devices. Besides, aqueous zinc-ion capacitors based on MnO_2 cathode and MXene anode were also reported.[153] Moreover, a porous 3D MXene-rGO aerogel cathode was synthesized for the zinc-ion capacitor, which displayed an ultralong cycle life with above 95% capacity retention over 75 000 cycles.[154] In addition, $MnO_x@Ti_3C_2T_x$ hierarchical structure was designed as the cathode of ZIBs.[155] The assembly exhibited excellent rate performance with 50% capacity retention when the rate increased from 0.1 to 10 A g^{-1}. Interestingly, Zhi et al. found an unusual capacity enhancement during cycling when using V_2CT_x MXene as the cathode for zinc-ion hybrid batteries.[156] Such an abnormality is originated from the exfoliation of MXene and its oxidization into V_2O_5 during the repeated cycling process. As a result, a capacity as high as 508 mAh g^{-1} and an energy density of 386.2 Wh kg^{-1} were achieved.

5.3.3. Aluminum-Ion Storage

Aluminum is the most abundant metal in the earth's upper crust. An Al-based redox couple involves three electron transfer and therefore theoretically provides more capacity compared to the LIBs. In addition, Al-ion batteries (AIBs) are much safer and cheaper than LIBs. However, the large size of solvated Al^{3+} ions in electrolytes and their strong bonding force with the host materials seriously hamper the development of AIBs. Previous simulations have predicted that bare MXenes and O-terminated MXenes exhibit high capacities toward the aluminum-ion storage.[52b] Unfortunately, up to now, only V_2CT_x MXene shows reasonable Al-ion storage capacity. Beidaghi et al. demonstrated that Al^{3+} could reversibly intercalate into the V_2CT_x MXene host.[33a] Moreover, the electrochemical performance can be improved by delaminating multilayer V_2CT_x into few-layer counterpart with the assistance of TBAOH (Figure 16i). The optimized MXene cathode can deliver a high capacity of over 300 mAh g^{-1} at a current density of 100 mA g^{-1}, along with good rate performance (Figure 16j–m). Although a continuous capacity decay was observed, the specific capacity, intercalation voltage, and cycle life reported here are among the best achieved for intercalation-type AIB cathodes.

To summarize, although theoretical predictions indicate that MXenes have very high capacities for various multivalent ions (e.g., Mg^{2+}, Zn^{2+}, Al^{3+}) storage, the experimental progress is still limited. According to the existing publications, the surface modification and structure manipulation are effective ways to improve the metal ion storage performance of MXenes. Further, the DFT calculation results suggest that bare MXenes or O-terminated MXenes generally exhibit better performance than the F- or OH-terminated ones.[52b,c] Therefore, the synthesis of MXene with controllable surface chemistry is of significant importance for the future development of MXene electrodes for multivalent metal ion storage.

5.4. Anode Protection for Metal Batteries

Currently, portable electronics and electric vehicles require energy storage devices with increasingly higher energy density. Metal batteries, including metal–sulfur, metal–air, metal–oxygen, and metal–CO_2 batteries exhibit much higher energy densities compare to LIBs owing to the high theoretical specific capacities of metal anodes (e.g., Li, Na, K, Zn). However, the development of metal anodes is hampered by their high reactivity, uneven dendrite formation, large volumetric changes during cycling, poor long-term durability as well as safety issues.[103g,157] A vast amount of work has therefore been conducted to tackle these problems, among which metal anode protection has been demonstrated to be an effective way. Approaches developed to protect metal anodes from uneven dendrite formation can be classified into three categories: i) metal anode modification (e.g., trapping metals in porous hosts by controlling metal diffusion, regulating metal deposition by manipulating electrochemical reactions); ii) building an (artificial) SEI film on the metal anodes; iii) electrolyte engineering for achieving safe and stable metal anodes.[103g,157] MXene-based materials have some favorable features that are beneficial for efficient metal anode protection. For instance, the high conductivity and hydrophilicity properties of MXenes allow fast electronic and ionic transport, the large interlayer spacing can greatly alleviate the volumetric changes during metal plating/stripping, the 2D structure induces uniform nucleation and growth of metals on MXene surface. Moreover, the fluorine termination could lead to the formation of uniform, dense and durable SEI films dominated with LiF salt at the anode/electrolyte interface.[158] As a consequence, tremendous efforts have been devoted to the protection of metal anodes using MXenes.

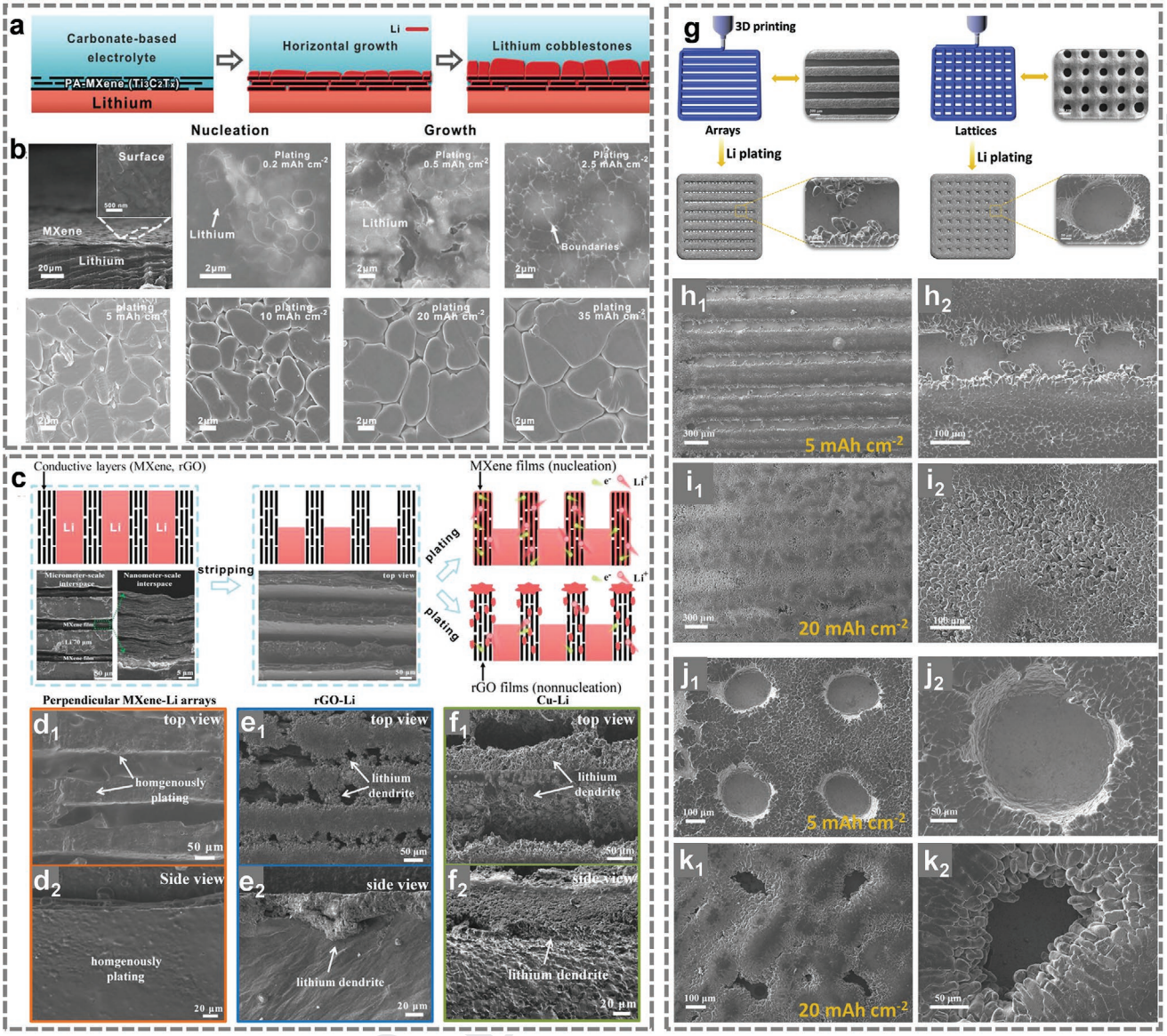

Figure 17. a) Schematic illustration of lithium plating on parallelly aligned MXene layers. b) SEM images of parallelly aligned MXene layers on lithium and MXene–lithium electrodes with various levels of lithium plating, showing the dendrite-free surface. Reproduced with permission.[158] Copyright 2019, Wiley. c) Schematic illustration of the stripping and plating states of perpendicular MXene–Li and rGO–Li arrays. Top-view and side-view SEM images of lithium plating on the d) perpendicular MXene–Li arrays, e) rGO–Li arrays, and f) Cu–Li arrays, respectively. Reproduced with permission.[159a] Copyright 2020, Wiley. g) Scheme of 3D printing MXene arrays and lattices to guide the nucleation and growth of lithium. SEM images of 3D printing-MXene arrays with h) 5 and i) 20 mAh cm^{-2} lithium plating at 0.5 mA cm^{-2}. SEM images of 3D printing-MXene lattices with j) 5 and k) 20 mAh cm^{-2} lithium plating at 0.5 mA cm^{-2}. Reproduced with permission.[159b] Copyright 2020, Elsevier.

5.4.1. Lithium Metal Anode

Yang's group developed several strategies to achieve dendrite-free lithium anodes via using different MXene architectures.[111,158,159] For example, the parallel alignment of MXene layers on top of the lithium anode can effectively induce the formation of horizontally orientated deposition of lithium (**Figure 17**a,b). This method greatly reduces the dendrite formation, thus leading to a long cycle life up to 900 h and an outstanding rate capability up to 35 mAh cm^{-2}.[158] Later, perpendicular MXene–Li arrays with dual periodic interphases, i.e., nanometer-scale interspaces in MXene walls and micrometer-scale interspaces between MXene walls, were fabricated through a rolling-cutting strategy.[159a] This unique structure not only enables fast ion transport upon lithium stripping and plating, but also effectively homogenizes the electric fields, which further prohibits the notorious lighting rod effect and accommodates the volumetric changes. The perpendicular MXene–Li arrays anode possessed a high capacity of 2056 mAh g^{-1}, good rate performance and long cycle life up to 1700 h, much superior to rGO-Li or Cu–Li arrays (Figure 17c–f). Recently, the emerging 3D printing technique was also applied

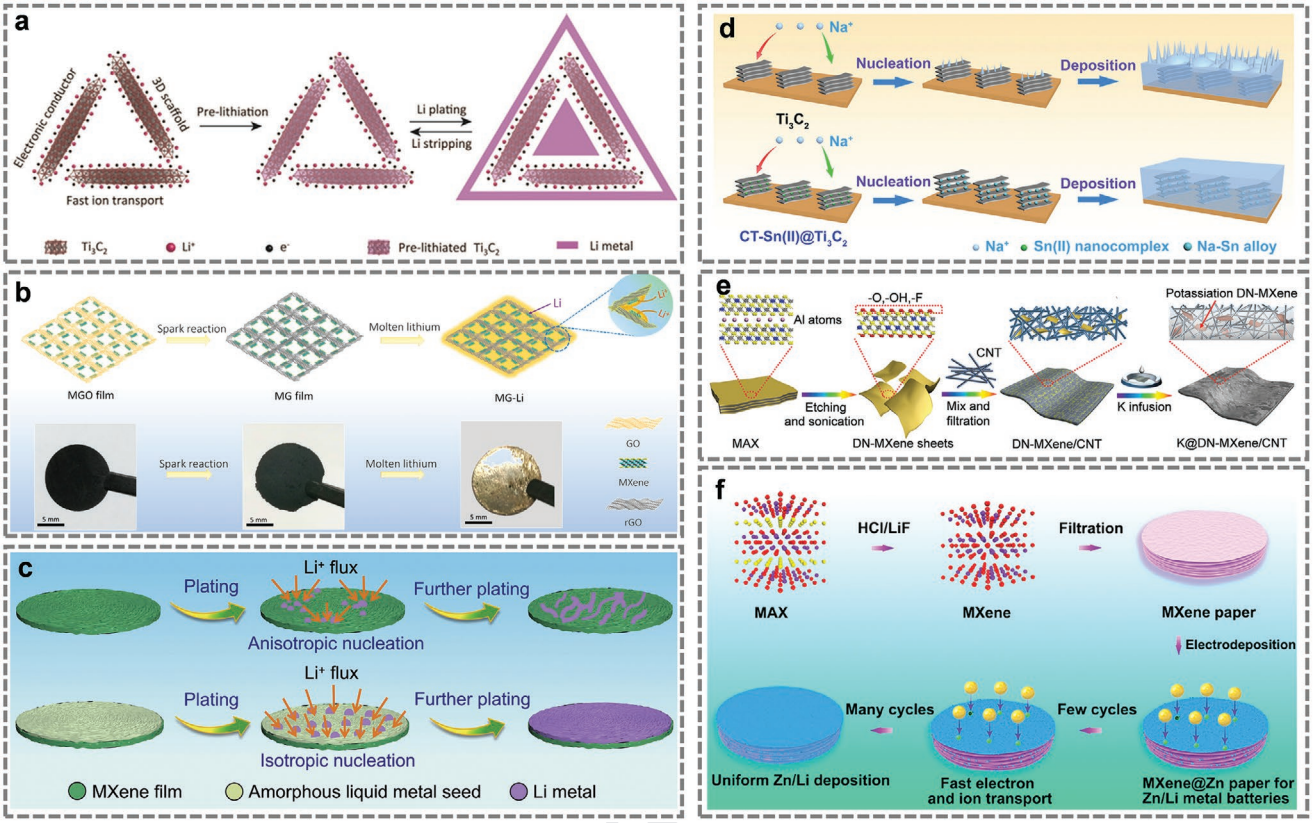

Figure 18. a) The lithium stripping/plating process on Ti_3C_2 MXene/rGO aerogel. Reproduced with permission.[160] Copyright 2018, Wiley. b) The fabrication process of the 3D MXene/graphene-Li anode and the corresponding photographs of the MXene/graphene oxide film, MXene/graphene film, and MXene/graphene-Li anode. Reproduced with permission.[161] Copyright 2019, American Chemical Society. c) The plating process of Li on MXene film and MXene/liquid metal film, respectively. Reproduced with permission.[163] Copyright 2020, Elsevier. d) The comparison of Na nucleation, deposition in Ti_3C_2 and CT-Sn(II)@Ti_3C_2 matrixes. Reproduced with permission.[164] Copyright 2019, Wiley. e) The preparation of the DN-MXene/CNT scaffold and K@DN-MXene/CNT metallic anodes. Reproduced with permission.[165] Copyright 2019, Wiley. f) The synthesis process of MXene paper and the Li/Zn deposition on it. Reproduced with permission.[166] Copyright 2019, American Chemical Society.

to fabricate MXene arrays and MXene lattices as lithium hosts (Figure 17g). Because of the largely available interspaces in MXene arrays, the growth of lithium was confined in the strip-shaped channels (Figure 17h–k).[159b]

Besides, other 3D scaffolds for Li metal anodes such as MXene/rGO aerogel (**Figure 18**a),[160] MXene/graphene framework (Figure 18b),[161] and interlayer-calated thin lithium electrode[162] were also designed for high performance and dendrite-free lithium metal batteries. Notably, Qian et al. developed a novel method by using an amorphous liquid metal nucleation seed on MXene films to induce isotropic lithium nucleation and growth, so as to inhibit the growth of lithium dendrite (Figure 18c).[163]

5.4.2. Other Metal Anodes (Na, K, Zn)

Apart from lithium metal anode, MXene-based materials have also been employed to protect other metal anodes from dendrite formation. For instance, Li et al. presented a Sn^{2+} pillared Ti_3C_2 MXene scaffold (CT-Sn(II)@Ti_3C_2) as a stable matrix for high-performance dendrite-free sodium metal anodes.[164] The intercalation of sodiophilic seeds (Sn^{2+}) into the MXene layers can effectively avoid the dendrite growth on the favorable sites. Meanwhile, the expanded interlayer distance can mitigate volumetric change and accommodate more sodium ions (Figure 18d). Wang et al. fabricated a defect-rich and nitrogen-containing MXene/CNT free-standing host for potassium metal (K@DN-MXene/CNT) and used it as anode for dendrite free K-S batteries (Figure 18e).[165] The fast K^+ diffusion and electronic transport in the highly conductive scaffold decreased the local current density and achieved the homogeneous ionic flux during plating/stripping. Both theoretical calculations and experimental results verified that the 3D scaffold could induce the homogeneous nucleation and thus a uniform distribution of potassium.[165] Notably, Qian et al. showed that the flexible and free-standing $Ti_3C_2T_x$ MXene@Zn paper could serve as a matrix for both aqueous zinc and nonaqueous lithium metal batteries (Figure 18f).[166] In the former case, the stable and reversible zinc plating/stripping process was enabled by the high conductivity and good hydrophilicity of the MXene@Zn films. While in the latter case, the zinc in the MXene@Zn host severed as the nucleation agent because of the Zn–Li alloy reaction.

It is evident from the above results that benefiting from the high conductivity, large interlayer spacing, and abundant surface functional groups (particularly the −F), MXene-based

materials have shown great potential in protecting metal anodes from the growth of dendrites. However, it should be noted that the application of MXenes in metal anode protection is still in the infancy stage and more work is required in this direction.

6. Conclusion and Perspective

In this review, we have summarized the synthetic strategies and properties of MXenes and the recent progress on using MXenes for energy storage applications. Specifically, we covered various strategies for designing MXene and MXene-based materials and their applications in alkali-ion (e.g., Na^+, K^+) storage, multivalent-ion (e.g., Mg^{2+}, Zn^{2+}, and Al^{3+}) storage, and metal batteries (**Figure 19**). The versatile MXenes with high conductivity and rich surface terminations have shown great potential and are being intensively evaluated as different components in energy storage devices, including electrodes, metal anode protective layers, sulfur hosts, separator interlayers, and conductive additives. Despite the significant progress that has been made in recent years, many challenges remain. In our view, there are several important research directions that are needed to make further progress in using MXenes and MXene-based materials for electrochemical energy storage applications.

The current synthesis methods of MXenes generally involve the use of HF, which is harmful and hazardous for human beings. Identifying other etchants that are safer than HF as well as developing low cost, efficient and environmentally-friendly etching processes are of great interest and importance for the large-scale production of high quality MXenes. The Lewis acid molten salts and electrochemical routes are good examples, while more cost-efficient and scalable methods are required. What's more, it is clear that the synthesis route of MXenes could also affect their conductivities. So exploring new etchants that have less environmental impacts might also lead to improved MXene conductivity. One the other hand, bottom-up methods (e.g., CVD) have shown their efficacy of directly synthesizing metal carbides and thus could also be a promising approach to synthesize high quality MXenes. Such a process avoids the use of etchants and therefore, can obtain "pure" MXenes without functional groups, which offers the opportunity to study the intrinsic properties of MXenes and could be appealing for many specific applications.

The surface chemistry of MXenes plays an essential role in determining their properties and therefore the electrochemical activity. These terminations can selectively interact with specific compounds (e.g., S termination with LiPSs) and thus affect the energy storage performance (e.g., specific capacity, coulombic efficiency). Regulating the surface termination, including the type and composition can further optimize the electrochemical performance of MXenes but remains challenging. The molten salts method has shown great ability to control and change the functional groups.[43–45] However, much more efforts are required to explore more facile approaches to synthesize MXenes with controllable terminations, especially those

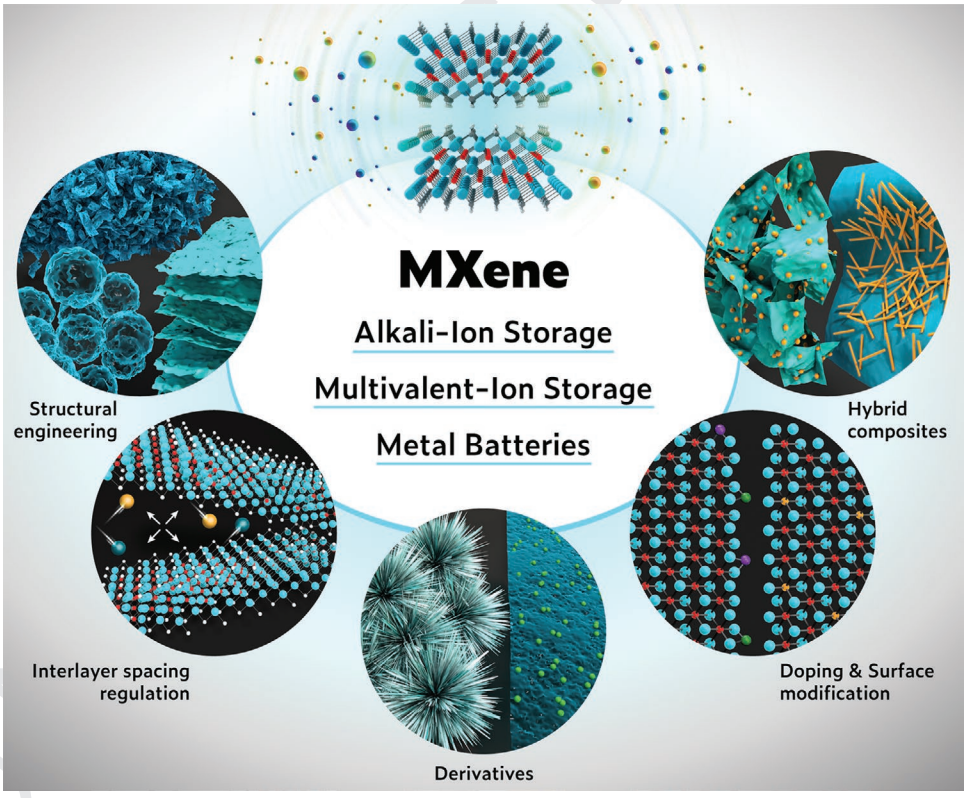

Figure 19. Schematic illustration of the various strategies that can be used to exploit MXenes to improve the performance of emerging batteries (beyond the Li ion).

with the same kind of moieties and those without any terminations. A careful selection of etchants and delicately designed etching process can be helpful. Further, post-treatment could be another direction to adjust the surface chemistry. For instance, plasma modification is verified to be an effective way to manipulate the surface chemistry of various materials.[167]

Delaminated MXene flakes possess more active sites and larger surface area but tend to restack or aggregate because of the van der Waals interaction and/or hydrogen bonding force. In this respect, hybridizing MXenes with other low-dimensional nanomaterials is an effective approach that not only prevents MXenes from restacking but also improves their performance. For instance, hybridizing MXenes with conductive polymers (e.g., polyaniline, polypyrrole), 2D nanosheets (e.g., MoS_2, $MoSe_2$), one-dimensional nanotube/nanorods (e.g., CNT), and 0D quantum dots has been shown enhanced electrochemical performance. Apart from traditional chemical methods, physical deposition (e.g., atomic layer deposition)[168] can be another possible direction to synthesize MXene-based composites with precisely controlled composition.

MXenes typically suffer from rapid oxidation/degradation in the air and water.[169] On the one hand, the surface oxides might enhance the electrochemical activity. On the other hand, they could reduce the conductivity and further bring about complexities in studying the intrinsic properties of MXenes. Thorough investigations on the oxidation behavior are required to better understand and control the oxidation process. In the meantime, preventing MXenes from oxidation is also pivotal as the high stability is a prerequisite for their practical applications. Therefore, it is crucial to develop effective approaches that can improve the stability of MXene under various conditions. It has demonstrated that storing the MXene colloidal solutions in hermetic inert gas-filled bottles at low temperatures (e.g., 5 °C) is an efficient way to eliminate the main oxidant (i.e., dissolved oxygen) of the MXene flakes.[169a] Besides, surface coatings also can effectively protect MXene flakes from irreversible oxidization,[170] yet the optimal composition of surface coating layers and the coating conditions that could prevent the oxidation but without affecting the electrochemical activity of MXenes remain to be further explored.

MXene electrodes typically show pseudocapacitive characteristic with heavily sloped discharge curves. Given the high electronic conductivities, MXene electrodes normally exhibit excellent rate performance and are good candidates for high rate hybrid ion capacitors, however, might be less appealing for high energy devices owing to their low capacitances. Fortunately, the versatile composition of MXenes enables the possibility of tuning their electrochemical performance; whereas further hybridizing MXenes with other high specific capacity materials provides the opportunity of using MXenes for high energy/power density devices.

In spite of the thriving development of MXenes in the field of energy storage, the ion dynamic and charge storage behavior of MXenes in various energy storage devices (especially the $K^+/Zn^{2+}/Al^{3+}$ ion batteries) are still not fully understood. A better understanding of the reaction mechanism is vital to provide valuable information for the design and optimization of MXene electrodes, which can be achieved by using various state-of-the-art in situ and ex situ characterizations and analyses, including TEM, NMR, and synchrotron investigations (e.g., XRD, X-ray absorption near-edge spectroscopy, soft X-ray absorption spectroscopy).

Despite the fact that more than 30 MXenes have been experimentally synthesized, the most studied and best optimized one is still the first MXene, i.e., $Ti_3C_2T_x$. Although it exhibits various unique and promising features, it is by no means the best MXene for every application. Different properties and performances can be reasonably expected given the large family of MXenes with various compositions. For example, M_2CT_x MXenes (e.g., V_2CT_x) possess the higher theoretical gravimetric capacity (>400 mAh g^{-1}) toward mobile ion storage because of their lighter molar mass than $Ti_3C_2T_x$.[52c] In addition, nitride MXenes have been predicted to have a higher conductivity and could provide faster electronic transport.[171] Unfortunately, the etching and exfoliation conditions for MXenes beyond $Ti_3C_2T_x$ are far from optimized because of the considerably less research activity (compared to that of $Ti_3C_2T_x$). On the other hand, this also means that there is a huge room for further improving the overall performance. We anticipate that more MXenes (beyond $Ti_3C_2T_x$) will be intensively investigated in the years ahead. A prerequisite for such development is the reliable methods for the preparation of these (non-Ti) MXenes, which unfortunately are still premature (especially for the nitride MXenes). More efforts should therefore be devoted to developing efficient methods for the large-scale and controllable synthesis of (nitride) MXenes. This will also help to understand the chemistry of these MXenes and further to optimize their properties.

Finally, it would be practically meaningless if the target material has no potential to transfer "from lab to fab." Although 2D materials have shown great potential in many fields, only few of them have successfully been commercialized. The main limitation is that the materials for laboratorial use are produced in very small quantities and the cost is often less considered. Further, there are also scalability issues since some precursors are not sufficiently abundant which would increase the overall cost. In this regard, Ti-based MXenes are the most appealing as the precursors (i.e., Ti, Al, C) are relatively abundant and cheap. Further, MXenes are generally produced by selectively etching the MAX precursors through scalable chemical routes, which has the potential to meet the requirements of industrial production. Another potential issue is whether MXenes produced at industrial scale (e.g., kilogram level) could preserve their desirable properties. A recent study demonstrated that there is no loss of properties of $Ti_3C_2T_x$ MXene when the batch size is increased from 1 to 50 g.[172] Though much larger size is required for industrial usage, it points out the possibility of producing MXenes at large scale without sacrificing their excellent properties. In fact, Murata Manufacturing Co., Ltd. is pushing forward with the production of MXenes at kilogram scale by using larger reactors.[173] Nonetheless, more efforts are still needed to reach larger scale, as well as to develop safer, more energy-efficient, and cost-efficient approaches. This requires not only the development of the best practices for processing MXenes in various forms (e.g., powder, films, etc.), but also the deep understanding of the synthesis–structure–property relationship. In addition, the electrochemical measurements of MXenes, especially those that hold the potential to be commercialized, should follow the standard procedure used in industry.

However, some MXenes, such as Sc-based MXenes, are highly unlikely to be used in widespread applications due to the high cost and therefore investigations at laboratorial level would be appropriate so as to study the fundamental properties. As both the scientist and engineer communities are working synergistically to overcome the challenges (e.g., safety, scalability, stability), we believe that major breakthroughs will be made in the commercialization of MXenes in the future.

Acknowledgements

F.M. and H.L. contributed equally to this work. The research reported in this publication was supported by King Abdullah University of Science and Technology (KAUST).

Conflict of Interest

The authors declare no conflict of interest.

Keywords

2D materials, energy storage, MXene, rechargeable batteries

Received: June 13, 2020
Revised: July 31, 2020
Published online:

[1] a) J.-M. Tarascon, M. Armand, *Materials for Sustainable Energy: A Collection of Peer-Reviewed Research and Review Articles from Nature Publishing Group*, World Scientific, Singapore **2011**, p. 171; b) J. R. Miller, P. Simon, *Science* **2008**, *321*, 651; c) M. Winter, R. J. Brodd, *Chem. Rev.* **2004**, *104*, 4245; d) W. Zhang, F. Zhang, F. Ming, H. N. Alshareef, *EnergyChem* **2019**, *1*, 100012; e) D. P. Dubal, O. Ayyad, V. Ruiz, P. Gomez-Romero, *Chem. Soc. Rev.* **2015**, *44*, 1777.

[2] M. Li, J. Lu, Z. Chen, K. Amine, *Adv. Mater.* **2018**, *30*, 1800561.

[3] a) C.-X. Zu, H. Li, *Energy Environ. Sci.* **2011**, *4*, 2614; b) F. Risacher, B. Fritz, *Aquat. Geochem.* **2009**, *15*, 123.

[4] a) L. Peng, Y. Zhu, D. Chen, R. S. Ruoff, G. Yu, *Adv. Energy Mater.* **2016**, *6*, 1600025; b) H. Kim, J. C. Kim, M. Bianchini, D.-H. Seo, J. Rodriguez-Garcia, G. Ceder, *Adv. Energy Mater.* **2018**, *8*, 1702384; c) Y. Li, Y. Lu, C. Zhao, Y.-S. Hu, M.-M. Titirici, H. Li, X. Huang, L. Chen, *Energy Storage Mater.* **2017**, *7*, 130; d) X. Xiang, K. Zhang, J. Chen, *Adv. Mater.* **2015**, *27*, 5343; e) J. C. Pramudita, D. Sehrawat, D. Goonetilleke, N. Sharma, *Adv. Energy Mater.* **2017**, *7*, 1602911; f) C. Vaalma, D. Buchholz, S. Passerini, *Curr. Opin. Electrochem.* **2018**, *9*, 41; g) Q. Zhang, Z. Wang, S. Zhang, T. Zhou, J. Mao, Z. Guo, *Electrochem. Energy Rev.* **2018**, *1*, 625; h) M. M. Huie, D. C. Bock, E. S. Takeuchi, A. C. Marschilok, K. J. Takeuchi, *Coord. Chem. Rev.* **2015**, *287*, 15; i) F. Ming, H. Liang, W. Zhang, J. Ming, Y. Lei, A.-H. Emwas, H. N. Alshareef, *Nano Energy* **2019**, *62*, 853; j) R. Mohtadi, M. Matsui, T. S. Arthur, S.-J. Hwang, *Angew. Chem., Int. Ed.* **2012**, *51*, 9780; k) L. Fu, N. Li, Y. Liu, W. Wang, Y. Zhu, Y. Wu, *Chin. J. Chem.* **2017**, *35*, 13; l) X. Zhang, Y. Tang, F. Zhang, C.-S. Lee, *Adv. Energy Mater.* **2016**, *6*, 1502588; m) S. K. Das, *Angew. Chem., Int. Ed.* **2018**, *57*, 16606; n) Y. Zhang, S. Liu, Y. Ji, J. Ma, H. Yu, *Adv. Mater.* **2018**, *30*, 1706310; o) F. Ming, H. Liang, Y. Lei, W. Zhang, H. N. Alshareef, *Nano Energy* **2018**, *53*, 11; p) C. Xu, B. Li, H. Du, F. Kang, *Angew. Chem., Int. Ed.* **2012**, *51*, 933; q) J. Ming, J. Guo, C. Xia, W. Wang, H. N. Alshareef, *Mater. Sci. Eng., R* **2019**, *135*, 58; r) P. He, Q. Chen, M. Yan, X. Xu, L. Zhou, L. Mai, C.-W. Nan, *EnergyChem* **2019**, *1*, 100022; s) B. Tang, L. Shan, S. Liang, J. Zhou, *Energy Environ. Sci.* **2019**, *12*, 3288; t) C. Li, X. Xie, S. Liang, J. Zhou, *Energy Environ. Mater.* **2020**, *3*, 146; u) F. Ming, H. Liang, Y. Lei, S. Kandambeth, M. Eddaoudi, H. N. Alshareef, *ACS Energy Lett.* **2018**, *3*, 2602; v) C. Xia, J. Guo, Y. Lei, H. Liang, C. Zhao, H. N. Alshareef, *Adv. Mater.* **2018**, *30*, 1705580.

[5] a) J. Besenhard, H. Fritz, *J. Electroanal. Chem. Interfacial Electrochem.* **1974**, *53*, 329; b) J. Besenhard, *Carbon* **1976**, *14*, 111; c) M. Arakawa, J.-I. Yamaki, *J. Electroanal. Chem. Interfacial Electrochem.* **1987**, *219*, 273; d) E. Peled, *J. Electrochem. Soc.* **1979**, *126*, 2047.

[6] a) K. Mizushima, P. Jones, P. Wiseman, J. B. Goodenough, *Mater. Res. Bull.* **1980**, *15*, 783; b) N. Godshall, I. Raistrick, R. Huggins, *Mater. Res. Bull.* **1980**, *15*, 561; c) G. Amatucci, J. Tarascon, L. Klein, *J. Electrochem. Soc.* **1996**, *143*, 1114.

[7] a) M. S. Whittingham, *Chem. Rev.* **2004**, *104*, 4271; b) M. S. Whittingham, *Science* **1976**, *192*, 1126; c) M. S. Whittingham, F. R. Gamble Jr., *Mater. Res. Bull.* **1975**, *10*, 363.

[8] K. S. Novoselov, A. K. Geim, S. V. Morozov, D. Jiang, Y. Zhang, S. V. Dubonos, I. V. Grigorieva, A. A. Firsov, *Science* **2004**, *306*, 666.

[9] M. Naguib, M. Kurtoglu, V. Presser, J. Lu, J. Niu, M. Heon, L. Hultman, Y. Gogotsi, M. W. Barsoum, *Adv. Mater.* **2011**, *23*, 4248.

[10] a) B. Anasori, M. R. Lukatskaya, Y. Gogotsi, *Nat. Rev. Mater.* **2017**, *2*, 16098; b) M. Naguib, V. N. Mochalin, M. W. Barsoum, Y. Gogotsi, *Adv. Mater.* **2014**, *26*, 992.

[11] a) M. Ghidiu, M. R. Lukatskaya, M.-Q. Zhao, Y. Gogotsi, M. W. Barsoum, *Nature* **2014**, *516*, 78; b) M.-Q. Zhao, X. Xie, C. E. Ren, T. Makaryan, B. Anasori, G. Wang, Y. Gogotsi, *Adv. Mater.* **2017**, *29*, 1702410; c) Z. Ling, C. E. Ren, M.-Q. Zhao, J. Yang, J. M. Giammarco, J. Qiu, M. W. Barsoum, Y. Gogotsi, *Proc. Natl. Acad. Sci. USA* **2014**, *111*, 16676.

[12] a) Z. Wang, H. Kim, H. N. Alshareef, *Adv. Mater.* **2018**, *30*, 1706656; b) C. Zhang, B. Anasori, A. Seral-Ascaso, S. H. Park, N. McEvoy, A. Shmeliov, G. S. Duesberg, J. N. Coleman, Y. Gogotsi, V. Nicolosi, *Adv. Mater.* **2017**, *29*, 1702678; c) G. Ying, S. Kota, A. D. Dillon, A. T. Fafarman, M. W. Barsoum, *FlatChem* **2018**, *8*, 25.

[13] a) Q. Jiang, N. Kurra, M. Alhabeb, Y. Gogotsi, H. N. Alshareef, *Adv. Energy Mater.* **2018**, *8*, 1703043; b) Q. Jiang, C. Wu, Z. Wang, A. C. Wang, J.-H. He, Z. L. Wang, H. N. Alshareef, *Nano Energy* **2018**, *45*, 266; c) Q. Jiang, N. Kurra, K. Maleski, Y. Lei, H. Liang, Y. Zhang, Y. Gogotsi, H. N. Alshareef, *Adv. Energy Mater.* **2019**, *9*, 1901061; d) N. Kurra, B. Ahmed, Y. Gogotsi, H. N. Alshareef, *Adv. Energy Mater.* **2016**, *6*, 1601372; e) B. Ahmed, D. H. Anjum, M. N. Hedhili, Y. Gogotsi, H. N. Alshareef, *Nanoscale* **2016**, *8*, 7580; f) N. Kurra, M. Alhabeb, K. Maleski, C.-H. Wang, H. N. Alshareef, Y. Gogotsi, *ACS Energy Lett.* **2018**, *3*, 2094; g) Y.-Y. Peng, B. Akuzum, N. Kurra, M.-Q. Zhao, M. Alhabeb, B. Anasori, E. C. Kumbur, H. N. Alshareef, M.-D. Ger, Y. Gogotsi, *Energy Environ. Sci.* **2016**, *9*, 2847; h) M. R. Lukatskaya, S. Kota, Z. Lin, M.-Q. Zhao, N. Shpigel, M. D. Levi, J. Halim, P.-L. Taberna, M. W. Barsoum, P. Simon, *Nat. Energy* **2017**, *2*, 17105; i) A. Byeon, A. M. Glushenkov, B. Anasori, P. Urbankowski, J. Li, B. W. Byles, B. Blake, K. L. Van Aken, S. Kota, E. Pomerantseva, *J. Power Sources* **2016**, *326*, 686; j) C. Zhan, M. Naguib, M. Lukatskaya, P. R. Kent, Y. Gogotsi, D.-e. Jiang, *J. Phys. Chem. Lett.* **2018**, *9*, 1223; k) M. Naguib, J. Come, B. Dyatkin, V. Presser, P.-L. Taberna, P. Simon, M. W. Barsoum, Y. Gogotsi, *Electrochem. Commun.* **2012**, *16*, 61.

[14] a) D. Xiong, X. Li, Z. Bai, S. Lu, *Small* **2018**, *14*, 1703419; b) J. Pang, R. G. Mendes, A. Bachmatiuk, L. Zhao, H. Q. Ta, T. Gemming, H. Liu, Z. Liu, M. H. Rummeli, *Chem. Soc. Rev.* **2019**, *48*, 72;

c) M. Greaves, S. Barg, M. A. Bissett, *Batteries Supercaps* **2020**, *3*, 214; d) X. Zhang, Z. Zhang, Z. Zhou, *J. Energy Chem.* **2018**, *27*, 73; e) H. Tang, Q. Hu, M. Zheng, Y. Chi, X. Qin, H. Pang, Q. Xu, *Prog. Nat. Sci.: Mater. Int.* **2018**, *28*, 133; f) L. Verger, V. Natu, M. Carey, M. W. Barsoum, *Trends Chem* **2019**, *1*, 656; g) Q. Jiang, Y. Lei, H. Liang, K. Xi, C. Xia, H. N. Alshareef, *Energy Storage Mater.* **2020**, *27*, 78; h) K. Li, M. Liang, H. Wang, X. Wang, Y. Huang, J. Coelho, S. Pinilla, Y. Zhang, F. Qi, V. Nicolosi, *Adv. Funct. Mater.* **2020**, 2000842; i) A. Zhang, R. Liu, J. Tian, W. Huang, J. Liu, *Chem. - Eur. J.* **2020**, *26*, 6342.

[15] a) S. Sun, C. Liao, A. M. Hafez, H. Zhu, S. Wu, *Chem. Eng. J.* **2018**, *338*, 27; b) X. Tang, X. Guo, W. Wu, G. Wang, *Adv. Energy Mater.* **2018**, *8*, 1801897.

[16] a) Q. Tao, M. Dahlqvist, J. Lu, S. Kota, R. Meshkian, J. Halim, J. Palisaitis, L. Hultman, M. W. Barsoum, P. O. Å. Persson, *Nat. Commun.* **2017**, *8*, 1; b) L. Qin, Q. Tao, A. El Ghazaly, J. Fernandez-Rodriguez, P. O. Å. Persson, J. Rosen, F. Zhang, *Adv. Funct. Mater.* **2018**, *28*, 1703808; c) R. Meshkian, M. Dahlqvist, J. Lu, B. Wickman, J. Halim, J. ThÄśrnberg, Q. Tao, S. Li, S. Intikhab, J. Snyder, *Adv. Mater.* **2018**, *30*, 1706409; d) P. Srimuk, J. Halim, J. Lee, Q. Tao, J. Rosen, V. Presser, *ACS Sustainable Chem. Eng.* **2018**, *6*, 3739; e) J. Halim, J. Palisaitis, J. Lu, J. Thörnberg, E. Moon, M. Precner, P. Eklund, P. O. Å. Persson, M. Barsoum, J. Rosen, *ACS Appl. Nano Mater.* **2018**, *1*, 2455; f) R. Meshkian, H. Lind, J. Halim, A. El Ghazaly, J. Thörnberg, Q. Tao, M. Dahlqvist, J. Palisaitis, P. O. Å. Persson, J. Rosen, *ACS Appl. Nano Mater.* **2019**, *2*, 6209.

[17] a) M. Naguib, O. Mashtalir, J. Carle, V. Presser, J. Lu, L. Hultman, Y. Gogotsi, M. W. Barsoum, *ACS Nano* **2012**, *6*, 1322; b) J.-C. Lei, X. Zhang, Z. Zhou, *Front. Phys.* **2015**, *10*, 276; c) M. Naguib, J. Halim, J. Lu, K. M. Cook, L. Hultman, Y. Gogotsi, M. W. Barsoum, *J. Am. Chem. Soc.* **2013**, *135*, 15966; d) R. Meshkian, L.-Å. Näslund, J. Halim, J. Lu, M. W. Barsoum, J. Rosen, *Scr. Mater.* **2015**, *108*, 147; e) J. Halim, S. Kota, M. R. Lukatskaya, M. Naguib, M.-Q. Zhao, E. J. Moon, J. Pitock, J. Nanda, S. J. May, Y. Gogotsi, *Adv. Funct. Mater.* **2016**, *26*, 3118; f) B. Soundiraraju, B. K. George, *ACS Nano* **2017**, *11*, 8892; g) A. Djire, A. Bos, J. Liu, H. Zhang, E. M. Miller, N. R. Neale, *ACS Appl. Nano Mater.* **2019**, *2*, 2785; h) P. Urbankowski, B. Anasori, K. Hantanasirisakul, L. Yang, L. Zhang, B. Haines, S. J. May, S. J. Billinge, Y. Gogotsi, *Nanoscale* **2017**, *9*, 17722; i) I. Persson, A. El Ghazaly, Q. Tao, J. Halim, S. Kota, V. Darakchieva, J. Palisaitis, M. W. Barsoum, J. Rosen, P. O. Å. Persson, *Small* **2018**, *14*, 1703676; j) J. Thörnberg, J. Halim, J. Lu, R. Meshkian, J. Palisaitis, L. Hultman, P. O. Å. Persson, J. Rosen, *Nanoscale* **2019**, *11*, 14720.

[18] a) Y. I. Jhon, J. Koo, B. Anasori, M. Seo, J. H. Lee, Y. Gogotsi, Y. M. Jhon, *Adv. Mater.* **2017**, *29*, 1702496; b) J. Zhou, X. Zha, F. Y. Chen, Q. Ye, P. Eklund, S. Du, Q. Huang, *Angew. Chem., Int. Ed.* **2016**, *55*, 5008; c) J. Zhou, X. Zha, X. Zhou, F. Chen, G. Gao, S. Wang, C. Shen, T. Chen, C. Zhi, P. Eklund, *ACS Nano* **2017**, *11*, 3841; d) B. Anasori, Y. Xie, M. Beidaghi, J. Lu, B. C. Hosler, L. Hultman, P. R. Kent, Y. Gogotsi, M. W. Barsoum, *ACS Nano* **2015**, *9*, 9507; e) R. Meshkian, Q. Tao, M. Dahlqvist, J. Lu, L. Hultman, J. Rosen, *Acta Mater.* **2017**, *125*, 476; f) Z. Jing, H. Wang, X. Feng, B. Xiao, Y. Ding, K. Wu, Y. Cheng, *J. Phys. Chem. Lett.* **2019**, *10*, 5721; g) J. Yang, X. Zhou, X. Luo, S. Zhang, L. Chen, *Appl. Phys. Lett.* **2016**, *109*, 203109; h) X. Zhan, C. Si, J. Zhou, Z. Sun, *Nanoscale Horiz.* **2020**, *5*, 235.

[19] a) P. Urbankowski, B. Anasori, T. Makaryan, D. Er, S. Kota, P. L. Walsh, M. Zhao, V. B. Shenoy, M. W. Barsoum, Y. Gogotsi, *Nanoscale* **2016**, *8*, 11385; b) M. H. Tran, T. Schäfer, A. Shahraei, M. Dürrschnabel, L. Molina-Luna, U. I. Kramm, C. S. Birkel, *ACS Appl. Energy Mater.* **2018**, *1*, 3908; c) J. Zhou, S. Lin, Y. Huang, P. Tong, B. Zhao, X. Zhu, Y. Sun, *Chem. Eng. J.* **2019**, *373*, 203; d) X. Wang, S. Lin, H. Tong, Y. Huang, P. Tong, B. Zhao, J. Dai, C. Liang, H. Wang, X. Zhu, *Electrochim. Acta* **2019**, *307*, 414; e) S. Zhao, X. Meng, K. Zhu, F. Du, G. Chen, Y. Wei, Y. Gogotsi, Y. Gao, *Energy Storage Mater.* **2017**, *8*, 42; f) M. Ghidiu, M. Naguib, C. Shi, O. Mashtalir, L. Pan, B. Zhang, J. Yang, Y. Gogotsi, S. J. Billinge, M. W. Barsoum, *Chem. Commun.* **2014**, *50*, 9517; g) R. Syamsai, A. N. Grace, *J. Alloys Compd.* **2019**, *792*, 1230; h) H. Lin, Y. Wang, S. Gao, Y. Chen, J. Shi, *Adv. Mater.* **2018**, *30*, 1703284; i) J. Yang, M. Naguib, M. Ghidiu, L.-M. Pan, J. Gu, J. Nanda, J. Halim, Y. Gogotsi, M. W. Barsoum, *J. Am. Ceram. Soc.* **2016**, *99*, 660; j) P. Cai, Q. He, L. Wang, X. Liu, J. Yin, Y. Liu, Y. Huang, Z. Huang, *Ceram. Int.* **2019**, *45*, 5761.

[20] G. Deysher, C. E. Shuck, K. Hantanasirisakul, N. C. Frey, A. C. Foucher, K. Maleski, A. Sarycheva, V. B. Shenoy, E. A. Stach, B. Anasori, *ACS Nano* **2020**, *14*, 204.

[21] G. Bei, B. J. Pedimonte, T. Fey, P. Greil, *J. Am. Ceram. Soc.* **2013**, *96*, 1359.

[22] M. Radovic, A. Ganguly, M. Barsoum, *J. Mater. Res.* **2008**, *23*, 1517.

[23] a) Y.-W. Cheng, J.-H. Dai, Y.-M. Zhang, Y. Song, *J. Phys. Chem. C* **2018**, *122*, 28113; b) J. Zhang, Y. Zhao, X. Guo, C. Chen, C.-L. Dong, R.-S. Liu, C.-P. Han, Y. Li, Y. Gogotsi, G. Wang, *Nat. Catal.* **2018**, *1*, 985; c) H. Kim, B. Anasori, Y. Gogotsi, H. N. Alshareef, *Chem. Mater.* **2017**, *29*, 6472.

[24] B. Ahmed, A. E. Ghazaly, J. Rosen, *Adv. Funct. Mater.* **2020**, 2000894.

[25] A. Petruhins, M. Dahlqvist, J. Lu, L. Hultman, J. Rosen, *Cryst. Growth Des.* **2020**, *20*, 55.

[26] a) M. Dahlqvist, J. Lu, R. Meshkian, Q. Tao, L. Hultman, J. Rosen, *Sci. Adv.* **2017**, *3*, e1700642; b) J. Lu, A. Thore, R. Meshkian, Q. Tao, L. Hultman, J. Rosen, *Cryst. Growth Des.* **2017**, *17*, 5704; c) L. Chen, M. Dahlqvist, T. Lapauw, B. Tunca, F. Wang, J. Lu, R. Meshkian, K. Lambrinou, B. Blanpain, J. Vleugels, *Inorg. Chem.* **2018**, *57*, 6237; d) M. Dahlqvist, A. Petruhins, J. Lu, L. Hultman, J. Rosen, *ACS Nano* **2018**, *12*, 7761.

[27] a) G. Eda, H. Yamaguchi, D. Voiry, T. Fujita, M. Chen, M. Chhowalla, *Nano Lett.* **2011**, *11*, 5111; b) X. Rui, Z. Lu, H. Yu, D. Yang, H. H. Hng, T. M. Lim, Q. Yan, *Nanoscale* **2013**, *5*, 556; c) J. Kang, J. D. Wood, S. A. Wells, J.-H. Lee, X. Liu, K.-S. Chen, M. C. Hersam, *ACS Nano* **2015**, *9*, 3596.

[28] M. W. Barsoum, T. El-Raghy, L. Farber, M. Amer, R. Christini, A. Adams, *J. Electrochem. Soc.* **1999**, *146*, 3919.

[29] T. El-Raghy, M. Barsoum, M. Sika, *Mater. Sci. Eng., A* **2001**, *298*, 174.

[30] M. Barsoum, J. Golczewski, H. Seifert, F. Aldinger, *J. Alloys Compd.* **2002**, *340*, 173.

[31] a) Y. Gogotsi, A. Nikitin, H. Ye, W. Zhou, J. E. Fischer, B. Yi, H. C. Foley, M. W. Barsoum, *Nat. Mater.* **2003**, *2*, 591; b) E. N. Hoffman, G. Yushin, M. W. Barsoum, Y. Gogotsi, *Chem. Mater.* **2005**, *17*, 2317; c) E. N. Hoffman, G. Yushin, T. El-Raghy, Y. Gogotsi, M. W. Barsoum, *Microporous Mesoporous Mater.* **2008**, *112*, 526; d) J. Chmiola, C. Largeot, P.-L. Taberna, P. Simon, Y. Gogotsi, *Science* **2010**, *328*, 480; e) V. Presser, J. McDonough, S.-H. Yeon, Y. Gogotsi, *Energy Environ. Sci.* **2011**, *4*, 3059.

[32] M. Naguib, V. Presser, N. Lane, D. Tallman, Y. Gogotsi, J. Lu, L. Hultman, M. W. Barsoum, *RSC Adv.* **2011**, *1*, 1493.

[33] a) A. VahidMohammadi, A. Hadjikhani, S. Shahbazmohamadi, M. Beidaghi, *ACS Nano* **2017**, *11*, 11135; b) B. Philippe, R. Dedryvère, M. Gorgoi, H. Rensmo, D. Gonbeau, K. Edström, *J. Am. Chem. Soc.* **2013**, *135*, 9829.

[34] N. Driscoll, A. G. Richardson, K. Maleski, B. Anasori, O. Adewole, P. Lelyukh, L. Escobedo, D. K. Cullen, T. H. Lucas, Y. Gogotsi, *ACS Nano* **2018**, *12*, 10419.

[35] O. Mashtalir, M. Naguib, B. Dyatkin, Y. Gogotsi, M. W. Barsoum, *Mater. Chem. Phys.* **2013**, *139*, 147.

[36] a) F. Shahzad, M. Alhabeb, C. B. Hatter, B. Anasori, S. M. Hong, C. M. Koo, Y. Gogotsi, *Science* **2016**, *353*, 1137; b) A. Lipatov,

M. Alhabeb, M. R. Lukatskaya, A. Boson, Y. Gogotsi, A. Sinitskii, *Adv. Electron. Mater.* **2016**, *2*, 1600255; c) X. Sang, Y. Xie, M.-W. Lin, M. Alhabeb, K. L. Van Aken, Y. Gogotsi, P. R. Kent, K. Xiao, R. R. Unocic, *ACS Nano* **2016**, *10*, 9193.

[37] C. Peng, P. Wei, X. Chen, Y. Zhang, F. Zhu, Y. Cao, H. Wang, H. Yu, F. Peng, *Ceram. Int.* **2018**, *44*, 18886.

[38] a) F. Liu, J. Zhou, S. Wang, B. Wang, C. Shen, L. Wang, Q. Hu, Q. Huang, A. Zhou, *J. Electrochem. Soc.* **2017**, *164*, A709; b) M. Wu, B. Wang, Q. Hu, L. Wang, A. Zhou, *Materials* **2018**, *11*, 2112; c) F. Liu, A. Zhou, J. Chen, J. Jia, W. Zhou, L. Wang, Q. Hu, *Appl. Surf. Sci.* **2017**, *416*, 781.

[39] J. Halim, M. R. Lukatskaya, K. M. Cook, J. Lu, C. R. Smith, L.-Å. Näslund, S. J. May, L. Hultman, Y. Gogotsi, P. Eklund, *Chem. Mater.* **2014**, *26*, 2374.

[40] L. Wang, H. Zhang, B. Wang, C. Shen, C. Zhang, Q. Hu, A. Zhou, B. Liu, *Electron. Mater. Lett.* **2016**, *12*, 702.

[41] T. Li, L. Yao, Q. Liu, J. Gu, R. Luo, J. Li, X. Yan, W. Wang, P. Liu, B. Chen, *Angew. Chem., Int. Ed.* **2018**, *57*, 6115.

[42] J. Mei, G. A. Ayoko, C. Hu, J. M. Bell, Z. Sun, *Sustainable Mater. Technol.* **2020**, *25*, e00156.

[43] M. Li, J. Lu, K. Luo, Y. Li, K. Chang, K. Chen, J. Zhou, J. Rosen, L. Hultman, P. Eklund, *J. Am. Chem. Soc.* **2019**, *141*, 4730.

[44] Y. Li, H. Shao, Z. Lin, J. Lu, L. Liu, B. Duployer, P. O. Å. Persson, P. Eklund, L. Hultman, M. Li, K. Chen, X.-H. Zha, S. Du, P. Rozier, Z. Chai, E. Raymundo-Piñero, P.-L. Taberna, P. Simon, Q. Huang, *Nat. Mater.* **2020**, *19*, 894.

[45] V. Kamysbayev, A. S. Filatov, H. Hu, X. Rui, F. Lagunas, D. Wang, R. F. Klie, D. V. Talapin, *Science* **2020**, eaba8311.

[46] a) W. Sun, S. Shah, Y. Chen, Z. Tan, H. Gao, T. Habib, M. Radovic, M. Green, *J. Mater. Chem. A* **2017**, *5*, 21663; b) S. Yang, P. Zhang, F. Wang, A. G. Ricciardulli, M. R. Lohe, P. W. Blom, X. Feng, *Angew. Chem., Int. Ed.* **2018**, *130*, 15717.

[47] a) C. Xu, L. Wang, Z. Liu, L. Chen, J. Guo, N. Kang, X.-L. Ma, H.-M. Cheng, W. Ren, *Nat. Mater.* **2015**, *14*, 1135; b) D. Geng, X. Zhao, Z. Chen, W. Sun, W. Fu, J. Chen, W. Liu, W. Zhou, K. P. Loh, *Adv. Mater.* **2017**, *29*, 1700072.

[48] O. Mashtalir, M. R. Lukatskaya, M.-Q. Zhao, M. W. Barsoum, Y. Gogotsi, *Adv. Mater.* **2015**, *27*, 3501.

[49] M. Naguib, R. R. Unocic, B. L. Armstrong, J. Nanda, *Dalton Trans.* **2015**, *44*, 9353.

[50] a) M. R. Lukatskaya, O. Mashtalir, C. E. Ren, Y. Dall'Agnese, P. Rozier, P. L. Taberna, M. Naguib, P. Simon, M. W. Barsoum, Y. Gogotsi, *Science* **2013**, *341*, 1502; b) O. Mashtalir, M. Naguib, V. N. Mochalin, Y. Dall'Agnese, M. Heon, M. W. Barsoum, Y. Gogotsi, *Nat. Commun.* **2013**, *4*, 1716.

[51] a) A. Lipatov, M. Alhabeb, H. Lu, S. Zhao, M. J. Loes, N. S. Vorobeva, Y. Dall'Agnese, Y. Gao, A. Gruverman, Y. Gogotsi, *Adv. Electron. Mater.* **2020**, *6*, 1901382; b) M. Lu, Z. Zhang, L. Kang, X. He, Q. Li, J. Sun, R. Jiang, H. Xu, F. Shi, Z. Lei, *J. Mater. Chem. A* **2019**, *7*, 12582; c) M. Alhabeb, K. Maleski, T. S. Mathis, A. Sarycheva, C. B. Hatter, S. Uzun, A. Levitt, Y. Gogotsi, *Angew. Chem., Int. Ed.* **2018**, *57*, 5444; d) H. Wu, M. Almalki, X. Xu, Y. Lei, F. Ming, A. Mallick, V. Roddatis, S. Lopatin, O. Shekhah, M. Eddaoudi, *J. Am. Chem. Soc.* **2019**, *141*, 20037; e) Z. Ma, X. Zhou, W. Deng, D. Lei, Z. Liu, *ACS Appl. Mater. Interfaces* **2018**, *10*, 3634.

[52] a) Y. Xie, M. Naguib, V. N. Mochalin, M. W. Barsoum, Y. Gogotsi, X. Yu, K.-W. Nam, X.-Q. Yang, A. I. Kolesnikov, P. R. Kent, *J. Am. Chem. Soc.* **2014**, *136*, 6385; b) Y. Xie, Y. Dall'Agnese, M. Naguib, Y. Gogotsi, M. W. Barsoum, H. L. Zhuang, P. R. Kent, *ACS Nano* **2014**, *8*, 9606; c) C. Eames, M. S. Islam, *J. Am. Chem. Soc.* **2014**, *136*, 16270.

[53] a) X. Liu, X. Shao, F. Li, M. Zhao, *Appl. Surf. Sci.* **2018**, *455*, 522; b) Q. Meng, J. Ma, Y. Zhang, Z. Li, C. Zhi, A. Hu, J. Fan, *Nanoscale* **2018**, *10*, 3385.

[54] a) Q. Peng, J. Guo, Q. Zhang, J. Xiang, B. Liu, A. Zhou, R. Liu, Y. Tian, *J. Am. Chem. Soc.* **2014**, *136*, 4113; b) R. B. Rakhi, B. Ahmed, M. N. Hedhili, D. H. Anjum, H. N. Alshareef, *Chem. Mater.* **2015**, *27*, 5314; c) R. Cheng, T. Hu, H. Zhang, C. Wang, M. Hu, J. Yang, C. Cui, T. Guang, C. Li, C. Shi, *J. Phys. Chem. C* **2019**, *123*, 1099.

[55] a) M. A. Hope, A. C. Forse, K. J. Griffith, M. R. Lukatskaya, M. Ghidiu, Y. Gogotsi, C. P. Grey, *Phys. Chem. Chem. Phys.* **2016**, *18*, 5099; b) M. Hu, T. Hu, Z. Li, Y. Yang, R. Cheng, J. Yang, C. Cui, X. Wang, *ACS Nano* **2018**, *12*, 3578.

[56] L. Li, *Comput. Mater. Sci.* **2016**, *124*, 8.

[57] a) Y. Xie, P. Kent, *Phys. Rev. B* **2013**, *87*, 235441; b) M. Khazaei, A. Ranjbar, M. Arai, S. Yunoki, *Phys. Rev. B* **2016**, *94*, 125152; c) M. Khazaei, M. Arai, T. Sasaki, C.-Y. Chung, N. S. Venkataramanan, M. Estili, Y. Sakka, Y. Kawazoe, *Adv. Funct. Mater.* **2013**, *23*, 2185; d) X. Zhang, Z. Ma, X. Zhao, Q. Tang, Z. Zhou, *J. Mater. Chem. A* **2015**, *3*, 4960.

[58] Q. Tang, Z. Zhou, P. Shen, *J. Am. Chem. Soc.* **2012**, *134*, 16909.

[59] a) K. J. Harris, M. Bugnet, M. Naguib, M. W. Barsoum, G. R. Goward, *J. Phys. Chem. C* **2015**, *119*, 13713; b) L. H. Karlsson, J. Birch, J. Halim, M. W. Barsoum, P. O. Persson, *Nano Lett.* **2015**, *15*, 4955; c) H.-W. Wang, M. Naguib, K. Page, D. J. Wesolowski, Y. Gogotsi, *Chem. Mater.* **2016**, *28*, 349.

[60] F. Chang, C. Li, J. Yang, H. Tang, M. Xue, *Mater. Lett.* **2013**, *109*, 295.

[61] M. Ghidiu, J. Halim, S. Kota, D. Bish, Y. Gogotsi, M. W. Barsoum, *Chem. Mater.* **2016**, *28*, 3507.

[62] J. Luo, W. Zhang, H. Yuan, C. Jin, L. Zhang, H. Huang, C. Liang, Y. Xia, J. Zhang, Y. Gan, *ACS Nano* **2017**, *11*, 2459.

[63] M. Ghidiu, S. Kota, J. Halim, A. W. Sherwood, N. Nedfors, J. Rosen, V. N. Mochalin, M. W. Barsoum, *Chem. Mater.* **2017**, *29*, 1099.

[64] a) D. Magne, V. Mauchamp, S. Celerier, P. Chartier, T. Cabioc'h, *Phys. Rev. B* **2015**, *91*, 201409; b) A. N. Enyashin, A. L. Ivanovskii, *J. Solid State Chem.* **2013**, *207*, 42; c) A. N. Enyashin, A. L. Ivanovskii, *J. Phys. Chem. C* **2013**, *117*, 13637.

[65] I. R. Shein, A. L. Ivanovskii, *Comput. Mater. Sci.* **2012**, *65*, 104.

[66] a) M. Kurtoglu, M. Naguib, Y. Gogotsi, M. W. Barsoum, *MRS Commun.* **2012**, *2*, 133; b) M. Khazaei, M. Arai, T. Sasaki, M. Estili, Y. Sakka, *Phys. Chem. Chem. Phys.* **2014**, *16*, 7841.

[67] M. Ashton, K. Mathew, R. G. Hennig, S. B. Sinnott, *J. Phys. Chem. C* **2016**, *120*, 3550.

[68] B. Anasori, C. Shi, E. J. Moon, Y. Xie, C. A. Voigt, P. R. C. Kent, S. J. May, S. J. L. Billinge, M. W. Barsoum, Y. Gogotsi, *Nanoscale Horiz.* **2016**, *1*, 227.

[69] H. Weng, A. Ranjbar, Y. Liang, Z. Song, M. Khazaei, S. Yunoki, M. Arai, Y. Kawazoe, Z. Fang, X. Dai, *Phys. Rev. B* **2015**, *92*, 075436.

[70] T. Hu, H. Zhang, J. Wang, Z. Li, M. Hu, J. Tan, P. Hou, F. Li, X. Wang, *Sci. Rep.* **2015**, *5*, 16329.

[71] A. D. Dillon, M. J. Ghidiu, A. L. Krick, J. Griggs, S. J. May, Y. Gogotsi, M. W. Barsoum, A. T. Fafarman, *Adv. Funct. Mater.* **2016**, *26*, 4162.

[72] a) Y. Dong, S. Chertopalov, K. Maleski, B. Anasori, L. Hu, S. Bhattacharya, A. M. Rao, Y. Gogotsi, V. N. Mochalin, R. Podila, *Adv. Mater.* **2018**, *30*, 1705714; b) S. Chertopalov, V. N. Mochalin, *ACS Nano* **2018**, *12*, 6109.

[73] a) S. Lai, J. Jeon, S. K. Jang, J. Xu, Y. J. Choi, J.-H. Park, E. Hwang, S. Lee, *Nanoscale* **2015**, *7*, 19390; b) J. Xu, J. Shim, J.-H. Park, S. Lee, *Adv. Funct. Mater.* **2016**, *26*, 5328.

[74] a) S. S. Zhang, *J. Power Sources* **2013**, *231*, 153; b) L. Ma, K. E. Hendrickson, S. Wei, L. A. Archer, *Nano Today* **2015**, *10*, 315; c) H.-J. Peng, J.-Q. Huang, X.-B. Cheng, Q. Zhang, *Adv. Energy Mater.* **2017**, *7*, 1700260; d) Z. Xiao, Z. Li, X. Meng, R. Wang, *J. Mater. Chem. A* **2019**, *7*, 22730; e) H.-J. Peng, Q. Zhang, *Angew. Chem., Int. Ed.* **2015**, *54*, 11018.

[75] X. Liang, L. F. Nazar, *2D Metal Carbides and Nitrides (MXenes)*, Springer, Berlin **2019**, p. 381.

[76] X. Liang, A. Garsuch, L. F. Nazar, *Angew. Chem., Int. Ed.* **2015**, *54*, 3907.
[77] X. Liang, Y. Rangom, C. Y. Kwok, Q. Pang, L. F. Nazar, *Adv. Mater.* **2017**, *29*, 1603040.
[78] D. Rao, L. Zhang, Y. Wang, Z. Meng, X. Qian, J. Liu, X. Shen, G. Qiao, R. Lu, *J. Phys. Chem. C* **2017**, *121*, 11047.
[79] E. S. Sim, G. S. Yi, M. Je, Y. Lee, Y.-C. Chung, *J. Power Sources* **2017**, *342*, 64.
[80] E. S. Sim, Y.-C. Chung, *Appl. Surf. Sci.* **2018**, *435*, 210.
[81] D. Wang, F. Li, R. Lian, J. Xu, D. Kan, Y. Liu, G. Chen, Y. Gogotsi, Y. Wei, *ACS Nano* **2019**, *13*, 11078.
[82] L.-C. Yin, J. Liang, G.-M. Zhou, F. Li, R. Saito, H.-M. Cheng, *Nano Energy* **2016**, *25*, 203.
[83] H. R. Jiang, W. Shyy, M. Liu, Y. X. Ren, T. S. Zhao, *J. Mater. Chem. A* **2018**, *6*, 2107.
[84] S. Mukherjee, L. Kavalsky, K. Chattopadhyay, C. V. Singh, *Nanoscale* **2018**, *10*, 21335.
[85] N. Li, Q. Meng, X. Zhu, Z. Li, J. Ma, C. Huang, J. Song, J. Fan, *Nanoscale* **2019**, *11*, 8485.
[86] H. Lin, D.-D. Yang, N. Lou, S.-G. Zhu, H.-Z. Li, *Ceram. Int.* **2019**, *45*, 1588.
[87] a) Y. Wang, J. Shen, L.-C. Xu, Z. Yang, R. Li, R. Liu, X. Li, *Phys. Chem. Chem. Phys.* **2019**, *21*, 18559; b) P. Liang, L. Zhang, D. Wang, X. Man, H. Shu, L. Wang, H. Wan, X. Du, H. Wang, *Appl. Surf. Sci.* **2019**, *489*, 677.
[88] X. Zhao, M. Liu, Y. Chen, B. Hou, N. Zhang, B. Chen, N. Yang, K. Chen, J. Li, L. An, *J. Mater. Chem. A* **2015**, *3*, 7870.
[89] W. Bao, L. Liu, C. Wang, S. Choi, D. Wang, G. Wang, *Adv. Energy Mater.* **2018**, *8*, 1702485.
[90] Y. Song, Z. Sun, Z. Fan, W. Cai, Y. Shao, G. Sheng, M. Wang, L. Song, Z. Liu, Q. Zhang, *Nano Energy* **2020**, *70*, 104555.
[91] a) H. Tang, W. Li, L. Pan, C. P. Cullen, Y. Liu, A. Pakdel, D. Long, J. Yang, N. McEvoy, G. S. Duesberg, *Adv. Sci.* **2018**, *5*, 1800502; b) H. Tang, W. Li, L. Pan, K. Tu, F. Du, T. Qiu, J. Yang, C. P. Cullen, N. McEvoy, C. Zhang, *Adv. Funct. Mater.* **2019**, *29*, 1901907.
[92] Z. Xiao, Z. Li, P. Li, X. Meng, R. Wang, *ACS Nano* **2019**, *13*, 3608.
[93] Z. Xiao, Z. Yang, Z. Li, P. Li, R. Wang, *ACS Nano* **2019**, *13*, 3404.
[94] a) W. Bao, X. Xie, J. Xu, X. Guo, J. Song, W. Wu, D. Su, G. Wang, *Chem. - Eur. J.* **2017**, *23*, 12613; b) J. Song, X. Guo, J. Zhang, Y. Chen, C. Zhang, L. Luo, F. Wang, G. Wang, *J. Mater. Chem. A* **2019**, *7*, 6507; c) W. Bao, D. Su, W. Zhang, X. Guo, G. Wang, *Adv. Funct. Mater.* **2016**, *26*, 8746; d) Q. Zhao, Q. Zhu, J. Miao, P. Zhang, B. Xu, *Nanoscale* **2019**, *11*, 8442; e) L.-P. Lv, C.-F. Guo, W. Sun, Y. Wang, *Small* **2019**, *15*, 1804338; f) N. Li, W. Cao, Y. Liu, H. Ye, K. Han, *Colloids Surf., A* **2019**, *573*, 128; g) R. Gan, N. Yang, Q. Dong, N. Fu, R. Wu, C. Li, Q. Liao, J. Li, Z. Wei, *J. Mater. Chem. A* **2020**, *8*, 7253; h) H.-Y. Zhou, Z.-Y. Sui, K. Amin, L.-W. Lin, H.-Y. Wang, B.-H. Han, *ACS Appl. Mater. Interfaces* **2020**, *12*, 13904.
[95] X. Zhang, H. Xie, C.-S. Kim, K. Zaghib, A. Mauger, C. Julien, *Mater. Sci. Eng., R* **2017**, *121*, 1.
[96] X. T. Gao, Y. Xie, X. D. Zhu, K. N. Sun, X. M. Xie, Y. T. Liu, J. Y. Yu, B. Ding, *Small* **2018**, *14*, 1802443.
[97] M.-S. Song, S.-C. Han, H.-S. Kim, J.-H. Kim, K.-T. Kim, Y.-M. Kang, H.-J. Ahn, S. Dou, J.-Y. Lee, *J. Electrochem. Soc.* **2004**, *151*, A791.
[98] a) H. Pan, X. Huang, R. Zhang, D. Wang, Y. Chen, X. Duan, G. Wen, *Chem. Eng. J.* **2019**, *358*, 1253; b) C. Du, J. Wu, P. Yang, S. Li, J. Xu, K. Song, *Electrochim. Acta* **2019**, *295*, 1067; c) L. Jiao, C. Zhang, C. Geng, S. Wu, H. Li, W. Lv, Y. Tao, Z. Chen, G. Zhou, J. Li, G. Ling, Y. Wan, Q.-H. Yang, *Adv. Energy Mater.* **2019**, *9*, 1900219; d) Y. Zhang, Z. Mu, C. Yang, Z. Xu, S. Zhang, X. Zhang, Y. Li, J. Lai, Z. Sun, Y. Yang, *Adv. Funct. Mater.* **2018**, *28*, 1707578; e) H. Zhang, Q. Qi, P. Zhang, W. Zheng, J. Chen, A. Zhou, W. Tian, W. Zhang, Z. Sun, *ACS Appl. Energy Mater.* **2019**, *2*, 705.
[99] X. Wang, C. Yang, X. Xiong, G. Chen, M. Huang, J.-H. Wang, Y. Liu, M. Liu, K. Huang, *Energy Storage Mater.* **2019**, *16*, 344.
[100] Y. Yao, W. Feng, M. Chen, X. Zhong, X. Wu, H. Zhang, Y. Yu, *Small* **2018**, *14*, 1802516.
[101] D. Guo, F. Ming, H. Su, Y. Wu, W. Wahyudi, M. Li, M. N. Hedhili, G. Sheng, L.-J. Li, H. N. Alshareef, *Nano Energy* **2019**, *61*, 478.
[102] a) Y.-S. Su, A. Manthiram, *Chem. Commun.* **2012**, *48*, 8817; b) Y.-S. Su, A. Manthiram, *Nat. Commun.* **2012**, *3*, 1166; c) J. He, Y. Chen, A. Manthiram, *Energy Environ. Sci.* **2018**, *11*, 2560; d) H.-J. Peng, D.-W. Wang, J.-Q. Huang, X.-B. Cheng, Z. Yuan, F. Wei, Q. Zhang, *Adv. Sci.* **2016**, *3*, 1500268; e) C.-H. Chang, S.-H. Chung, A. Manthiram, *J. Mater. Chem. A* **2015**, *3*, 18829.
[103] a) N.-W. Li, Y. Shi, Y.-X. Yin, X.-X. Zeng, J.-Y. Li, C.-J. Li, L.-J. Wan, R. Wen, Y.-G. Guo, *Angew. Chem., Int. Ed.* **2018**, *57*, 1505; b) E. Cha, M. D. Patel, J. Park, J. Hwang, V. Prasad, K. Cho, W. Choi, *Nat. Nanotechnol.* **2018**, *13*, 337; c) X. Zhang, Q. Zhang, X. G. Wang, C. Wang, Y. N. Chen, Z. Xie, Z. Zhou, *Angew. Chem., Int. Ed.* **2018**, *130*, 12996; d) J. Liang, X. Li, Y. Zhao, L. V. Goncharova, G. Wang, K. R. Adair, C. Wang, R. Li, Y. Zhu, Y. Qian, *Adv. Mater.* **2018**, *30*, 1804684; e) K. Liao, S. Wu, X. Mu, Q. Lu, M. Han, P. He, Z. Shao, H. Zhou, *Adv. Mater.* **2018**, *30*, 1705711; f) T. Kang, Y. Wang, F. Guo, C. Liu, J. Zhao, J. Yang, H. Lin, Y. Qiu, Y. Shen, W. Lu, *ACS Cent. Sci.* **2019**, *5*, 468; g) Z. A. Ghazi, Z. Sun, C. Sun, F. Qi, B. An, F. Li, H.-M. Cheng, *Small* **2019**, *15*, 1900687.
[104] C. Lin, W. Zhang, L. Wang, Z. Wang, W. Zhao, W. Duan, Z. Zhao, B. Liu, J. Jin, *J. Mater. Chem. A* **2016**, *4*, 5993.
[105] J. Song, D. Su, X. Xie, X. Guo, W. Bao, G. Shao, G. Wang, *ACS Appl. Mater. Interfaces* **2016**, *8*, 29427.
[106] L. Yin, G. Xu, P. Nie, H. Dou, X. Zhang, *Chem. Eng. J.* **2018**, *352*, 695.
[107] N. Li, Y. Xie, S. Peng, X. Xiong, K. Han, *J. Energy Chem.* **2020**, *42*, 116.
[108] G. Jiang, N. Zheng, X. Chen, G. Ding, Y. Li, F. Sun, Y. Li, *Chem. Eng. J.* **2019**, *373*, 1309.
[109] Y. Dong, S. Zheng, J. Qin, X. Zhao, H. Shi, X. Wang, J. Chen, Z.-S. Wu, *ACS Nano* **2018**, *12*, 2381.
[110] J. Huang, R. Meng, L. Zu, Z. Wang, N. Feng, Z. Yang, Y. Yu, J. Yang, *Nano Energy* **2018**, *46*, 20.
[111] B. Li, D. Zhang, Y. Liu, Y. Yu, S. Li, S. Yang, *Nano Energy* **2017**, *39*, 654.
[112] a) D. Er, J. Li, M. Naguib, Y. Gogotsi, V. B. Shenoy, *ACS Appl. Mater. Interfaces* **2014**, *6*, 11173; b) Y.-X. Yu, *J. Phys. Chem. C* **2016**, *120*, 5288; c) V. Shukla, N. K. Jena, S. R. Naqvi, W. Luo, R. Ahuja, *Nano Energy* **2019**, *58*, 877.
[113] a) Y. Wu, P. Nie, J. Wang, H. Dou, X. Zhang, *ACS Appl. Mater. Interfaces* **2017**, *9*, 39610; b) J. Zhu, M. Wang, M. Lyu, Y. Jiao, A. Du, B. Luo, I. Gentle, L. Wang, *ACS Appl. Nano Mater.* **2018**, *1*, 6854; c) G. Lv, J. Wang, Z. Shi, L. Fan, *Mater. Lett.* **2018**, *219*, 45; d) X. Wang, S. Kajiyama, H. Iinuma, E. Hosono, S. Oro, I. Moriguchi, M. Okubo, A. Yamada, *Nat. Commun.* **2015**, *6*, 6544; e) M. Naguib, R. A. Adams, Y. Zhao, D. Zemlyanov, A. Varma, J. Nanda, V. G. Pol, *Chem. Commun.* **2017**, *53*, 6883.
[114] M. R. Lukatskaya, O. Mashtalir, C. E. Ren, Y. Dall-Agnese, P. Rozier, P. L. Taberna, M. Naguib, P. Simon, M. W. Barsoum, Y. Gogotsi, *Science* **2013**, *341*, 1502.
[115] S. Kajiyama, L. Szabova, K. Sodeyama, H. Iinuma, R. Morita, K. Gotoh, Y. Tateyama, M. Okubo, A. Yamada, *ACS Nano* **2016**, *10*, 3334.
[116] S.-M. Bak, R. Qiao, W. Yang, S. Lee, X. Yu, B. Anasori, H. Lee, Y. Gogotsi, X.-Q. Yang, *Adv. Energy Mater.* **2017**, *7*, 1700959.
[117] a) D. Zhao, M. Clites, G. Ying, S. Kota, J. Wang, V. Natu, X. Wang, E. Pomerantseva, M. Cao, M. W. Barsoum, *Chem. Commun.* **2018**, *54*, 4533; b) V. Natu, M. Clites, E. Pomerantseva, M. W. Barsoum, *Mater. Res. Lett.* **2018**, *6*, 230.
[118] P. Lian, Y. Dong, Z.-S. Wu, S. Zheng, X. Wang, S. Wang, C. Sun, J. Qin, X. Shi, X. Bao, *Nano Energy* **2017**, *40*, 1.
[119] Y. Dall'Agnese, P.-L. Taberna, Y. Gogotsi, P. Simon, *J. Phys. Chem. Lett.* **2015**, *6*, 2305.

[120] J. Luo, J. Zheng, J. Nai, C. Jin, H. Yuan, O. Sheng, Y. Liu, R. Fang, W. Zhang, H. Huang, *Adv. Funct. Mater.* **2019**, *29*, 1808107.
[121] S. Sun, Z. Xie, Y. Yan, S. Wu, *Chem. Eng. J.* **2019**, *366*, 460.
[122] J. Li, D. Yan, S. Hou, Y. Li, T. Lu, Y. Yao, L. Pan, *J. Mater. Chem. A* **2018**, *6*, 1234.
[123] J. Luo, C. Fang, C. Jin, H. Yuan, O. Sheng, R. Fang, W. Zhang, H. Huang, Y. Gan, Y. Xia, *J. Mater. Chem. A* **2018**, *6*, 7794.
[124] X. Xie, K. Kretschmer, B. Anasori, B. Sun, G. Wang, Y. Gogotsi, *ACS Appl. Nano Mater.* **2018**, *1*, 505.
[125] X. Xie, M.-Q. Zhao, B. Anasori, K. Maleski, C. E. Ren, J. Li, B. W. Byles, E. Pomerantseva, G. Wang, Y. Gogotsi, *Nano Energy* **2016**, *26*, 513.
[126] X. Guo, X. Xie, S. Choi, Y. Zhao, H. Liu, C. Wang, S. Chang, G. Wang, *J. Mater. Chem. A* **2017**, *5*, 12445.
[127] Y. Wu, P. Nie, L. Wu, H. Dou, X. Zhang, *Chem. Eng. J.* **2018**, *334*, 932.
[128] Y. Zhang, B. Guo, L. Hu, Q. Xu, Y. Li, D. Liu, M. Xu, *J. Alloys Compd.* **2018**, *732*, 448.
[129] Y. Tian, Y. An, S. Xiong, J. Feng, Y. Qian, *J. Mater. Chem. A* **2019**, *7*, 9716.
[130] a) D. Zhao, R. Zhao, S. Dong, X. Miao, Z. Zhang, C. Wang, L. Yin, *Energy Environ. Sci.* **2019**, *12*, 2422; b) R. Meng, J. Huang, Y. Feng, L. Zu, C. Peng, L. Zheng, L. Zheng, Z. Chen, G. Liu, B. Chen, *Adv. Energy Mater.* **2018**, *8*, 1801514; c) R. Zhao, Z. Qian, Z. Liu, D. Zhao, X. Hui, G. Jiang, C. Wang, L. Yin, *Nano Energy* **2019**, *65*, 104037; d) X. Guo, W. Zhang, J. Zhang, D. Zhou, X. Tang, X. Xu, B. Li, H. Liu, G. Wang, *ACS Nano* **2020**, *14*, 3651.
[131] a) Y. Wu, P. Nie, J. Jiang, B. Ding, H. Dou, X. Zhang, *ChemElectroChem* **2017**, *4*, 1560; b) J. Li, B. Rui, W. Wei, P. Nie, L. Chang, Z. Le, M. Liu, H. Wang, L. Wang, X. Zhang, *J. Power Sources* **2020**, *449*, 227481.
[132] H. Huang, J. Cui, G. Liu, R. Bi, L. Zhang, *ACS Nano* **2019**, *13*, 3448.
[133] C.-F. Du, Q. Liang, Y. Zheng, Y. Luo, H. Mao, Q. Yan, *ACS Appl. Mater. Interfaces* **2018**, *10*, 33779.
[134] Y. Zhang, R. Zhan, Q. Xu, H. Liu, M. Tao, Y. Luo, S. Bao, C. Li, M. Xu, *Chem. Eng. J.* **2019**, *357*, 220.
[135] M. Tao, Y. Zhang, R. Zhan, B. Guo, Q. Xu, M. Xu, *Mater. Lett.* **2018**, *230*, 173.
[136] F. Wu, Y. Jiang, Z. Ye, Y. Huang, Z. Wang, S. Li, Y. Mei, M. Xie, L. Li, R. Chen, *J. Mater. Chem. A* **2019**, *7*, 1315.
[137] X. Guo, J. Zhang, J. Song, W. Wu, H. Liu, G. Wang, *Energy Storage Mater.* **2018**, *14*, 306.
[138] a) S. Tu, F. Ming, J. Zhang, X. Zhang, H. N. Alshareef, *Adv. Mater.* **2019**, *31*, 1806860; b) S. Tu, M. Mizohata, G. Sheng, L. Liu, F. Ming, C.-N. Xu, D. Tu, X. Zhang, H. N. Alshareef, *Adv. Funct. Mater.* **2020**, *88*, 1909843; c) J. Tang, X. Huang, T. Lin, T. Qiu, H. Huang, X. Zhu, Q. Gu, B. Luo, L. Wang, *Energy Storage Mater.* **2020**, *26*, 550; d) Y. Dong, Z.-S. Wu, S. Zheng, X. Wang, J. Qin, S. Wang, X. Shi, X. Bao, *ACS Nano* **2017**, *11*, 4792; e) R. Wang, S. Wang, Y. Zhang, D. Jin, X. Tao, L. Zhang, *J. Mater. Chem. A* **2018**, *6*, 1017; f) Y. Fang, R. Hu, B. Liu, Y. Zhang, K. Zhu, J. Yan, K. Ye, K. Cheng, G. Wang, D. Cao, *J. Mater. Chem. A* **2019**, *7*, 5363; g) W. Zhong, M. Tao, W. Tang, W. Gao, T. Yang, Y. Zhang, R. Zhan, S.-J. Bao, M. Xu, *Chem. Eng. J.* **2019**, *378*, 122209; h) M. Tao, G. Du, Y. Zhang, W. Gao, D. Liu, Y. Luo, J. Jiang, S. Bao, M. Xu, *Chem. Eng. J.* **2019**, *369*, 828; i) C. Zeng, F. Xie, X. Yang, M. Jaroniec, L. Zhang, S.-Z. Qiao, *Angew. Chem., Int. Ed.* **2018**, *57*, 8540.
[139] M. Tao, G. Du, T. Yang, W. Gao, L.-C. Zhang, W. Du, J. Jiang, S.-J. Bao, M.-W. Xu, *J. Mater. Chem. A* **2020**, *8*, 3018.
[140] D. Aurbach, Z. Lu, A. Schechter, Y. Gofer, H. Gizbar, R. Turgeman, Y. Cohen, M. Moshkovich, E. Levi, *Nature* **2000**, *407*, 724.
[141] a) Y.-s. Guo, F. Zhang, J. Yang, F.-f. Wang, Y. NuLi, S.-i. Hirano, *Energy Environ. Sci.* **2012**, *5*, 9100; b) H. D. Yoo, I. Shterenberg, Y. Gofer, G. Gershinsky, N. Pour, D. Aurbach, *Energy Environ. Sci.* **2013**, *6*, 2265; c) E. Levi, Y. Gofer, D. Aurbach, *Chem. Mater.* **2010**, *22*, 860.
[142] M. Xu, S. Lei, J. Qi, Q. Dou, L. Liu, Y. Lu, Q. Huang, S. Shi, X. Yan, *ACS Nano* **2018**, *12*, 3733.
[143] M. Xu, N. Bai, H.-X. Li, C. Hu, J. Qi, X.-B. Yan, *Chin. Chem. Lett.* **2018**, *29*, 1313.
[144] Q. Gao, J. Come, M. Naguib, S. Jesse, Y. Gogotsi, N. Balke, *Faraday Discuss.* **2017**, *199*, 393.
[145] M.-Q. Zhao, C. E. Ren, M. Alhabeb, B. Anasori, M. W. Barsoum, Y. Gogotsi, *ACS Appl. Energy Mater.* **2019**, *2*, 1572.
[146] F. Liu, Y. Liu, X. Zhao, X. Liu, L.-Z. Fan, *J. Mater. Chem. A* **2019**, *7*, 16712.
[147] H. Kaland, J. Hadler-Jacobsen, F. H. Fagerli, N. P. Wagner, Z. Wang, S. M. Selbach, F. Vullum-Bruer, K. Wiik, S. K. Schnell, *Sustainable Energy Fuels* **2020**, *4*, 2956.
[148] a) T. Gao, F. Han, Y. Zhu, L. Suo, C. Luo, K. Xu, C. Wang, *Adv. Energy Mater.* **2015**, *5*, 1401507; b) Y. Cheng, H. J. Chang, H. Dong, D. Choi, V. L. Sprenkle, J. Liu, Y. Yao, G. Li, *J. Mater. Res.* **2016**, *31*, 3125; c) X. Fan, R. R. Gaddam, N. A. Kumar, X. S. Zhao, *Adv. Energy Mater.* **2017**, *7*, 1700317; d) S. Su, Y. NuLi, Z. Huang, Q. Miao, J. Yang, J. Wang, *ACS Appl. Mater. Interfaces* **2016**, *8*, 7111.
[149] a) A. Byeon, M.-Q. Zhao, C. E. Ren, J. Halim, S. Kota, P. Urbankowski, B. Anasori, M. W. Barsoum, Y. Gogotsi, *ACS Appl. Mater. Interfaces* **2017**, *9*, 4296; b) F. Liu, Y. Liu, X. Zhao, K. Liu, H. Yin, L.-Z. Fan, *Small* **2020**, *16*, 1906076.
[150] A. Volta, *Philos. Trans. R. Soc. London* **1800**, 403.
[151] T. Yamamoto, T. Shoji, *Inorg. Chim. Acta* **1986**, *117*, L27.
[152] a) P. A. Maughan, N. Tapia-Ruiz, N. Bimbo, *Electrochim. Acta* **2020**, *341*, 136061; b) Q. Yang, Z. Huang, X. Li, Z. Liu, H. Li, G. Liang, D. Wang, Q. Huang, S. Zhang, S. Chen, *ACS Nano* **2019**, *13*, 8275.
[153] a) S. Wang, Q. Wang, W. Zeng, M. Wang, L. Ruan, Y. Ma, *Nano-Micro Lett.* **2019**, *11*, 70; b) J. Shi, S. Wang, Q. Wang, X. Chen, X. Du, M. Wang, Y. Zhao, C. Dong, L. Ruan, W. Zeng, *J. Power Sources* **2020**, *446*, 227345.
[154] Q. Wang, S. Wang, X. Guo, L. Ruan, N. Wei, Y. Ma, J. Li, M. Wang, W. Li, W. Zeng, *Adv. Electron. Mater.* **2019**, *5*, 1900537.
[155] S. Luo, L. Xie, F. Han, W. Wei, Y. Huang, H. Zhang, M. Zhu, O. G. Schmidt, L. Wang, *Adv. Funct. Mater.* **2019**, *29*, 1901336.
[156] X. Li, M. Li, Q. Yang, H. Li, H. Xu, Z. Chai, K. Chen, Z. Liu, Z. Tang, L. Ma, *ACS Nano* **2020**, *14*, 541.
[157] a) L. Wang, Z. Zhou, X. Yan, F. Hou, L. Wen, W. Luo, J. Liang, S. X. Dou, *Energy Storage Mater.* **2018**, *14*, 22; b) X.-B. Cheng, R. Zhang, C.-Z. Zhao, Q. Zhang, *Chem. Rev.* **2017**, *117*, 10403.
[158] D. Zhang, S. Wang, B. Li, Y. Gong, S. Yang, *Adv. Mater.* **2019**, *31*, 1901820.
[159] a) Z. Cao, Q. Zhu, S. Wang, D. Zhang, H. Chen, Z. Du, B. Li, S. Yang, *Adv. Funct. Mater.* **2020**, *30*, 1908075; b) K. Shen, B. Li, S. Yang, *Energy Storage Mater.* **2020**, *24*, 670.
[160] X. Zhang, R. Lv, A. Wang, W. Guo, X. Liu, J. Luo, *Angew. Chem., Int. Ed.* **2018**, *57*, 15028.
[161] H. Shi, C. J. Zhang, P. Lu, Y. Dong, P. Wen, Z.-S. Wu, *ACS Nano* **2019**, *13*, 14308.
[162] X. Chen, M. Shang, J. Niu, *Nano Lett.* **2020**, *20*, 2639.
[163] C. Wei, H. Fei, Y. Tian, Y. An, H. Guo, J. Feng, Y. Qian, *Energy Storage Mater.* **2020**, *26*, 223.
[164] J. Luo, C. Wang, H. Wang, X. Hu, E. Matios, X. Lu, W. Zhang, X. Tao, W. Li, *Adv. Funct. Mater.* **2019**, *29*, 1805946.
[165] X. Tang, D. Zhou, P. Li, X. Guo, B. Sun, H. Liu, K. Yan, Y. Gogotsi, G. Wang, *Adv. Mater.* **2020**, *32*, 1906739.
[166] Y. Tian, Y. An, C. Wei, B. Xi, S. Xiong, J. Feng, Y. Qian, *ACS Nano* **2019**, *13*, 11676.
[167] a) H. Liang, F. Ming, H. N. Alshareef, *Adv. Energy Mater.* **2018**, *8*, 1801804; b) H. Liang, C. Xia, A.-H. Emwas, D. H. Anjum, X. Miao, H. N. Alshareef, *Nano Energy* **2018**, *49*, 155.
[168] B. Ahmed, D. H. Anjum, Y. Gogotsi, H. N. Alshareef, *Nano Energy* **2017**, *34*, 249.
[169] a) C. J. Zhang, S. Pinilla, N. McEvoy, C. P. Cullen, B. Anasori, E. Long, S.-H. Park, A. Seral-Ascaso, A. Shmeliov, D. Krishnan, *Chem. Mater.* **2017**, *29*, 4848; b) T. Habib, X. Zhao, S. A. Shah, Y. Chen, W. Sun, H. An, J. L. Lutkenhaus, M. Radovic, M. J. Green, *npj 2D Mater. Appl.* **2019**, *3*, 8; c) R. Lotfi, M. Naguib, D. E. Yilmaz,

J. Nanda, A. C. T. Van Duin, *J. Mater. Chem. A* **2018**, *6*, 12733; d) Y. Lee, S. J. Kim, Y.-J. Kim, Y. Lim, Y. Chae, B.-J. Lee, Y.-T. Kim, H. Han, Y. Gogotsi, C. W. Ahn, *J. Mater. Chem. A* **2020**, *8*, 573.

[170] a) X. Wu, Z. Wang, M. Yu, L. Xiu, J. Qiu, *Adv. Mater.* **2017**, *29*, 1607017; b) C.-W. Wu, B. Unnikrishnan, I. W. P. Chen, S. G. Harroun, H.-T. Chang, C.-C. Huang, *Energy Storage Mater.* **2020**, *25*, 563.

[171] N. Zhang, Y. Hong, S. Yazdanparast, M. A. Zaeem, *2D Mater.* **2018**, *5*, 045004.

[172] C. E. Shuck, A. Sarycheva, M. Anayee, A. Levitt, Y. Zhu, S. Uzun, V. Balitskiy, V. Zahorodna, O. Gogotsi, Y. Gogotsi, *Adv. Eng. Mater.* **2020**, *22*, 1901241.

[173] C. E. Shuck, Y. Gogotsi, *Chem. Eng. J.* **2020**, *401*, 125786.

Fangwang Ming received his master degree in chemical engineering in 2017 from Xiamen University. He is currently a Ph.D. student under the supervision of professor Husam N. Alshareef at King Abdullah University of Science & Technology (KAUST). His research interest relates to functional nanomaterials, especially 2D materials, for efficient energy storage and conversion.

Hanfeng Liang received his Ph.D. in applied chemistry in 2015 from Xiamen University. As a visiting graduate student, he studied at University of Wisconsin - Madison from 2013 to 2015. He is currently a postdoc in Prof. Husam N. Alshareef's group at KAUST. His research focuses on earth-abundant materials for catalysis and electrochemical energy storage and conversion.

Husam N. Alshareef is a professor of Materials Science and Engineering at King Abdullah University of Science and Technology (KAUST). He obtained his Ph.D. at North Carolina State University, Raleigh, USA. He then did his postdoctoral work at Sandia National Laboratory, USA. Following ten years in the semiconductor industry, he joined KAUST in 2009, where he has been running a research group focused on developing inorganic nanomaterials for energy and electronics.

ADVANCED MATERIALS

Please complete this form and return it via E-Mail to the Editorial Office:
advmat@wiley-vch.de

Reprint Order Form

Manuscript No.: _____

Customer No.: (if available) _____

Purchase Order No.: _____

Author: _____

Charges for Reprints in Euro (excl. VAT), prices are subject to change. Minimum order 50 copies; single issues for authors at a reduced price.

No. of pages	50 copies	100 copies	150 copies	200 copies	300 copies	500 copies
1– 4	345,—	395,—	425,—	445,—	548,—	752,—
5– 8	490,—	573,—	608,—	636,—	784,—	1077,—
9–12	640,—	739,—	786,—	824,—	1016,—	1396,—
13–16	780,—	900,—	958,—	1004,—	1237,—	1701,—
17–20	930,—	1070,—	1138,—	1196,—	1489,—	2022,—
every additional 4 pages	147,—	169,—	175,—	188,—	231,—	315,—

Information regarding VAT: The charges for publication of *reprints/ issues/poster* are considered to be "supply of services" and therefore subject to German VAT. However, if you are an institutional customer outside Germany, the tax can be waived if you provide us with the valid VAT number of your company. Non-EU customers may have a VAT number starting with "EU" instead of their country code, if they are registered with the EU tax authorities. If you do not have a valid EU VAT number and you are a taxable person doing business in a non-EU country, please provide a certification from your local tax authorities confirming that you are a taxable person under local tax law. Please note that the certification must confirm that you are a taxable person and are conducting an economic activity in your country. **Note:** certifications confirming that you are a tax-exempt legal body (non-profit organization, public body, school, political party, etc.) in your country do not exempt you from paying German VAT.

Please send me send bill me for

☐ no. of reprints

☐ no. of issue
(1 copy: 28 Euro)

☐ high-resolution PDF file (330 Euro excl. VAT)
E-mail address: _____

❖ Special Offer:
If you order 200 or more reprints you will get a PDF file for half price.

Please note: It is not permitted to present the PDF file on the internet or on company homepages.

Cover Posters (prices excl. VAT)
Posters of published covers are available in two sizes:

☐ DIN A2 42 x 60 cm / 17 x 24in (one copy: 39 Euro)

☐ DIN A1 60 x 84 cm / 24 x 33in (one copy: 49 Euro)

Postage for shipping (prices excl. VAT)
overseas +25 Euro
within Europe +15 Euro

_____
Date, Signature

VAT number: _____

Mail reprints / copies of the issue to:

_____
_____
_____
_____
_____

Send bill to:

_____
_____
_____
_____

☐ **I will pay by bank transfer**

☐ **I will pay by credit card**

VISA, Mastercard and AMERICAN EXPRESS
For your security please use this link (Credit Card Token Generator) to create a secure code Credit Card Token and include this number in the form instead of the credit card data. Click here:
https://www.wiley-vch.de/editorial_production/index.php

CREDIT CARD TOKEN NUMBER

						V									

Wiley-VCH Verlag GmbH & Co. KGaA – A company of John Wiley & Sons, Inc. -
Location of the Company: Weinheim - Trade Register: Mannheim, HRB 432833.
Chairman of the Supervisory Board: John Kritzmacher
General Partner: John Wiley & Sons GmbH, Location: Weinheim –
Trade Register Mannheim, HRB 432296 – Managing Director: Sabine Haag and Dr. Guido Herrmann

WILEY-VCH